PhD degree in Molecular Medicine (curriculum in Molecular Oncology)

European School of Molecular Medicine (SEMM),

University of Milan and University of Naples "Federico II"

Settore disciplinare: Bio/10

CROSS-TALK BETWEEN THE PROTEOLYTIC AND NON-PROTEOLYTIC FUNCTIONS OF THE UROKINASE RECEPTOR

Valentina De Lorenzi

IFOM, Milan

Matricola n. R09395

Supervisor: Dr. Nicolai Sidenius

IFOM, Milan

Anno accademico 2013-2014

TABLE OF CONTENTS

1. LIST OF ABBREVIATIONS 6

2. FIGURES INDEX 9

3. ABSTRACT 12

4. INTRODUCTION 14

4.1 PLASMINOGEN ACTIVATION SYSTEM 15

4.1.1 Plasminogen / Plasmin 15

4.1.2 Regulation of plasmin generation and activity 16

4.2 UROKINASE-TYPE PLASMINOGEN ACTIVATOR SYSTEM 18

4.2.1 uPA 18

4.2.2 PAI-1 19

4.2.3 uPAR 22

4.2.4 VN 25

4.3 uPAR FUNCTIONS 27

4.3.1 Proteolytic functions 27

4.3.2 Non proteolytic functions 29

4.4 uPAR SIGNALLING AND ADHESIVE FUNCTIONS ARE INTIMATELY CONNECTED 33

4.5 CROSS-TALK BETWEEN THE PROTEOLYTIC AND NON-PROTEOLYTIC FUNCTIONS OF uPAR 35

4.6 OBJECTIVES OF THIS STUDY 37

5. MATERIALS AND METHODS 39

5.1 MATERIAL 39

5.2 CELL CULTURE AND TRANSFECTIONS 39

5.3 EXPRESSION VECTOR CONSTRUCTION 40

5.4 OLIGONUCLEOTIDE SEQUENCES 42

5.5 EXPRESSION AND PURIFICATION OF RECOMBINANT PROTEINS 43

5.6 TIME-LAPSE IMAGING 43

5.7 DIFFERENTIAL INTERFERENCE CONTRAST (DIC) MICROSCOPY 44

5.8 CELL LYSIS AND WESTERN BLOTTING 44

5.9 LABEL-FREE REAL-TIME CELL-BASED ASSAY (RTCA) EXPERIMENTS 45

5.10 VN FRAGMENTS RELEASE EXPERIMENTS 46

5.11 MATRIX-ASSISTED LASER DESORPTION/IONIZATION TIME OF FLIGHT (MALDI-TOF) MASS SPECTROMETRY (MS) 46

5.12 ANTIBODIES GENERATION 47

5.13 TIME-RESOLVED FLUORESCENCE BASED ASSAYS 48

5.13.1 Screening of sera/supernatants 49

5.13.2 Antibody epitope mapping experiments *50*
5.13.3 Immunoassays for the detection of N-terminal SMB-containing VN fragments *50*
5.13.4 Binding assays *51*
5.14 PREPARATION OF CALIBRATOR SAMPLES 52
5.15 GENERATION OF THE VN(1-61) STANDARD 52
5.16 CREATININE ASSAY 52
6. RESULTS 53
6.1 NEGATIVE FEEDBACK BETWEEN UPAR PROTEOLYTIC AND NON-PROTEOLYTIC FUNCTIONS 53
6.1.1 Plasminogen activation exerts a negative feedback on cell adhesion to VN *53*
6.1.2 The catalytic activity of both uPA and Pli contributes to the negative feedback *56*
6.1.3 The negative feedback is partially caused by uPAR cleavage *57*
6.1.4 Pli cleaves the RGD-motif in VN *59*
6.1.5 Cleavage of the RGD-motif in VN is responsible for the negative feedback between plasminogen activation and cell adhesion *65*
6.1.6 Development of an immunoassay for the detection of N-terminal VN fragments *68*
6.1.7 uPAR-expressing cells accelerate the cleavage of matrix VN by uPA and Pli *70*
6.1.8 Binding of VN to uPAR accelerates cleavage by uPA *74*
6.1.9 SMB-containing VN fragments are released by cancer cell lines *79*
6.1.10 N-terminal VN fragments are detectable in human urines *82*
6.2 OPTIMIZATION AND VALIDATION OF THE HU3/HF6 IMMUNOASSAY FOR USE AS A CLINICAL GRADE ASSAY FOR THE DETECTION AND QUANTIFICATION OF URINARY N-TERMINAL VN-FRAGMENTS 85
6.2.1 Dynamic range and assay precision *85*
6.2.2 Linearity of the assay *87*
6.2.3 Assay recovery *88*
6.2.4 Assay variability *89*
6.2.5 Assay robustness *90*
6.2.6 Circadian variability *91*
6.3 UPA·PAI-1 IS A SUPER-AGONIST OF THE UPAR-VN INTERACTION 93
6.3.1 The uPA·PAI-1 complex is a super-agonist of the uPAR mediated cell adhesion to VN 93
6.3.2 PAI-1 counteracts the negative feedback and behaves as a proteolysis-dependent agonist of the uPAR-mediated cell adhesion on VN *96*
6.3.3 uPA·PAI-1 complex directly enhances uPAR-VN interaction *98*
6.3.4 Mechanism of the PAI-1·uPA·uPAR·VN complex formation *99*
7. DISCUSSION 109
7.1 NEGATIVE FEEDBACK BETWEEN UPAR INDUCED EXTRACELLULAR PROTEOLYSIS AND CELL ADHESION TO VN 109

7.1.1 uPAR cleavage *109*
7.1.2 VN cleavage *110*
7.1.3 uPAR "catalyzes" the cleavage of VN mediated by uPA *110*
7.1.4 Cancer cells lines release SMB-containing fragments in vitro *111*
7.1.5 Implications and future perspectives *112*
7.3 SMB-CONTAINING FRAGMENTS ARE PRESENT *IN VIVO* 113
7.4 THE USE OF N-TERMINAL VN FRAGMENTS AS CANCER BIOMARKER 115
7.5 VALIDATION OF THE HU3/HF6 IMMUNOASSAY 117
7.6 THE UPA·PAI-1 COMPLEX IS A SUPER-AGONIST OF THE UPAR/VN INTERACTION 118
7.6.1 Future investigations *119*
7.6.2 Implications *120*
8. REFERENCES 123

1. LIST OF ABBREVIATIONS

293/uPAR = HEK293 cells overexpressing uPAR

ATF = amino terminal fragment of uPA

BSA = bovine serum albumin

CFA = complete Freund's Adjuvant

CHO = chinese hamster ovary cells

CNS = central nervous system

CV = coefficient of variation

D1 = domain 1 of uPAR

D2 = domain 2 of uPAR

D3 = domain 3 of uPAR

DELFIA = dissociation-enhanced lanthanide fluorescence immunoassay

DIC = Differential Interference Contrast microscopy

ECM = extracellular matrix

EGF = epidermal growth factor

EGFR = epidermal growth factor receptor

ER+ = estrogen receptor expressing cells

ERK = extracellular signal-regulated kinase

FAK = focal adhesion kinase

FGF2 = fibroblast growth factor 2

fMLP = formyl-Met-Leu-Phe peptide

FN = fibronectin

FPR = fMLP receptor

FPRL-1 = fMLP receptor like-1

FPRL-2 = fMLP receptor like-2

GFD = growth factor-like domain

GPCR = G protein-coupled receptor

GPI = glycophosphatidylinositol

HEK293 = human embryonic kidney 293 cells

HGF = hepatocytes growth factor

HIF1α = hypoxia-inducible factor 1α

HPLC = high-performance liquid chromatography

IFA = Incomplete Freund's Adjuvant

IgG = immunoglobulin G

IP = intraperitoneal injection

KD = kringle domain

LDLR = low density lipoprotein receptor

LPS = lipopolysaccharide

LRP-1A = low density lipoprotein receptor-related protein-1A

LRP-1B = low density lipoprotein receptor-related protein-1B

LRP2 = low density lipoprotein receptor-related protein-2

m/z = mass over charge ratio

mAb = monoclonal antibody

MALDI-TOF = Matrix-Assisted Laser Desorption/Ionization Time of Flight

MAPK = mitogen-activated protein kinase

MMP = matrix metalloproteinase

MS = mass spectrometry

MW = molecular weight

NFκB = nuclear factor kappa B

O/N = overnight

PAI-1 = plasminogen activator inhibitor 1

PAI-2 = plasminogen activator inhibitor 2

PAN = Pan-apple domain

PBS = phosphate buffered saline

PBS-T = phosphate buffered saline containing 0.1% Tween-20

PDGFRβ = platelet derived growth factor receptor β

PFA = paraformaldehyde

PLAU = uPA gene name

PLAUR = uPAR gene name

Plg = plasminogen

Pli = plasmin

PMSF = phenylmethanesulfonylfluoride

PN-1 = protease nexin-1

RCL = reactive centre loop

RT = room temperature

RTCA = Real-Time Cell-based Assay

S/N = signal to noise ratio

sc-uPA = single-chain uPA

SD = standard deviation

SDS-PAGE = Sodium Dodecyl Sulphate - PolyAcrylamide Gel Electrophoresis

SEM = standard error of the mean

serpin = serine proteases inhibitor

SMB = somatomedin B

SPD = serine protease domain

suPAR = soluble uPAR

TAFI = thrombin-activatable fibrinolytic inhibitor

tc-uPA = two-chain uPA

TGFβ = transforming growth factor β

TKR = tyrosine kinase receptor

TNFα = tumour necrosis factor α

tPA = tissue-type plasminogen activator

TR-FIA = Time-Resolved Fluorescence Immunoassay

uPA = urokinase-type plasminogen activator

UTR = untraslated region

VEGF = vascular endothelial growth factor

VLDLR = very low density lipoprotein receptor

VN = vitronectin

w/w = weight/weight ratio

α2M = α2-macroglobulin

α2AP = α2-antiplasmin

2. FIGURES INDEX

Figure 1: Schematic representation of human plasminogen. 15
Figure 2: Schematic representation of human uPA. 19
Figure 3: Inhibitory mechanism and dynamics of PAI-1. 21
Figure 4: The urokinase receptor. 23
Figure 5: Schematic representation of human VN. 26
Figure 6: Overview of the functions of uPAR. 27
Figure 7: Effect of plasminogen activation on 293/uPAR cells morphology. 54
Figure 8: Plasminogen activation exerts a negative feedback on cell adhesion to VN. 55
Figure 9: Plasminogen activation down-modulates uPAR-induced cell signalling on VN. 56
Figure 10: The catalytic activity of both uPA and Pli contributes to the negative feedback between plasminogen activation and cell adhesion. 57
Figure 11: The cleavage of uPAR contributes partially to the negative feedback. 58
Figure 12: $uPAR^{WT}$ but not $uPAR^{R83/89A}$ is cleaved by both uPA and Pli. 59
Figure 13: Pre-treatment of VN with Pli, but not uPA, inhibits subsequent cell adhesion mediated by uPAR and integrins. 60
Figure 14: Cartoon illustrating the domain structure of human VN and the VN(1-64)-Fc chimera. 61
Figure 15: Cleavage site(s) responsible for the negative feedback are in the N-terminal region of VN. 61
Figure 16: R45A mutation makes VN insensitive to Pli pre-treatment. 62
Figure 17: The R45A mutation in VN strongly impairs the negative feedback. 63
Figure 18: Pli cleaves VN in the RGD-motif after Arg45. 64
Figure 19: R45A mutation in VN strongly impairs tc-uPA mediated negative feedback. . 65
Figure 20: Cleavage of VN in the RGD-motif is responsible of the negative feedback. 66
Figure 21: Cleavage of uPAR by uPA and Pli contributes to the negative feedback. 67
Figure 22: Mapping of the binding epitopes of HF6, HU3 and IO35. 68
Figure 23: Cartoon illustrating the binding epitopes for HU3, HF6 and IO35 in VN. 69
Figure 24: Recognition of short N-terminal VN fragments by HF6, HU3 and IO35. 70
Figure 25: Plasminogen activation results in the release of N-terminal VN-fragments containing the SMB-domain. 71
Figure 26: tc-uPA mediated release is not due to trace amount of Pli in the preparation. .. 72
Figure 27: The generation of soluble VN-fragments containing the SMB-domain requires binding of both uPA and VN to uPAR. 73

Figure 28: Cartoon illustrating the mechanism of action of the different compounds/mutations used in Fig. 27 73
Figure 29: uPAR accelerate the generation of SMB-containing VN-fragments by uPA. ... 74
Figure 30: Levels of uPAR binding to VN and the release of VN fragments are strongly correlated. 75
Figure 31: Monomeric soluble uPAR induces tc-uPA mediated cleavage of VN. 76
Figure 32: The VN-binding capability of uPAR determines the extent of cleavage acceleration. 76
Figure 33: uPAR increases more than 100-fold the cleavage of VN mediated by tc-uPA. 77
Figure 34: uPAR catalyzes uPA-mediated cleavage of the ^{45}RG peptide bond – MALDI spectra. 78
Figure 35: uPAR catalyzes uPA-mediated cleavage of ^{45}RG peptide bond in VN – peak intensity 78
Figure 36: VN fragments are released by cancer cell lines. 80
Figure 37: uPA expression but not uPAR correlates with the released SMB levels. 81
Figure 38: Human urines contain short N-terminal VN fragments. 83
Figure 39: Three different molecular species of VN fragments are present in human urines. 84
Figure 40: Dynamic range of the HU3/HF6 immunoassay. 86
Figure 41: S/N ratio and Z-factor of the assay. 87
Figure 42: Assay linearity. 88
Figure 43: Assay recovery. 89
Figure 44: Intra- and inter-assay variability. 90
Figure 45: Assay robustness. 91
Figure 46: Long-term variations in urinary VN-antigen levels. 92
Figure 47: Short-term variations in urinary VN-antigen levels. 92
Figure 48: uPA·PAI-1 complex is a super-agonist of uPAR-mediated cell adhesion to VN. 94
Figure 49: Morphology of 293/uPAR cells treated with different ligands. 94
Figure 50: uPA·PAI-1 super-agonistic effect on uPAR-mediated adhesion to VN is not due to increased cell spreading. 95
Figure 51: Effect of uPAR ligands on 2D cell migration on VN. 96
Figure 52: uPA generated during plasminogen activation stimulates cell adhesion to VN-coated matrices in the presence of PAI-1. 97
Figure 53: The uPA·PAI-1 complex is a super-agonist of the interaction between uPAR and VN. 98

Figure 54: uPA·PAI-1 super-agonistic activity is not due to higher affinity of the uPA·PAI-1 complex for uPAR. 99
Figure 55: Complex formation between uPA and PAI-1 is required to promote uPAR binding to VN. 100
Figure 56: Pre-incubation of VN with PAI-1 increases subsequent uPAR binding induced by uPA and the catalytic activity of uPA is dispensable. 102
Figure 57: The VN binding site is required for tc-uPA mediated uPAR binding and dispensable for tc-uPA^{S356A} induced binding. 103
Figure 58: The VN binding site in uPAR is required for both sc-uPA and uPA·PAI-1 induced VN binding. 104
Figure 59: The VN binding site in PAI-1 is dispensable for the super-agonistic activity of the uPA·PAI-1 complex in inducing uPAR binding to VN. 105
Figure 60: Cartoon depicting the mechanism responsible for uPAR binding to VN mediated by complex formation between uPA and PAI-1. 106
Figure 61: Cartoon illustrating the molecular mechanism of the cross-talk between plasminogen activation and cell adhesion to VN. 108

3. ABSTRACT

Urokinase (uPA) and its cell surface receptor (uPAR) have been implicated in a wide variety of biological processes related to tissue homeostasis. Moreover the uPA-system plays an important role in many pathological events, such as tumour cell migration and dissemination. On the one hand, the binding of uPA to uPAR favours extracellular proteolysis by enhancing cell surface plasminogen activation. On the other hand, it promotes cell adhesion and signalling through binding of the provisional matrix protein vitronectin (VN). Although the existence of feedback loops between the functions of uPAR in extracellular proteolysis, cell adhesion and signalling has been described, some aspects of this cross-talk are still poorly understood and not characterized experimentally.

We here report that cell surface plasminogen activation induces a potent negative feedback on cell adhesion to VN. The feedback is predominantly caused by proteolytic cleavage of the RGD-motif in VN catalyzed by both uPA and plasmin. In this process the cell-adhesive properties of VN are impaired by disruption of the integrin binding site and release of the somatomedin B (SMB) domain responsible for binding of uPAR. Cleavage of VN by uPA displays a remarkable receptor-dependence and requires concomitant binding of both uPA and VN to uPAR suggesting that the hydrolysis is accelerated by a mechanism of substrate presentation. VN represents the first described uPAR-dependent substrate of uPA and our findings therefore identify a potential novel function of uPAR in focusing the proteolytic activity of the plasminogen activation system onto extracellular matrix-associated VN.

Additionally, SMB-containing N-terminal VN fragments are released by several cancer cell lines *in vitro* and are detectable in human urines samples. We have thus developed a clinical grade immunoassay for the detection and quantification of such fragments in urine samples with the aim of using the levels of urinary VN fragments as a novel cancer biomarker. Our working hypothesis is that this biomarker may be used as an indirect functional measurement of the uPA-system activity in the tumour tissue.

Finally, we show that the specific urokinase inhibitor, plasminogen activator inhibitor 1 (PAI-1), blocks the negative feedback mediated by uPA and behaves as a potent uPA-dependent agonist of the interaction between uPAR and VN. Indeed, we report for the first time that the covalent complex between uPA and PAI-1 is endowed with higher agonistic activity compared to uPA. Taken together, these data might represent a molecular explanation of the poor clinical outcome observed in cancer patients with high levels of uPA and PAI-1.

4. INTRODUCTION

Proteases are present in all organisms from prokaryotes to eukaryotes. In the human genome there are more than 500 genes encoding for proteases[1], which are involved in a variety of physiological processes. Their functions range from simple and non specific reactions, such those involved in food digestion, to highly orchestrated processes such as the blood clotting cascade, wound healing, immune and inflammatory cell migration and activation, apoptosis and angiogenesis. In addition, they have an important role in protein post-translational processing as well as in protein degradation.

Proteases are classified in six classes: aspartic, glutamic, cysteine, serine, threonine and metallo proteases; depending on the mechanism of catalysis. In particular, serine proteases utilize a serine residue as the nucleophile to attack and hydrolyse the target peptide bond of the substrate. Indeed, the catalytic mechanism relies on the so-called catalytic triad, composed of three amino acids located in the active site of the enzyme: serine, histidine and aspartic acid. The histidine and the aspartic acid cooperate to polarize and activate the serine residue.

Proteolytic reactions are highly regulated. In fact, most proteases are synthesised as inactive precursors, called zymogens, that are activated upon proteolytic cleavage, to ensure activation at the proper time in the correct localization. In addition, proteases often act within complex networks of inhibitors, receptors, substrates and binding proteins, which represent an additional layer of modulation. Accordingly, deregulated proteolytic events have been implicated in many human diseases including cancer, arthritis and cardiovascular diseases.

One such network is the urokinase-type plasminogen activation system that exerts multiple functions, both proteolytic and non-proteolytic, in an integrated and reciprocally regulated manner.

4.1 PLASMINOGEN ACTIVATION SYSTEM

4.1.1 Plasminogen / Plasmin

Plasminogen (Plg) is the zymogen form of the serine protease plasmin (Pli). It is mainly synthesised by hepatocytes in the liver[2] as well as by other organs and tissues[3] and is present in the blood stream at high concentration and in interstitial fluids.

The zymogen is secreted as a single-chain glycoprotein, 791 amino acids long. It is composed of seven domains: an N-terminal Pan-apple domain followed by 5 kringle domains (KD), containing Lys-binding sites responsible for binding to fibrin and to the cell surface, and the C-terminal serine protease domain (SPD), containing the catalytic triad (His603, Asp646 and Ser741).

The conversion of Plg to Pli is mediated by cleavage at the Arg561-Val562 peptide bond[4], which results in the generation of two polypeptide chains (namely: α and β chain) tethered together by two disulphide bonds. The two primary enzymes responsible for the proteolytic activation of Plg are tissue-type plasminogen activator (tPA) and urokinase-type plasminogen activator (uPA), with the former mainly acting in the blood stream and the latter involved in plasminogen activation mostly in extravascular tissues.

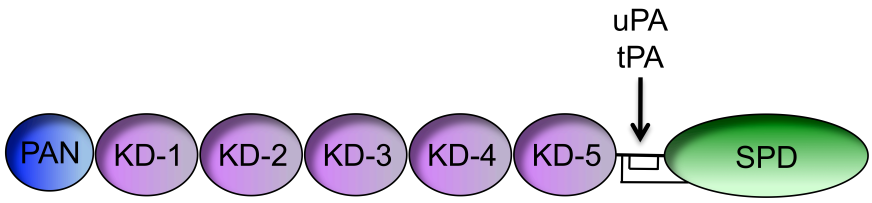

Figure 1: Schematic representation of human plasminogen.

Human Plg contains an N-terminal Pan-apple domain (PAN), 5 kringle domains (KD-1 to 5) and a SPD at the C-terminus. The activation site and the two inter-chain disulphide bonds are depicted.

Once activated, Pli displays a broad trypsin-like specificity and can consequently cleave a variety of diverse substrates. Pli has been recognized for a long time as the major

fibrinolytic enzyme; indeed, it cleaves fibrin at multiple lysine residues leading to the fibrin clots degradation. However, Pli has also been shown to activate and release from the extracellular matrix (ECM) several growth factors and chemokines, such as the transforming growth factor β (TGFβ)[5, 6], the fibroblast growth factor 2 (FGF2)[7, 8] and the hepatocytes growth factor (HGF)[9]. Furthermore, Pli can degrade ECM components, including laminin, fibronectin (FN)[10] and vitronectin (VN)[11], and cleave specific transmembrane as well as membrane-bound receptors (reviewed in [12]). In addition to these direct effects, Pli activity is further amplified and diversified by its ability to activate many members of the matrix metalloproteinase (MMP) family as the interstitial collagenase MMP1[13] and the two gelatinase MMP2 and MMP9[14].

Consistently with its broad substrate specificity, Pli has been implicated in a plethora of different biological processes, besides its well-characterized role in fibrinolysis and haemostasis. For instance, plasminogen activation has been shown to play a key role in tissue remodelling and wound healing, as evidenced by impaired resolution of skin wounds in Plg-deficient mice[15], and in cell migration and inflammation, as Plg-deficient mice display a largely compromised monocytes recruitment in the thioglycollate induced inflammation model[16].

4.1.2 Regulation of plasmin generation and activity

Being Pli such a broad and potent protease, its temporal activation and spatial localization are tightly regulated by a complex network of receptors, activators and inhibitors.

The main physiological inhibitor of Pli is the serpin α2-antiplasmin (α2AP)[17], which forms irreversible complex with the protease through an extremely fast kinetic reaction. At a lesser extent, Pli is also inhibited by the broad serine protease inhibitor α2-macroglobulin (α2M). Remarkably, Pli is resistant to inhibition by both α2AP and α2M when bound to the cell surface[18].

In addition to protection toward inhibition, membrane-bound Plg is more prone to activation due to a conformational change occurring upon cell surface binding[19, 20]. Localization at the plasma membrane is therefore of critical importance for Pli generation and activity.

The interaction of Plg/Pli with the cell surface occurs between the Lys-binding sites present in the KDs of Plg[19, 21] and cell membrane proteins containing a C-terminal basic residue[22, 23]. Many cellular Plg receptors have been identified in the last decades, the majority of which are cytoplasmic or nuclear proteins with well-established intracellular functions, such as the glycolytic enzyme α-enolase that was among the firsts to be identified[24]. These molecules represent atypical membrane receptors and the mechanism of their translocation to the cell membrane is still unknown. In sharp contrast, the latest identified Plg-R_{KT} was shown to be a Plg receptor with a C-terminal Lys exposed on the cell surface and two predicted transmembrane domains[25]. Remarkably, Plg-R_{KT} has been shown to regulate peripheral blood monocytes migration and invasion *in vitro* and macrophages recruitment at sites of inflammation *in vivo*[26], thus recapitulating a phenotype observed in Plg-deficient mice[16].

The key regulators of Plg activation are the two Plg activators: tPA and uPA. They have different structures, tissue expression pattern and, indeed, they have been shown to exert divergent functions *in vivo*[27, 28]. $tPA^{-/-}$ mice display a reduced rate of plasma clots lysis that is not observed in $uPA^{-/-}$ mice. On the other hand, inactivation of the uPA gene results in phenotypes that are not observed in $tPA^{-/-}$ mice, such as the occasional occurrence of small fibrin deposits in the liver and rectal prolapse. Remarkably, however, the double $uPA^{-/-}$ /$tPA^{-/-}$ mice have much more severe phenotypes compared with single knock-out animals. For instance, they have reduced life-span and fertility, extensive spontaneous fibrin deposition, a higher incidence of rectal prolapse compared to $uPA^{-/-}$ mice and more reduced clots lysis rate than $tPA^{-/-}$ mice[28]. uPA and tPA can therefore partially compensate each other absence and cooperate in diverse vascular as well as extravascular processes.

4.2 UROKINASE-TYPE PLASMINOGEN ACTIVATOR SYSTEM

The main components of the uPA system are the serine protease uPA, its cell surface receptor uPAR and its inhibitor, plasminogen activator inhibitor 1 (PAI-1). This system has been extensively studied over the last decades for its direct link with extracellular proteolysis and ECM degradation, in particular in the context of cancer. However, along the years a growing body of evidences has documented the existence of a variety of functions, which do not require the catalytic activity of uPA but are likewise important in physiological and pathological conditions. An emerging "new" component of the uPA system is the extracellular protein VN, which has been shown to interact with and modulate the activity of virtually all the components of the uPA system.

4.2.1 uPA

uPA is secreted by cells as an inactive polypeptide called single-chain uPA (sc-uPA) or pro-uPA. It is a 411 residues long protein, consisting of the N-terminal growth factor-like domain (GFD), a KD domain, a connective peptide containing the activation site and the C-terminal SPD, harbouring the catalytic triad (His204, Asp255 and Ser356). The N-terminal modular region, composed of the GFD and the KD domains, is called amino terminal fragment (ATF).

Zymogen activation occurs through a single specific cleavage after Lys158 mediated by Pli that leads to the generation of active two-chain uPA (tc-uPA). In addition, other proteases, including cathepsin B[29], matriptase[30, 31] and hepsin[32], have been shown to cleave and activate sc-uPA *in vitro*. Using $Plg^{-/-}$ mice, it has also been reported that glandular kallikrein 6 can activate sc-uPA *in vivo*[33].

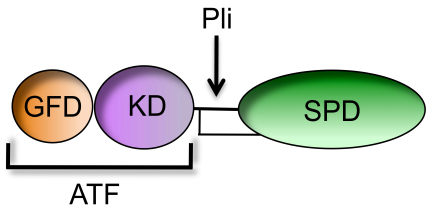

Figure 2: Schematic representation of human uPA.

The so-called amino terminal fragment (ATF) of uPA is composed of the N-terminal GFD domain and a KD. The SPD is located in the C-terminal part of the protein. The activation site and the single disulphide bond, tethering the two chains of the active form, are depicted.

uPA expression is highly regulated. Many transcription factors have been identified to interact with both promoter and enhancer regions. In addition, instability elements have been mapped in the 3' untraslated region (UTR) of the transcript and are key regulators of the mRNA stability (reviewed in [34]).

4.2.2 PAI-1

The glycoprotein PAI-1 belongs to the serpin (serine proteases inhibitor) protein family and is the primary and specific inhibitor of both uPA and tPA. Other serpins, such as plasminogen activator inhibitor 2 (PAI-2)[35, 36] and protease nexin 1 (PN-1)[37], have been shown to inhibit uPA and tPA *in vitro*, but with a slower kinetic compared to PAI-1[38].

PAI-1 is expressed by many cells in various tissues throughout the body, including endothelial cells, adipocytes and vascular smooth muscle cells[39-41]. It has been suggested that the liver may be the primary source of PAI-1 present in the plasma[39]. However, platelets could represent another important source of plasma PAI-1, as it has been recently shown that they *de novo* synthesize and release active PAI-1, in a process that can be further stimulated by thrombin[42, 43].

PAI-1 expression is regulated both transcriptionally, by several cytokines (e.g. tumour necrosis factor α, TNFα), hormones (e.g. insulin) and growth factors (such as TGFβ and

epidermal growth factor, EGF), and post-transcriptionally through the regulation of the mRNA stability (review in [34]).

The cDNA of human PAI-1 was cloned in 1986 by four groups[44-47]. It encodes for a 402 residues long immature protein with two alternative cleavage sites for the signal peptidase in the N-terminal part of the protein. Mature PAI-1 is therefore present in two isoforms, having 379 or 381 amino acids[44].

As most serpins, PAI-1 displays a highly ordered globular structure with 3 β-sheets, 9 α-helices and an exposed peptide loop called reactive centre loop (RCL), which is the key element for its inhibitory activity. The RCL contains the P_1-P_1' peptide bond (Arg346-Met347) that acts as substrate for the target protease. The P_1 residue is the major determinant for PAI-1 specificity; indeed, it has been shown that a basic residue at this position in necessary for uPA inhibition[48]. During the inhibitory reaction, the P_1-P_1' peptide bond is inserted within the active site of uPA leading to the formation of a reversible Michaelis complex between uPA and PAI-1. uPA is therefore able to cleave the P_1-P_1' bond and is consequently blocked in an irreversible complex through the formation of a covalent ester bond between the serine of the active site of uPA (Ser356) and the Arg346 of PAI-1 (reviewed in [49]). In addition, it has been shown that upon protease cleavage, PAI-1 can also behave as a substrate with no inhibitory activity. In this case, PAI-1 is inactivated while uPA retains full functionality[50].

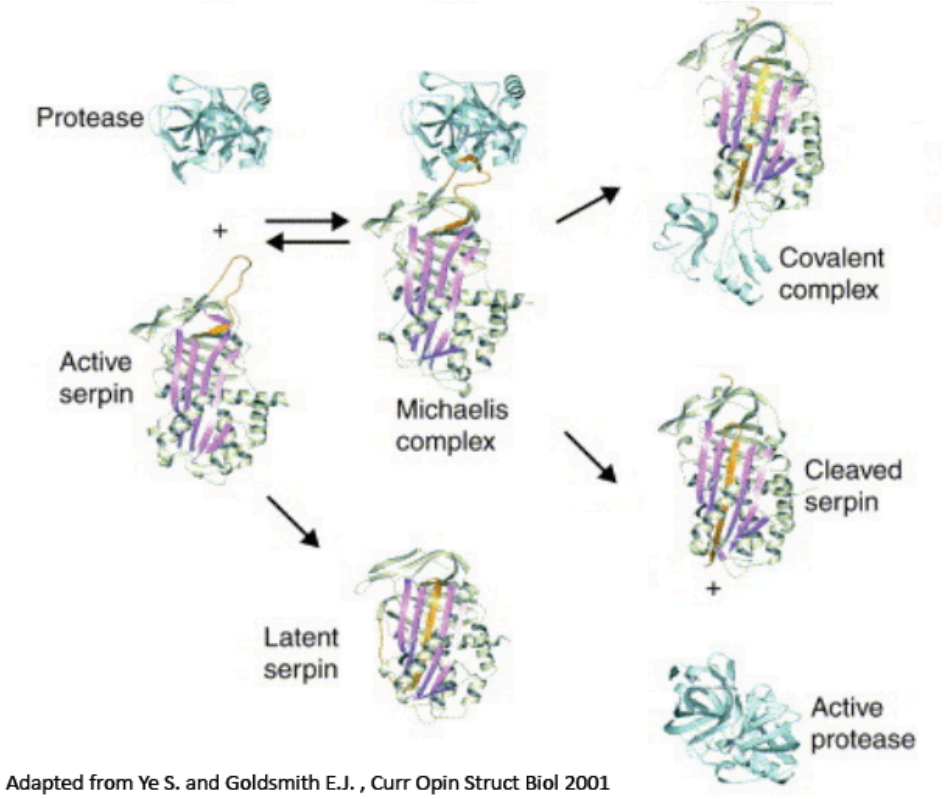

Figure 3: Inhibitory mechanism and dynamics of PAI-1.

The RCL loop of PAI-1 interacts with the serine in the active site of uPA leading to the formation of a reversible Michaelis complex. uPA activity is therefore inhibited through the formation of a covalent complex between uPA and PAI-1. Alternatively, PAI-1 is cleaved and inactivated while uPA remains catalytically active. The spontaneous latency transition of PAI-1 results in the generation of an inactive latent molecule, which does not bind VN and does not inhibit uPA.

A unique feature of PAI-1 compared with all the other serpins is its capability to undergo a spontaneous conversion of the active protein into a non-reactive stable form, called latent PAI-1[51]. This transition occurs under physiological conditions and is due to the insertion of the N-terminal part of the RCL in the central β-sheetA, which causes massive structural changes in the protein and the distortion of the key peptide bond P_1-P_1'. Measured half-life for active PAI-1 *in vitro* is about 1-2 hours at 37°C.

Binding to VN increases the stability of PAI-1 with about 2-fold increase of the measured half-life[52]. Active PAI-1 binds VN within the N-terminal somatomedin B (SMB) domain of the protein[53] with a very high affinity interaction (K_d in the subnanomolar range); on the contrary latent PAI-1 displays at least 200-fold lower affinity[54]. Recently, it has been

suggested the existence of an additional lower affinity PAI-1 binding site in VN, outside the SMB domain[55, 56].

Accordingly with this high affinity, PAI-1 in plasma and in the ECM is present in complex with VN[57, 58]. It has been suggested that PAI-1/VN interaction may actually have a double function: stabilization of PAI-1 as well as regulation of the spatial localization of the active protein[59].

4.2.3 uPAR

uPAR is a highly glycosylated extracellular receptor bound to the external leaflet of the plasma membrane through a glycophosphatidylinositol (GPI) anchor. uPAR cDNA was cloned in 1990[60]: it encodes for a precursor protein 335 residues long that is secreted by the cells after removal of the N-terminal signal peptide and the C-terminal hydrophobic sequence responsible for GPI-anchor attachment[61]. The mature protein comprises 283 amino acids and is composed of three homologous LU-domains (called D1, D2 and D3). The first crystal structure of soluble uPAR (suPAR) in complex with a uPA-binding antagonist peptide was solved in 2005[62] and showed the expected three-finger fold for the LU-domains and extensive interactions among the β-strands of the individual domains leading to a croissant-like topology.

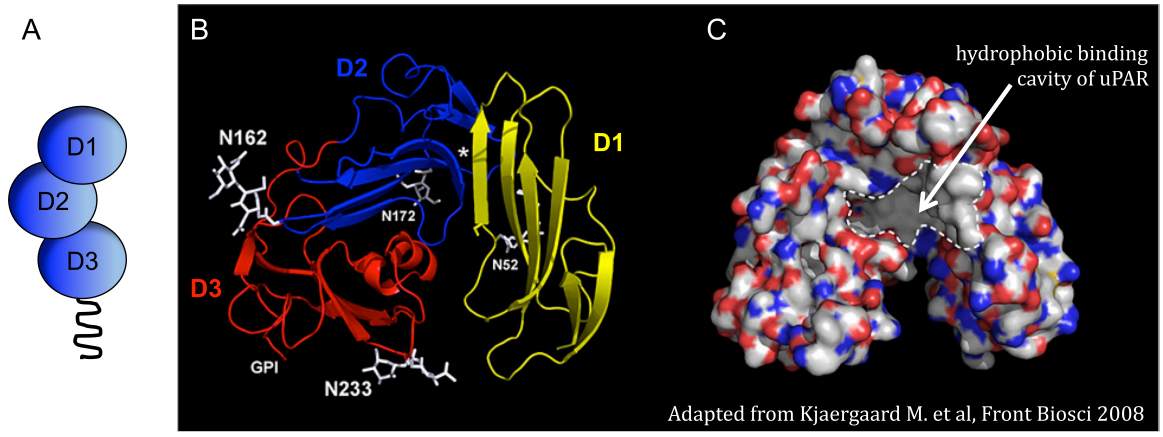

Figure 4: The urokinase receptor.

(A) Schematic representation of the domain organization of uPAR: the three homologous domains (D1-3) are tethered to the plasma membrane through a GPI-anchor. (B) Ribbon diagram of the structure of uPAR. Interactions among the three domains form a 13-strand antiparallel β-sheet. (C) Equivalent surface representation in which carbon and hydrogen atoms are depicted in gray, oxygen in red, nitrogen in blue and sulphur in yellow. The hydrophobic central cavity of uPAR responsible for the uPA binding is depicted.

uPAR gene (*PLAUR*) expression is subjected to a tight regulation. *PLAUR* promoter contains binding sequences for different transcription factors including nuclear factor kappa B (NFκB), SP1 and AP2, which mediate the regulation of uPAR gene expression by several molecules such as TGFβ, vascular endothelial growth factor (VEGF) and the mitogen-activated protein kinase (MAPK) pathway (also known as extracellular signal-regulated kinase, ERK, pathway) (reviewed in [34]). Remarkably, it has been shown that uPAR expression is induced in tumour-associated hypoxic conditions through the binding of hypoxia-inducible factor 1α (HIF1α) to a hypoxia responsive element present in the promoter of the gene[63]. Moreover, the stability of the *PLAUR* mRNA is regulated post-transcriptionally through the binding of RNA-binding proteins and miRNAs[64] to AU-rich regions located in the 3'UTR of the transcript. Notably, similar AU-rich regions are also present in the 3'UTR of uPA and PAI-1, suggesting the existence of common regulatory mechanisms (reviewed in [34]).

Under physiological conditions, uPAR is only moderately expressed in various tissues and organs including lungs, spleen, kidney and liver. On the other hand, organs undergoing

massive tissue remodelling are highly positive for uPAR[65]. Indeed, it has been shown that uPAR is present in migrating keratinocytes at the wound edges, but not in the resting counterpart in mouse skin[65, 66], in trophoblast cells in mouse placenta[65] and in human gestational tissues[67]. In addition, uPAR expression was found to be significantly increased upon injury, such as traumatic brain injury and cerebral ischemia, where major uPAR-expressing cells were infiltrating granulocytes, activated macrophages and endothelial cells[68]. uPAR is also expressed in other cells of the immune system, including activated neutrophils[69], monocytes[70] and T-cells[71], and in a subset of hematopoietic stem/progenitor cells[72].

Many pathological conditions are associated with uPAR overexpression. In particular, a huge amount of clinical and experimental data over the last decades has strongly linked uPAR, as well as the other components of the uPA system (i.e. uPA and PAI-1), with cancer. These molecules are overexpressed in a variety of human tumours including breast, lung, colon, ovarian and gastric carcinomas (review in[73]). Remarkably, they are present not only in the cancer cells but also in the tumour stroma: in human colon adenocarcinomas, it has been shown that uPAR is expressed by cancer cells at the invasive foci as well as by tumour infiltrating macrophages and neutrophils[74, 75]. In the same tumours, uPA was not expressed by malignant epithelial cells but only present in fibroblast-like stromal cells[74, 76]. Similar expression pattern has also been shown for human invasive ductal breast carcinomas, where the expression of the uPA system components was only rarely observed in cancer cells but rather detected in stromal cells. In fact, uPAR was found to be mainly expressed by tumour-associated macrophages[77], while myofibroblasts have been identified as the primary source of uPA[78, 79] and PAI-1[80].

It has been shown that the uPA system affects many biological processes involved at multiple stages of cancer formation and progression including ECM degradation, cancer cell proliferation, migration and intravasation (reviewed in [81]). Accordingly, high levels of

uPA system components in tumour tissues are significant prognostic factors of poor clinical outcome in several cancer types[73].

4.2.4 VN

VN was discovered as an adhesive protein capable to support spreading and growth of cultured cells[82] and called serum spreading factor[83]. The name "vitronectin" was proposed in 1983 because of its ability to bind glass and its adhesive properties[84]. It is now described as a matricellular protein, meaning a protein that does not have a structural function but rather acts as modulator of the cell-matrix interface, binding both ECM components and cell surface receptors or other proteins present in the pericellular space.

The primary source of VN is the liver[85], even if evidences of extrahepatic synthesis (e.g. in brain, adipose tissues, heart and skeletal muscles) have been reported[86].

Mature VN is a highly glycosylated protein, 459 amino acids long. It circulates as a single chain (75 kDa) or a disulphide-bridge two-chain form (65 + 10 kDa), which is generated upon proteolytic cleavage at the Arg379, by yet undefined enzymes. It is composed of: the N-terminal SMB domain (residues: 1-44), followed by a ^{45}RGD motif (i.e. integrin binding site), a highly acidic connecting region, harbouring a collagen binding site[87] and a transglutaminase cross-linking site at Gln93[88], and two hemopexin-like domains containing an additional collagen binding site[89] and the basic heparin binding domain, responsible for heparin and other glycosaminoglycans binding.

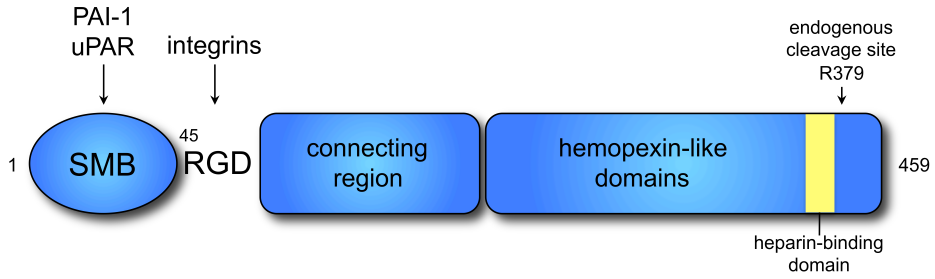

Figure 5: Schematic representation of human VN.

The N-terminal SMB domain of VN harbours an overlapping epitope for uPAR and PAI-1. Integrins bind to the flanking ^{45}RGD motif of the protein that is followed by a highly acidic connecting region and two hemopexin-like domains. The basic heparin-binding site and the endogenous cleavage site in the C-terminus of the protein are depicted.

VN is present in the circulation at high concentration and also in platelets α-granules, where it is found in complex with PAI-1[90]. Most of the plasma VN is in a closed folded conformation with limited ligand binding activity[91], whereas VN present in platelets and in association with the ECM in different tissues is in a high molecular weight multimeric form[92, 93]. VN deposition in normal tissues is limited, but increases in pathological conditions, such as atherosclerosis[94], liver fibrosis[95] and cancer[96-98]. In addition, VN is involved in the early response to acute tissue injury, supporting thrombus formation.

It has been shown that VN oligomerization can be induced by ligand binding, such as PAI-1[99]. The resulting VN multimers display a very different reactivity compared to native monomeric VN, with enhanced affinity for ECM components and cell surface receptors, such as the VN-receptor $\alpha_V\beta_3$ integrin[100]. Indeed, multimeric VN has been reported to interact with a variety of different proteins and molecules (reviewed in [101]). As mentioned above, VN interacts with all the core components of the uPA system: it is well-described that both uPAR[102] and PAI-1[53] bind to the SMB domain, whereas Plg[103] and uPA[104] have been documented to interact with the heparin binding region of the protein.

uPAR can orchestrate a variety of different cellular processes in both physiological and pathological conditions. uPAR functions are classically categorized as "proteolytic" and "non proteolytic" depending on the requirement of the catalytic activity of uPA.

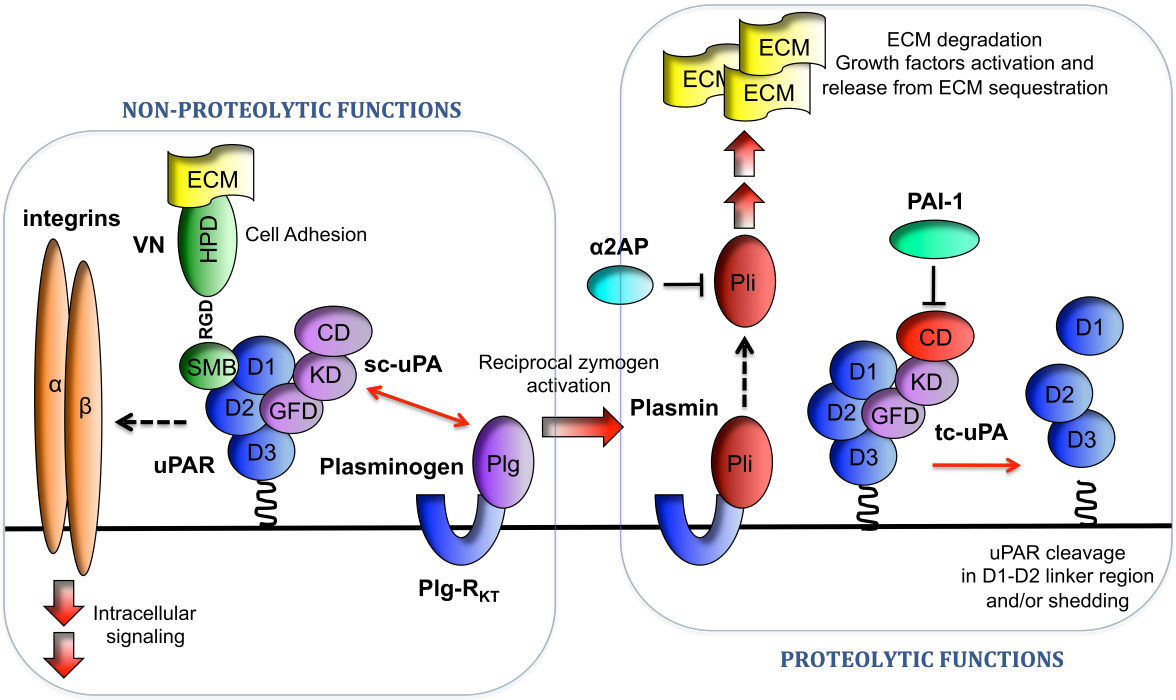

Figure 6: Overview of the functions of uPAR.

uPAR functions can be divided in proteolytic and non-proteolytic. On the one hand, it accelerates Plg activation through the high affinity binding to uPA. On the other hand, it directly mediates cell adhesion and affects intracellular signalling through the direct interaction with the extracellular protein VN and the cross-talk with transmembrane receptors, such as integrins.

4.3.1 Proteolytic functions

uPAR proteolytic functions were the first to be identified and characterized, as indeed, uPAR was discovered in 1985 as the cellular binding protein for uPA[105]. uPAR binds to either sc-uPA or tc-uPA with relatively high affinity (K_d in the low nanomolar range). The interaction is mediated by the N-terminal GFD domain of uPA[106] and a large hydrophobic surface located in the central cavity of uPAR, as clearly shown by the crystal structure of

the ATF·uPAR complex solved in 2006[107]. The binding surface in uPAR comprises residues belonging to all the three domains; therefore, an intact and folded receptor is necessary for uPA binding[108].

sc-uPA binding to uPAR localizes the zymogen at the cell surface, where it can encounter cell-bound Plg. As a consequence, the reciprocal zymogen activation is accelerated[109]. uPAR is thus able to activate and concentrate cell-associated proteolytic activity at specific cellular localization, such as at the leading edge of migrating cells[110]. The ability of uPAR to enhance pericellular proteolysis has been documented also *in vivo*. The combined overexpression of uPA and uPAR, but not the individual proteins, in the basal epidermis and hair follicles of transgenic mice, has been reported to increase Pli, MMP2 and MMP9 activity and cause extensive alopecia and epidermal thickening[111]. These effects are mediated only by catalytically active uPA[111] through the uPA/uPAR induced Plg activation, as the overexpression of the two proteins in $Plg^{-/-}$ mice fails to induce the pathological phenotype[112].

However, the study of the real physiological significance of the uPA/uPAR interaction has been complicated by the fact that both uPA and uPAR have functions that do not require the presence of the binding partner[113, 114]. The generation of knock-in animals expressing a uPAR-binding deficient but catalytically active mouse uPA ($Plau^{GFDhu/GFDhu}$ mice) has allowed to reliably dissect the uPA/uPAR contribution[115]. $Plau^{GFDhu/GFDhu}$ mice remarkably differ from $uPA^{-/-}$ mice and display normal life span, tissue regeneration and leukocytes recruitment in standard models of inflammation. By contrast, they exhibit fibrin deposits in the hepatic tissues accompanied by increased leukocytes infiltration, thus indentifying a role of the uPA/uPAR interaction in fibrin surveillance and in the suppression of fibrin-associated inflammation.

In addition, uPAR can modulate pericellular proteolysis also through the internalization of uPA-inhibitor complexes (i.e. complexes with PAI-1, PAI-2[116, 117], and PN-1[118]). It has been shown that the process requires the interaction with members of the low density

lipoprotein receptor (LDLR) family[119] (including the low density lipoprotein receptor-related protein-1A and -1B, LRP-1A and LRP-1B, LRP-2 and the very low density lipoprotein receptor, VLDLR) and induces the lysosomal degradation of uPA and the inhibitor, while uPAR is recycled back to the plasma membrane[120]. The outcome is therefore to favour proteolysis through degradation of inactive complexes and regeneration of free uPAR on the cell surface.

4.3.2 Non proteolytic functions

As mentioned above, a variety of uPAR biological functions do not require the presence of active uPA. Several studies have clearly documented the existence of uPAR activities mediated by binding catalytically inactive uPA variants or due to the overexpression of the receptor even in the absence of uPA. These processes have been ascribed to physical and/or functional interactions between uPAR and plasma membrane or pericellular proteins.

4.3.2.1 uPAR as adhesion receptor

uPAR directly binds to the matrix form of VN, in a RGD- and divalent cation-independent process[121-123]. It may therefore be defined as a *bona fide* non-integrin VN receptor.

The interaction between uPAR and the SMB domain of VN has been well-characterized by the resolution of the crystal structure of the suPAR·ATF·SMB complex[124], in accordance with two independent complete alanine-scans of uPAR[125, 126] and a non-exhaustive scan of the SMB[102, 126]. The GFD moiety of uPA is inserted in the central cavity of the receptor, while the SMB interacts with the outer side, with an epitope comprising residues belonging to D1 as well as to the D1-D2 linker region of uPAR. The binding interface consists of an arginine recognition site, composed of the residues Phe13, Asp22 and Tyr28 of VN, which

interact with the Arg91 of uPAR, and a hydrophobic binding area consisting mainly of residues Tyr27 and Tyr28 of VN inserted in a large cavity of the receptor where they interact with residues Trp32 and Ile63 of uPAR.

uPA, or GFD-containing uPA derivatives, ligation greatly increases the affinity of uPAR to VN[122, 126]. It has been proposed that this effect is mediated by receptor conformational changes occurring upon uPA binding[107, 127] as well as by uPA-induced receptor oligomerization and lipid raft partition[128-130].

As mentioned above, also PAI-1 binds to the SMB domain with very high affinity. Indeed, the two binding-sites for uPAR and PAI-1 are overlapping and consistently it has been shown that the two proteins can compete for VN binding. In line with a much higher affinity for the PAI-1/SMB interaction compared to uPAR/SMB[131], it has been shown that PAI-1 antagonises uPAR-mediated cell adhesion, resulting in cell detachment. Of note, this effect is reverted by active tc-uPA, which displaces PAI-1 from VN through the formation of the uPA·PAI-1 complex[102]. In addition, PAI-1 binding to the SMB domain also inhibits integrin-mediated cell adhesion, by sterically blocking the binding of integrins to the RGD motif of VN[132].

4.3.2.2 uPAR as signalling receptor

uPAR lacks transmembrane or cytoplasmic domains, therefore it can not directly transduce signals across the plasma membrane. However, a huge amount of independent studies have clearly shown that uPAR is a signalling receptor, able to promote cell migration, proliferation and survival, independently of uPA catalytic activity. Indeed, uPAR overexpression or ligation to uPA and VN can trigger the activation of many intracellular signalling molecules, such as the focal adhesion kinase (FAK), the tyrosine kinase Src, the small GTPase Rac1 and the MAPK pathway. These signal transduction events are mediated by functional and/or direct interaction with other transmembrane receptors,

including members of the integrin family, tyrosine kinase receptors (TKRs) and G protein-coupled receptors (GPCRs) (reviewed in [133]).

It is well-documented that integrins are signalling co-receptors for uPAR. However, it is still a matter of debate whether uPAR and integrins interact directly or rather functionally. On the one hand, co-localization and co-immunoprecipitation data argue for a physical interaction. Consistently, it has been shown that uPAR and integrin co-immunoprecipitation is inhibited by synthetic peptides corresponding to the integrin sequence of the putative binding surfaces (reviewed in [134]). On the other hand, experiments aimed to specifically detect protein-protein interactions with purified proteins have given controversial results. For instance, it has been reported a direct binding between suPAR and immobilized Fc-tagged $\alpha_5\beta_1$ integrin[135] that could not be reproduced by an independent study[136]. In addition, a complete alanine-scan of uPAR, in a model of uPAR overexpression in two different cell lines, has shown that the only important residues for uPAR-induced cell spreading and ERK activation are those involved in VN binding. In particular, alanine substitution of all the residues previously described as integrin binding sites, either individually or in combination, has no effect on the ability of uPAR to induce spreading and intracellular signalling[125]. Along the same line, a recent study from our lab has documented the existence of a uPAR-integrin signalling axis which is RGD independent and does not require direct physical interactions between uPAR and integrins, but rather relies on the plasma membrane tension, generated upon uPAR-mediated adhesion to VN, for the transduction of the signal[137].

Despite this controversy about the nature of the interaction between uPAR and integrins, many studies document the relevance of this cross-talk.

The first identified uPAR co-receptor is MAC1 (also know as $\alpha_M\beta_2$)[138]. MAC1 is mainly expressed in leukocytes, including neutrophils and macrophages, and is involved in cell adhesion and chemotaxis in condition of acute inflammation. uPAR-MAC1 interaction has

been reported to affect adhesive properties of MAC1, increasing its ability to bind fibrinogen[139] and to be required for neutrophils chemotaxis *in vitro*[140].

β_3-containing integrins are another class of integrins known to interact with uPAR. β_3 subunits form heterodimers with α_V and α_{IIb} subunits. The resulting $\alpha_V\beta_3$ receptor can bind VN as well as FN, while the $\alpha_{IIb}\beta_3$ receptor is specific for platelets and is involved in physiological processes such as platelet aggregation, through binding to fibrinogen. uPAR-β_3 signalling has been shown to induce cell motility through the activation of Rac1, a small GTPase crucial in mesenchymal-type cell migration. In mouse kidney podocytes, it has been shown *in vitro* and *in vivo* that lipopolysaccharide (LPS)-induced uPAR expression triggers $\alpha_V\beta_3$ activation and increases Rac-driven cell motility and proteinuria[141]. The molecular mechanism of Rac activation by uPAR-β_3 has been investigated in cancer cell lines. It involves the tyrosine phosphorylation of the adaptor protein p130Cas and the consequent formation of the p130Cas-Crk complex that leads to Rac activation through the guanidine nucleotide exchange factor DOCK180. This signalling pathway results in increased cancer cell migration and invasion[142].

Among the β_1-containing integrins, uPAR has been shown to interact with the laminin-5 receptor $\alpha_3\beta_1$ and with the FN receptor $\alpha_5\beta_1$. Cross-talk with $\alpha_3\beta_1$ modulates matrix adhesion and mediates epithelial-to-mesenchymal transition in kidney epithelial cells in a Src-dependent process[143]. Similarly, uPAR-$\alpha_5\beta_1$ has been reported to modulate FN adhesion and to increase cell migration[135], through the Src/Rac signalling pathway[144].

uPAR-β_1 signalling has also been shown to impact on the epidermal growth factor receptor (EGFR) activation. In particular, it has been shown that it can promote receptor activation and consequently ERK activation, in a FAK-dependent manner. Ultimately, this leads to induction of Hep3 human carcinoma cell proliferation *in vivo*[145]. In addition, uPAR signalling through EGFR has been shown to induce sustained ERK activation in estrogen receptor positive (ER+) breast cancer cell lines, thus providing selective advantage when cells were deprived of estrogen[146].

Among the TKRs, uPAR has been reported to interact also with the platelet derived growth factor receptor β (PDGFRβ) and to promote proliferation and migration of human vascular smooth muscle cells[147].

Another class of uPAR transducers are the GPCRs. Indeed, uPA ligation to uPAR has been shown to induce a chemotactic response in different cell lines, independently of its catalytic activity[148] and in a pertussis toxin sensitive manner[149]. The signal transducers are members of the formyl-Met-Leu-Phe peptide (fMLP) receptor family, which comprises three GPCRs: the high affinity fMLP receptor (FPR) and two homologous proteins (FPRL-1 and FPRL-2). It has been reported that uPA induced migration requires FPRL-1 in peripheral monocytes[150] and involves both FPRL-1 and -2 in basophils[151]. fMLP itself is a potent leukocytes chemoattractant. Remarkably, fMLP induced directional migration requires uPAR[152]. In particular, a crucial chemotactic sequence in the D1-D2 linker region (^{88}SRSRY^{92}) has been identified, as truncated uPAR missing this sequence fails to sustain fMLP migration[149, 152]. Mechanistically, it has been proposed that the conformational changes occurring in the receptor upon ATF ligation[107, 127] might unmask the chemotactic sequence in the D1-D2 linker region, thus leading to the functional interaction with fMLP receptors.

4.4 uPAR SIGNALLING AND ADHESIVE FUNCTIONS ARE INTIMATELY CONNECTED

The tight connection between uPAR-induced signalling and uPAR-mediated adhesion to VN, has been well-documented by a study employing a complete alanine scan of uPAR[125]. uPAR overexpression in two cell lines results in increased VN adhesion accompanied by changes in cell morphology (e.g. reduction of cell-cell contact and lamellipodia formation) and induction of intracellular signalling (i.e. ERK activation) and cell migration. Remarkably, alanine substitution of the residues belonging to the VN binding epitope of

uPAR, but not of the residues thought to interact with integrins, strongly affects the ability of uPAR to induce these cellular changes. Moreover, the expression of an artificial GPI-receptor, with no sequence homology with uPAR but sharing the same binding site on VN, triggers morphological and cellular changes identical to the WT receptor. This study therefore demonstrates that uPAR-VN binding is required and sufficient to induce downstream signalling of uPAR[125].

Independent observations corroborate this finding. First of all, it has been reported that the interaction between uPAR and VN is also necessary and sufficient to induce cytoskeleton rearrangements and cell migration in murine fibroblasts, through the p130Cas/Rac signalling pathway[153]. Moreover, uPAR/EGFR-induced ERK activation in ER+ breast cancer cell lines relies on the expression of VN-binding competent uPAR, as the expression of a VN-binding deficient mutant ($uPAR^{W32A}$) fails to activate ERK[146]. In addition, uPAR-β_3 mediated cell migration has been shown to be VN-dependent both in cancer cell lines[142] as well as in kidney podocytes[141]. In the former study, migration and invasion of the breast cancer cell line MDA-MB-231 and of the colon carcinoma cell line B3 are strongly impaired in the absence of VN and inhibited by an anti-VN antibody. In the latter study, $VN^{-/-}$ mice are protected toward LPS-induced and uPAR/Rac-driven proteinuria.

Taken together, these studies strongly support the concept that uPAR adhesive and signalling functions are deeply linked. Two possible, and not mutually exclusive, scenarios can be envisioned. On the one hand, uPAR-mediated adhesion to VN could generate discrete areas of strong cell adhesion within the cells, thus placing surface receptors, such as integrins, in close proximity with their ligands in the ECM. This would therefore trigger integrin outside-in signalling. On the other hand, uPAR adhesion to VN could cause physical distortion of the focal adhesion components thus modulating their arrangement and activity. In this model, the uPAR signal would be transduced mechanically. Supporting this view, a recent study from our lab has characterized a novel ligand-independent

integrin signalling pathway, in which integrins, in an active conformation, transduce the signal even if they are not directly ligated to the ECM. In this process, adhesion is mediated by another receptor (i.e. uPAR binding to VN) and the physical contact between adhesion and signalling receptors is not direct but is provided by the plasma membrane[137].

4.5 CROSS-TALK BETWEEN THE PROTEOLYTIC AND NON-PROTEOLYTIC FUNCTIONS OF uPAR

The linker region between D1 and D2 of uPAR is highly susceptible to proteolytic cleavage by several proteases including chymotrypsin[154] and cathepsin G (^{87}Y↓S and ^{92}Y↓L)[155], various MMPs such as MMP-12 (^{86}T↓Y)[156], neutrophil elastase (^{85}V↓T)[155], human tissue kallikrein 4[157], Pli and uPA itself (^{83}R↓A and ^{89}Y↓S)[158].

uPA-mediated cleavage of purified suPAR is a slow kinetic reaction and occurs regardless of the binding of uPA to uPAR[158], suggesting that the activity of uPAR-bound uPA is not primarily directed to the binding uPAR molecule. By contrast, cleavage of cell surface uPAR is strongly accelerated and required the interaction between the two proteins[159]. Notably, it has been shown that uPAR on the cell surface can form dimers that preferentially localize in specific membrane domains called lipid rafts[129]. uPAR cleavage, catalyzed by uPA in the lipid rafts, was found to be highly accelerated, likely due to the high local concentration of uPAR[129]. In addition, it has been reported that the presence of the GPI-anchor changes the exposure of the linker region, being therefore necessary for efficient cleavage[160].

In addition to proteolytic cleavage at the D1-D2 linker region, uPAR can undergo a process that is called “shedding”, in which the entire protein is released from the cell surface. uPAR shedding can be mediated by the GPI-specific phospholipase C and D[61, 161] as well as by proteases that cleave close to the C-terminus of the protein, such as Pli (^{281}R↓S)[162] and cathepsin G (^{280}Y↓R and ^{281}R↓S)[155].

Cleavage and shedding of uPAR are irreversible processes that can occur singularly or in combination leading to the generation of different forms of suPAR, which indeed can be found *in vivo*[163].

Chymotrypsin cleaved suPAR, but not intact suPAR, displays chemotactic properties in different cell lines[148, 149]. Active suPAR fragments contain the chemotactic sequence ^{88}SRSRY^{92} either at their N- or C-terminus[149]. Consistently, synthetic peptides harbouring this sequence (i.e. uPAR(84-95) and (88-95)) are endowed with chemotactic properties, which resemble those of uPA[149]. Their effects are, in fact, pertussis toxin sensitive and they have been reported to induce monocytes and basophils migration, through the interaction with FPRL-1 and FPRL-1 and -2, respectively[150, 151]. In addition, uPAR(84-95) has been shown to induce hematopoietic stem cell migration *in vitro*[164], via interaction with FPR, and to trigger hematopoietic stem cell mobilization *in vivo*[165].

On the other hand, several independent studies describe the scavenger effect of intact suPAR. Indeed, it has been shown that suPAR, by binding uPA, can reduce proliferation and invasion of different cancer cell lines both *in vitro* and *in vivo* (reviewed in [166]). An additional mechanism of action for suPAR has been proposed, in which the soluble molecule functions by binding uPA/uPAR protein adaptors[167]. The outcome depends on the uPA and uPAR expression of the cells. In uPAR-negative cells, such as HEK293, suPAR is a weak signal agonist able to induce ERK activation. By contrast, in cells expressing uPA and uPAR, such as MDA-MB-231, it behaves as a negative regulator of ERK activation, cell proliferation and invasion, presumably displacing uPA/uPAR from adaptor proteins. Notably, cleavage of suPAR by chymotrypsin increases its signalling promoting activity and reverts its inhibitory functions[167].

On the cell surface, uPAR shedding reduces the number of receptor molecules, while cleavage results in the generation of a truncated D2D3 surface receptor. Truncated uPAR can not interact with uPA[108, 158], therefore it can no longer promote pericellular proteolysis. Similarly, VN binding and the interaction with integrins are also abolished upon receptor

cleavage[152, 168-170]. On the other hand, uPAR cleavage has been shown to be necessary for fibroblast differentiation in myofibroblasts[171] and for ERK activation in uPA mediated cell migration[172].

Taken together, these data suggest the possibility that the activity of uPAR is subjected to a feedback regulation by extracellular proteolysis. On the one hand, uPA activation can result in receptor cleavage and therefore negatively regulates uPAR binding to uPA, uPAR-mediated VN adhesion and consequently uPAR-integrin intracellular signalling, thus representing a potential negative feedback regulation of the uPAR activities. On the other hand, receptor cleavage and shedding have been shown to generate fragments as well as to unmask epitopes endowed with chemotactic and signal agonist properties, therefore representing a possible positive loop. Indeed, uPA activation and subsequent uPAR cleavage have been proposed as the molecular switch regulating the different activities of uPAR. Similarly, Pli, generated in the uPAR-dependent proteolytic cascade, may have a dual role: behaving as a negative regulator, cleaving uPAR and VN, or being a positive regulator, activating and releasing growth factors from the ECM. In this scenario, the capability of uPAR to accelerate and localize the activation of Plg and sc-uPA is not only a way to enhance pericellular proteolysis but is also a key factor in the regulation of the multiple uPAR functions.

4.6 OBJECTIVES OF THIS STUDY

The different uPAR functions have been extensively studied and are well characterized. However, some aspects of the cross-talk between proteolytic and non-proteolytic functions are still not fully understood.

In particular, little is know about how plasminogen activation affects uPAR-VN interaction and therefore uPAR-mediated cell adhesion to VN. More broadly, the impact of the uPAR proteolytic function on the ligand binding capability of VN is still poorly documented. It

has been shown for long time that both uPA and Pli may cleave uPAR and in addition Pli can cleave VN at multiple locations. It has been suggested that this may represents a negative feedback regulation, but the existence and the mechanism of such loop have not been characterized experimentally.

On the other way around, it is still unclear what is the role of the uPAR-VN interaction in the plasminogen activation system. The binding of uPA to uPAR enhances the receptor affinity for VN, thus potentially localizing active proteases at specific sites of action. However, VN also binds and stabilizes active PAI-1 and remarkably uPAR and PAI-1 binding to the SMB domain of VN are mutually exclusive. How all these binding interactions are connected and how they do operate both in physiological and pathological conditions are still partially understood aspects.

In this context, the aim of the present work is to specifically study the cross-talk between uPAR-induced extracellular proteolysis and uPAR-mediated cell adhesion to VN, focusing on the role of the uPAR-VN interaction.

5. MATERIALS AND METHODS

5.1 MATERIAL

HEK293 Flp-In T-REx cells, pcDNA5/FRT/TO vector and pOG44 vector were purchased from Invitrogen. Human VN urea-purified was obtained from Promega and human FN from Trimital. Fugene 6 was obtained from Roche. Human Glu Plg, human Pli and human α2AP were purchased from Molecular Innovations. Aprotinin and anti-vinculin antibody (hVIN-1) were purchased by SIGMA. Anti-phosphorylated p130Cas antibody (cat no. 4011) was from Cell Signalling Technology. Anti-uPAR monoclonal antibodies R2 and R3 are a kind gift of Dr. Gunilla Hoyer-Hansen (Finsen Laboratory, Denmark). GFD was kindly provided by Dr. Steve Rosenberg. sc-uPA was kindly provided by Dr. Jack Henkin (Abbott Laboratories, Abbott Park, IL). To obtain active tc-uPA, sc-uPA was incubated with Pli (100:1, w:w ratio) for 30 minutes at 37°C and Pli was subsequently inhibited with an excess of α2AP. PAI^{WT}, PAI^{R346A}, $PAI\text{-}1^{R103A/M112A/Q125A}$, uPA·PAI-1 complex and $sc\text{-}uPA^{S356A}$ were kindly provided by Dr. Peter A. Andreasen (University of Aarhus). $sc\text{-}uPA^{S356A}$ was activated as described above for sc-uPA WT. Monomeric suPAR was kindly provided by Dr. Michael Ploug (Finsen Laboratory, Denmark). The monoclonal antibody (mAb) 8B12 is a competitive antagonist of the uPAR-VN interaction. Briefly, it has been generated using an engineered uPAR variant as antigen and its epitope includes the Arg91 of uPAR (unpublished data).

5.2 CELL CULTURE AND TRANSFECTIONS

NCI-60 panel cell lines were grown in RPMI 1640 supplemented with 10% FBS, 100 U/mL penicillin, 100 U/mL streptomycin and 5 mM L-glutamine. HeLa cells were grown in MEM supplemented with 10% FBS, 100 U/mL penicillin, 100 U/mL streptomycin, 1

mM sodium pyruvate and 0.1 mM non-essential amino acids. Human embryonic kidney (HEK293) Flp-In T-Rex cells were cultured in DMEM supplemented with 10% FBS, 100 U/mL penicillin, 100 U/mL streptomycin, 5 mM L-glutamine, 15 μg/mL blasticidin and 100 μg/mL zeocin. Chinese hamster ovary (CHO) Flp-In cells were grown in Ham's F12 medium supplemented with 10% FBS, 100 U/mL penicillin, 100 U/mL streptomycin, 5 mM L-glutamine and 100 μg/mL zeocin. All cell lines were cultured at 37°C in 5% CO_2.

The Flp-In system is an easy tool for the generation of isogenic stable cell lines without the need of clones selection. In addition, the Flp-In T-REx system allows for a tetracycline-induced expression of the construct of interest. Cells were co-transfected with Flp-In expression vectors (pcDNA5/FRT/TO vectors) and the Flp-recombinase vector (pOG44) with a 1:10 (weight/weight, w:w) ratio, using Fugene. Selection of stable transfectants was performed by substituting zeocin with hygromycin B in the culture medium, at the final concentration of 150 μg/mL for HEK293 cells and 500 μg/mL for CHO cells. The co-transfection leads to the integration of a single copy of the expression vector to the same genomic position in every cell and therefore ensures comparable gene expression and avoids potential artefacts due to vector random insertion. Expression in HEK293 Flp-In T-REx was induced by adding tetracycline at the final concentration of 1 μg/mL to the culture medium overnight (O/N).

5.3 EXPRESSION VECTOR CONSTRUCTION

pcDNA5/FRT/TO-uPAR^{WT}, pcDNA5/FRT/TO-uPAR^{R83A}, pcDNA5/FRT/TO-uPAR^{R89A} and pcDNA5/FRT/TO-uPAR^{R91A} have already been described[125]. pcDNA5/FRT/TO-uPAR$^{R83/89A}$ and pcDNA5/FRT/TO-uPAR$^{W32A/R91A}$ were made by site-directed mutagenesis as previously described[125].

Generation of pcDNA5/FRT/TO-VN-His and pcDNA5/FRT/TO-VN^{G46A}-His has already been described[137]. pcDNA5/FRT/TO-VN^{R45A}-His was generated in a two-step overlapping

PCR procedure. Firstly, pcDNA5/FRT/TO-VN-His was amplified with oligos hVnu/R45AR and R45AF/HISNOTR. Secondly, the two PCR products were mixed, co-amplified using oligos hVnu /HISNOTR and cloned BamHI/NotI in pcDNA5/FRT-TO.

The expression vectors for recombinant proteins tagged with a human immunoglobulin G (IgG) constant region (Fc) are based on the pcDNA5/FRT/TO-hFc plasmid[125], however, a number of modifications was introduced to facilitate the shuffling of different coding regions as well as to improve protein yields. Firstly, an XhoI restriction site, located in the vector sequence downstream of the Fc coding region, was destroyed by site-directed mutagenesis using oligos dXu/dXd. Secondly, a linker encoding a cleavage sequence for the PreScission protease, made by annealing oligos PreF/PreR, was inserted in the XhoI site located at the signal peptide/Fc junction. Since the removal of the intron present in the Fc region of the construct was found to increase the yield of recombinant protein (our unpublished observations), the vector was transfected into CHO cells, RNA extracted, reverse transcribed. The cDNA was then amplified with oligos hVNukpn/FcNr and cloned KpnI/NotI into pcDNA5/FRT-TO (Invitrogen corp.) to generate pcDNA5/FRT/TO-Fc. pcDNA5/FRT/TO-VN(1-64)-Fc, pcDNA5/FRT/TO-VN(1-64)^{R45A}-Fc, pcDNA5/FRT/TO-VN(1-64)^{G46A}-Fc were generated amplifying pcDNA5/FRT/TO-VN-His, pcDNA5/FRT/TO-VN^{R45A}-His and pcDNA5/FRT/TO-VN^{G46A}-His, respectively, with oligos hVNuKpn/VN64DX and cloning the product KpnI/XhoI in pcDNA5/FRT/TO-Fc. To introduce the K78Q mutation in the tag, pcDNA5/FRT/TO-VN(1-64)-Fc was amplified using oligos FcSuKQ/FcNr and the PCR product was digested XhoI/NotI and cloned in pcDNA5/FRT/TO-VN(1-64)-Fc, pcDNA5/FRT/TO-VN(1-64)^{R45A}-Fc to generate pcDNA5/FRT/TO-VN(1-64)-Fc^{K78Q} and pcDNA5/FRT/TO-VN(1-64)^{R45A}-Fc^{K78Q}, respectively. pcDNA5/FRT/TO-VN(1-66)-Fc has already been described[125], vectors carrying single-point mutations were generated by site-directed mutagenesis.

To generate pcDNA5/FRT/TO-VN(1-45) and pcDNA5/FRT/TO-VN(1-66), pcDNA5/FRT/TO-VN(1-66)-Fc was amplified with oligos hVNuKpn/VN45RN and

hVNuKpn/VN66RN respectively, digested KpnI/NotI and cloned in pcDNA5/FRT/TO-VN(1-64)-Fc.

To obtain pcDNA5/FRT/TO-$VN^{(1-61)}$-EK-hFc, pcDNA5/FRT/TO-$VN^{(1-64)}$-hFc was amplified with oligos hVNuKpn and VN61EKR, digested KpnI/XhoI and cloned in pcDNA5/FRT/TO-hFc.

Construct encoding human suPAR tagged with an Fc, pcDNA5/FRT/TO-uPAR-Fc, was made by amplification of a full-length uPAR cDNA with oligos URskF/UpreR2D and cloning KpnI/XhoI in pcDNA5/FRT/TO-Fc. To obtain mutant uPAR-Fc constructs, pcDNA5/FRT/TO-$uPAR^{R83/89A}$ and pcDNA5/FRT/TO-$uPAR^{W32A/R91A}$ were amplified with oligos urskf/upre2d and cloned KpnI/XhoI in pcDNA5/FRT/TO-Fc to generate pcDNA5/FRT/TO-$uPAR^{R83/89A}$-Fc and pcDNA5/FRT/TO-$uPAR^{W32A/R91A}$-Fc, respectively.

5.4 OLIGONUCLEOTIDE SEQUENCES

hVnu: 5’-GCGGATCCAGCCCTGCCATGGCACCCCTGAG-3’

hVNd: 5’-CGGGGTACCATGGCACCCCTGAGA-3’

XbNhisF: 5’-CTAGAGGGCATCATCACCATCACCATTGAGC-3’

XbNhisR: 5’-GGCCGCTCAATGGTGATGGTGATGATGCCCT-3’

R45AF: 5’-AAGCCCCAAGTGACTGCCGGGGATGTGTTCACT-3’

R45AR: 5’-AGTGAACACATCCCCGGCAGTCACTTGGGGCTT-3’

HISNOTR: 5’-CAGCGGCCGCTCAATGGTGATGGTGATGATG-3’

dXu: 5’-GTAAATGAGCGGCCGCGTCGAGTCTAGAGGG-3’

dXd: 5’-CCCTCTAGACTCGACGCGGCCGCTCATTTA-3’

PreF: 5’-TCGAGCTGGAAGTTCTGTTCCAGGGGCCCA-3’

PreR: 5’-AGCTACCCGGGGACCTTGTCTTGAAGGTCG-3’

hVNukpn: 5’-CGGGGTACCATGGCACCCCTGAGA-3’

FcNr: 5’-TTGCGGCCGCTCATTTACCCGGAGACAG-3’

VN64DX: 5’-GGCTCGAGCTCCTCGCCATCGTCATA-3’

FcSuKQ: 5’- GGCTCGAGGGCAGTGGACCCCAATCTTGTGACAAAACT-3’

VN45RN: 5’-CCGCGGCCGCTTAGCGAGTCACTTGGGGCTT-3’

VN66RN: 5’- CCGCGGCCGCTTAGTTTTTCTCCTCGCCATC-3’

Urskf: 5’-GCGTCGACGGTACCCGCCACCATGGGTCACCCGCCGCTGCTG-3’

upre2d: 5’GCCTCGAGGGGCCCCTGGAACAGAACTTCCAGATCCAGGTCTGG GTGGTTACAGCCACT-3’

VN61EKR: 5’-GCCCTCGAGGCCTTTATCGTCATCGTCATAGACCGTGTACTC ATC-3’

5.5 EXPRESSION AND PURIFICATION OF RECOMBINANT PROTEINS

The expression vectors described above were transfected into CHO Flip-In cells (Invitrogen Corp.) and the recombinant proteins expressed under serum-free conditions as previously described[125, 173]. Recombinant proteins tagged with Fc were purified from the conditioned media by standard Protein A affinity chromatography and dialyzed extensively against phosphate buffered saline (PBS). His-tagged proteins were purified by immobilized metal-affinity chromatography and dialyzed extensively against PBS.

5.6 TIME-LAPSE IMAGING

Time-lapse live cell imaging was performed at 37°C, 5% CO_2 with an inverted microscope (IX80, Olympus) equipped with an incubation chamber (OKOlab). 12-well-plates were coated with recombinant VN (5 μg/mL) O/N at 4°C and then blocked with 5% heat inactivated bovine serum albumin (BSA) in PBS for 1 h at 37°C. 293/uPAR cells (250.000 cells/well) were plated in Opti-MEM® supplemented with 100 U/mL penicillin, 100 U/mL streptomycin and 1 μg/ml tetracycline. 2 h after seeding, sc-uPA was added to a final

concentration of 10 nM and about 1 h later Plg was added to 30 nM. Cells were imaged at regular intervals (2 minutes) using a 20x objective.

For cell migration experiments, 293/uPAR cells were plated and allowed to adhere as described above. After about 2 h of adhesion, cells were treated with 10 nM sc-uPA, PAI-1, uPA·PAI-1 or vehicle and imaged at regular intervals (5 minutes) using a 10x objective. Cell migration was quantified by manual tracking using ImageJ software and the "manual tracking" plugin. To obtain a time-resolved quantification of cell velocity, for every time-point, we calculated the average migration speed over the 30 minutes preceding the time point and followed 50 or more individual cells per condition. Adjustment of brightness/contrast was done with ImageJ and applied to the entire image.

5.7 DIFFERENTIAL INTERFERENCE CONTRAST (DIC) MICROSCOPY

Adherent cells were fixed with 4% paraformaldehyde (PFA) in PBS for 10 minutes at room temperature (RT). Fixed cells were washed with PBS and DIC imaging of cells was performed using an inverted microscope Olympus IX81. Cells were viewed through a high-aperture 60x objective lens (UIS2 60x TIRFM PlanApo N, NA 1.45; Olympus). Images were acquired using Hamamatsu Orca-ER digital camera with the software Metamorph 7.5.6.0. Cell-matrix contact area was quantified using ImageJ. Adjustment of brightness/contrast was done with ImageJ and applied to the entire image.

5.8 CELL LYSIS AND WESTERN BLOTTING

Cells were lysed directly on the culture dish in hot Laemli buffer. Equal volumes were separated by Sodium Dodecyl Sulphate - PolyAcrylamide Gel Electrophoresis (SDS-PAGE) and probed as indicated.

5.9 LABEL-FREE REAL-TIME CELL-BASED ASSAY (RTCA) EXPERIMENTS

The RTCA technology is a label-free system that allows for real-time monitoring of cellular events. The instrument measures electrical impedance through microelectrodes located at the bottom of each well. Cells attached on the electrode alter the local ionic environment at the electrode/medium interface and therefore cause an increase of electrode impedance. The electrical impedance measured for the cell population in the well is the sum of mainly two contributions: on the one hand it reflects the number of cells that are attached to the electrode (i.e. the more they are, the higher is the impedance), on the other hand it depends also on the quality and quantity of cell-electrode interactions (e.g. the more cells spread, the larger is the increase in impedance). Accordingly, electrical impedance can be employed to follow many cellular processes such as cell proliferation, adhesion and spreading. The read-out of the machine is a dimensionless parameter called cell index that is defined as the relative change in measured impedance at a given time-point respect to the background measurement.

RTCA experiments were conducted as described below. 96-well E-plates (Roche Corp.) were coated with FN (10 μg/mL), recombinant VN or VN variants (5 μg/mL) O/N at 4°C. Non-specific binding sites on the electrode surface were saturated with 5% BSA in PBS for ≥ 1 h at 37°C. Cells (15000 cells/well) were plated in serum-free Opti-MEM® medium supplemented with 100 U/mL penicillin, 100 U/mL streptomycin and 1 μg/mL tetracycline. To reduce the so-called edge well effect, the plate was left outside the incubator for 15 minutes after cell seeding to allow the cells to attach. Subsequently, the plate was transferred to the real time cell analyzer instrument (RTCA, xCELLigence SP, Roche Corp.) located in a humidified cell culture incubator (37˚C and 5% CO_2) and the impedance was measured at regular intervals. Cells were subjected to one or more treatments and the times at which treatments were performed are depicted in the graphs by vertical lines. Reagent concentrations were the following: 10 nM sc-uPA, tc-uPA, GFD,

PAI-1 and uPA·PAI-1, 30 nM Plg and Pli, 100 nM α2AP. To calculate the normalized cell index, all the measured cell indexes were divided over the cell index recorded in the same well at the time of the first treatment. This normalization reduces variability caused by the number of cells seeded in the individual wells, making the normalized cell index more comparable between the wells.

5.10 VN FRAGMENTS RELEASE EXPERIMENTS

For 293/uPAR cells release experiments, 12-well plates were coated with VN (5 μg/mL) O/N at 4°C and residual binding sites saturated with blocking buffer (5% heat-inactivated BSA in PBS) for 1 h at 37°C. 293/uPAR cells (500.000/well) were seeded in Opti-mem® and allowed to adhere for about 2 h before further treatments. The final concentrations of reagents used in the release experiments were: 10 nM sc-uPA and tc-uPA, 30 nM Plg and Pli, 100 nM α2AP and 300 nM aprotinin. The antagonists GFD (300 nM) and the mAb 8B12 (30 μg/mL) were added to the cells 30 minutes prior to the addition of proteases. The conditioned media were harvested 2 h after treatment, filtered and added phenylmethanesulfonylfluoride (PMSF) to 1 mM.

For release experiments conducted using the NCI-60 cell lines, 48-well plates were coated with VN as described above. 50.000 cells/well were seeded in Opti-mem® in the presence or absence of 30 nM Plg and 100 nM α2AP. Supernatants were collected after 16 h and treated as described above.

5.11 MATRIX-ASSISTED LASER DESORPTION/IONIZATION TIME OF FLIGHT (MALDI-TOF) MASS SPECTROMETRY (MS)

MALDI-TOF MS is a soft ionization technique that allows for the determination of intact proteins or peptides molecular weight. The read-out of the machine is a mass over charge

ratio (m/z). Since ions analyzed are usually monocharged, it coincides with the molecular weight (MW) of the peptides. In particular, when experiments are carried out in linear mode, as in the experiments described below, the obtained mass values correspond to the average molecular mass.

For *in vitro* fragments generation, VN (Promega) or recombinant VN variants were subjected to proteolytic digestion with Pli or tc-uPA for 2 h at 37°C. Where indicated a 3-fold excess of uPAR-Fc was added to the reaction mixture. The reaction was carried out in PBS with a 10:1 (weight/weight, w/w) ratio of VN to protease. Two picomoles of digested VN were deposited onto a MALDI plate and allowed to air-dry. Matrix (5 mg/mL α-cyano-hydroxy-cinnamic acid in 50% acetonitrile /0.1% trifluoroacetic acid) was spotted directly on top.

Regarding the analysis of human urine samples, a pull-down assay using HF6-conjugated beads was performed. Urine samples were supplemented with Tris-HCl pH 7.5 at a final concentration of 50 mM and PMSF at a final concentration of 1 mM and VN fragments were immunoprecipitated using HF6-conjugated beads. Eluted material was desalted using C8 zip-tip before spotting it on the MALDI plate.

Mass spectra were acquired in linear mode on a 4800 MALDI-TOF/TOF mass spectrometer (Applied Biosystems, Foster City, CA) equipped with a 336 nm nitrogen laser. Ions were accelerated with a 20 kV pulse. Spectra were generated in the mass range 2–20 kDa by averaging 40 sub-spectra for each of 25 randomized positions within the spot (1000 spectra/spot). Laser intensity was set at 4000 V to optimize the signal-to-noise (S/N) ratio and the resolution of mass peaks of the analyte.

5.12 ANTIBODIES GENERATION

Five 2-month-old male C57Bl/6 $VN^{-/-}$ mice were immunized by intraperitoneal (IP) injection with 100 μg VN(1-66)/hFc in 200 μL immunogen in PBS and 100 μL of

Complete Freund's Adjuvant (CFA). The immunized animals were boosted 3 times, at 3-week intervals, by IP injection of 100 μL VN(1-66)/hFc in 200 μL of 1:1 emulsion between 100 μL immunogen in PBS and 100 μL of Incomplete Freund's Adjuvant (IFA). After a 7-week rest period and 4 days before the fusion, the two best mice, chosen depending on sera titration (see Screening of sera/supernatants), were subjected to a final pre-fusion IP boost using 200 μg VN(1-66)/hFc in 200 μL PBS.

Spleens were removed and the splenocytes fused to the mouse SP2/0 myeloma cell line by the polyethylene glycol method using standard procedure[174]. After fusion, the cells were cultured for one day in non-selective medium (Iscove, 10% FBS, 1xHFCS) and then plated in 96 well-plates (35000 splenocytes/well) in selective HAT medium (Iscove, 1xHAT) supplemented with 1xHFCS (Hybridoma Fusion and Cloning Supplement, Roche Corp.). Hybridomas positive for the production of immunoglobulin specific for the antigen were identified by Time-Resolved Fluorescence Immunoassay (TR-FIA, see Screening of sera/supernatants), expanded in 12-well plates and frozen. Selected hybridomas were sub-cloned by limiting dilution in 96-well plates. Cells were plated in HT medium (Iscove, 1xHT) supplemented with 1xHFCS at a density ranging from 0.4 to 0.1 cells/well. When necessary, the sub-cloning procedure was repeated until all sub-clones scored positive by TRF-assay. The isotypes of the immunoglobulin produced by the different hybridomas were determined using a commercially available ELISA kit (Mouse Immunoglobulin Isotyping ELISA Kit, BD Pharmingen Corp.). In this way, three IgG1 monoclonal antibodies (namely HU3, HF6 and IO35) with non-overlapping epitopes were obtained.

5.13 TIME-RESOLVED FLUORESCENCE BASED ASSAYS

Immunoassays and binding assays were performed using Eu^{3+}-labeled reagents as detection system. This technology has many advantages compared to the conventional fluorescence. Firstly, Eu-complexes display higher sensitivity and can be used to measure

Eu^{3+} down to the sub-picomolar range (10^{-13} moles/L). Secondly, the use of Eu leads to very low background signal, due to a long decay time of the emitted fluorescence. This allows for a delayed measurement after the excitation and therefore for the exclusion of the background short-lived autofluorescence signals coming from solvents and reagents. In addition, Eu^{3+} ion is endowed with an extremely large Stokes shift (very different excitation and emission wavelengths) and a very narrow emission band, which contribute to increase the S/N ratio. In particular, we took advantage of the DELFIA® (dissociation-enhanced lanthanide fluorescence immunoassay) technology. In this system, the Eu^{3+} ion is dissociated from the labeled antibody bound to the solid phase by addition of a low pH chelating detergent solution (called DELFIA enhancement solution) to form a new highly fluorescent complex in a micellar solution, which ultimately leads to a further increase in sensitivity.

5.13.1 Screening of sera/supernatants

Black 96-well plates (MAXI-SORP, NUNC Corp.) were coated with SMB-GFP, 1 μg/mL in coating buffer (50 mM sodium carbonate, pH 9.6). After washing with PBS containing 0.1% Tween-20 (PBS-T, wash buffer), wells were blocked with 2% BSA in PBS, washed and incubated with sera/cell culture supernatants, properly diluted in 1% BSA in PBS. Bound mouse immunoglobulins were detected using a Eu^{3+}-labeled anti-mouse Fc antibody (1:5000, Perkin Elmer Corp.). Before reading the plates, wells were extensively washed and incubated with DELFIA enhancement solution (Perkin Elmer Corp.). The Eu^{3+}-label was detected by measuring time-resolved fluorescence intensity using an Envision Xcite plate reader (Perkin Elmer Corp.) employing the DELFIA label protocol.

5.13.2 Antibody epitope mapping experiments

Black 96-well immunoplates were coated with the monoclonal antibodies of interest (0.5 µg/mL) diluted in coating buffer O/N at 4°C. After washing with PBS-T, plates were blocked with The Blocking Solution (CANDOR Bioscience GmbH) for ≥ 2 h at RT shaking. Wells were incubated with the antigen VN(1-66)/Fc WT or carrying point mutations. Antigen binding was detected by incubation for 1 h at RT with Eu^{3+}-labeled anti-human Fc antibody (1:1000, Perkin Elmer Corp.). The Eu^{3+}-label was detected as described above.

5.13.3 Immunoassays for the detection of N-terminal SMB-containing VN fragments

We developed two immunoassays (namely HU3/HF6 and HU3/IO35) for the detection of N-terminal VN fragments. They have slightly different specificity: HU3/IO35 assay detects only fragments longer than 1-65; on the contrary, HU3/HF6 can detect also shorter fragments (e.g. 1-45).

Black 96-well immunoplates were coated with the monoclonal antibody HU3 (0.5 µg/mL) diluted in coating buffer at 4°C O/N. Plates were washed with PBS-T and blocked with The Blocking Solution for ≥ 2 h at RT shaking. After washing with PBS-T, wells were incubated with samples (loaded in duplicate) properly diluted in PBS-T. The binding was allowed to occur 1-2 h at RT shaking. Bound VN fragments were detected by sequential incubations with biotinylated HF6 or IO35 monoclonal antibody (0.5 µg/ml) and Eu^{3+}-labelled Streptavidin (1:10000, Perkin Elmer Corp.) for 1 h at RT shaking. The Eu^{3+}-label was detected as described above.

For HU3/HF6 assay, VN(1-61) was used as standard and a 7-point standard curve was made starting from 0.12 nM with a 2-fold dilution. When comparing HU3/HF6 and HU3/IO35 assays, the standard curve was done using conditioned medium of CHO cells

expressing VN(1-66). Background binding was measured in wells incubated with PBS-T and was subtracted from the total binding. The standard curve was fitted to the experimental data and the unknown concentrations were interpolated by non-linear regression using the log[agonist] vs. response – variable slope (four parameter) algorithm and the GraphPad Prism (V6.0b) software.

5.13.4 Binding assays

Binding assays were performed in black 96-well immunoplates coated with recombinant VN (5 μg/mL) in coating buffer at 4˚C O/N. Plates were washed with PBS-T and the remaining binding sites saturated with The Blocking Solution for ≥ 2 h at RT. After washing with PBS-T, wells were incubated with the indicated concentrations of uPAR-Fc or uPAR$^{W32A/R91A}$-Fc diluted in PBS-T in the presence of 10 nM sc-uPA and tc-uPA or with a dilution curve of the different ligands. Where indicated a pre-incubation with 10 nM PAI-1 or PAI-1 mutants was performed at 4°C for 2 h. After 1-2 h at RT, unbound reagents were removed by rinsing with wash buffer. The binding of the different uPAR-Fc variants was detected by incubation with a Eu^{3+}-labeled anti-human Fc antibody (1:1000). When comparing untagged and Fc-tagged uPAR, the extent of uPAR binding to VN was evaluated by subsequent incubation with the anti-uPAR monoclonal antibody R2 (0.5 μg/mL) and Eu^{3+}-labeled anti-mouse Fc antibody (1:5000). The Eu^{3+}-label was detected as described above. Background binding was measured in wells incubated with no receptor and was subtracted from the total binding.

uPAR-Fc binding to sc-uPA was assayed as described for binding to VN, using 1 μg/mL sc-uPA as coating.

5.14 PREPARATION OF CALIBRATOR SAMPLES

Four different "calibrator" urine samples were prepared. The first three (termed "High", "Medium" and "Low") were made by pooling 20 urine samples of colorectal cancer patients falling within the upper quartile (High), lower quartile (Low) or close to median (Medium) of all the measurements, n = 165 (data not shown). A fourth calibrator, "Matrice", is a single urine sample provided by a young healthy volunteer. All four calibrators were aliquoted and stored at -80˚C.

5.15 GENERATION OF THE VN(1-61) STANDARD

To obtain a highly pure standard for VN fragments immunoassays, we generated a chimera protein composed of the first 61 amino acids of human VN fused with the human Fc region with a cleavage site for enterokinase located in the linker region between VN residues and the Fc region (see Expression vectors construction section for the generation of pcDNA5/FRT/TO-VN$^{(1-61)}$-EK-hFc vector and Expression and purification of recombinant proteins section for the purification of Fc-tagged proteins). The purified protein was digested with enterokinase and the VN(1-61) fragment was purified by high-performance liquid chromatography (HPLC). The concentration of purified VN(1-61) fragment (>90% purity as estimated by HPLC and SDS-PAGE, data not shown) was accurately determined by amino acid analysis. This reference protein was used to generate standard curves and for spike in experiments.

5.16 CREATININE ASSAY

For creatinine assay, the Parameter^{TM} kit from R&D Systems was used according to manufacturer's instructions.

6. RESULTS

6.1 NEGATIVE FEEDBACK BETWEEN uPAR PROTEOLYTIC AND NON-PROTEOLYTIC FUNCTIONS

6.1.1 Plasminogen activation exerts a negative feedback on cell adhesion to VN

To investigate existence and mechanisms of feedback loops between the function of uPAR in extracellular proteolysis, cell adhesion and signalling, we used uPAR overexpressing HEK293 (293/uPAR) cells as model system. HEK293 cells express neither uPAR nor uPA[122] and are therefore a suitable model to perform structure-function studies. It has been previously shown that the ectopic expression of uPAR in HEK293 cells leads to extensive changes in cell morphology, increase in cell adhesion to VN and basal random cell migration and activation of migratory and proliferative signalling pathways[125, 137].

To test whether uPAR-initiated proteolysis mediates feedback mechanisms on uPAR-induced cell adhesion and spreading, we conducted time-lapse microscopy on 293/uPAR cells seeded on VN and exposed to consecutive additions of sc-uPA and Plg to trigger the plasminogen activation cascade (Fig. 7 and Movie 1). When seeded on VN, 293/uPAR cells displayed an adherent phenotype characterized by extensive lamellipodia formation that was further enhanced by sc-uPA addition. Treatment with Plg, however, rapidly reversed the pro-adhesive effect of sc-uPA as evidenced by lamellipodia retraction and the acquisition of rounded cell morphology, similarly to what has previously been reported for endothelial cells[175].

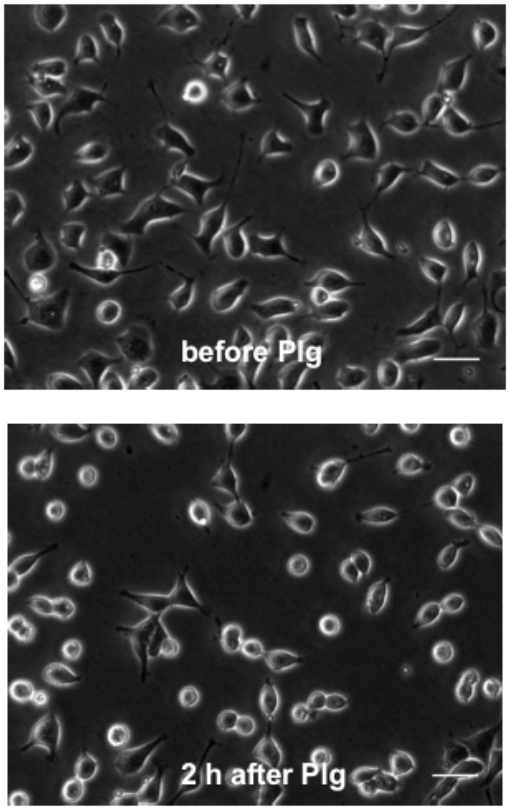

Figure 7: Effect of plasminogen activation on 293/uPAR cells morphology.

293/uPAR cells were seeded on VN and imaged by time-lapse microscopy. Cells were treated with subsequent additions of sc-uPA and Plg and representative phase contrast images, taken just before and 2 hours after addition of Plg, are shown. The complete time-lapse recording can be found as Movie 1. Scale bar, 20 μM.

To quantitatively analyze the negative feedback, we took advantage of a RTCA instrument, which allows for the continuous and non-invasive evaluation of the extent and quality of cell-matrix interactions by impedance measurements[176] (see material and methods for a more detailed description of the technique). The data obtained by RTCA analysis (Fig. 8A) closely paralleled the time-lapse microscopy recordings: after an initial adhesion phase, treatment with sc-uPA caused a marked increase in cell adhesion that was rapidly reverted upon subsequent addition of Plg. The inhibitory effect of plasminogen activation on cell adhesion to VN was mediated by cell surface associated Pli and/or tc-uPA activity as the addition of α2AP, which inhibits free but not membrane bound Pli[18], had limited effect on the proteolytic feedback. When cells were seeded on FN, the triggering of plasminogen activation did not impair cell adhesion, but rather resulted in a delayed and transient increase (Fig. 8B). In contrast to VN, the transient increase in FN adhesion is mediated by the activity of free Pli as it was fully inhibited by α2AP.

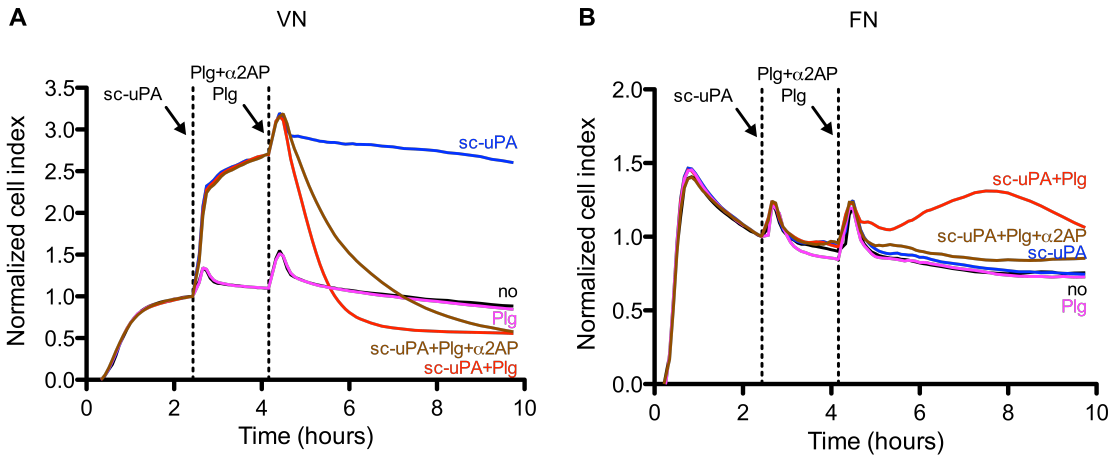

Figure 8: Plasminogen activation exerts a negative feedback on cell adhesion to VN.

RTCA analysis of 293/uPAR cells seeded in VN- (A) or FN-coated (B) wells is shown. Cell adhesion and spreading were followed over time by recording the changes in electrical impedance, named cell index (see Material and methods section for a more detailed description of the system). Stippled vertical lines indicate the time-points at which the cells were treated. Each condition was recorded in quadruplicates and the curves represent the average cell index as a function of time. Cell index values are normalized to the cell index measured before the first treatment. Data are from a representative experiment.

It has been shown that uPAR binding to VN is required and sufficient to induce p130Cas substrate domain phosphorylation through the Src/FAK signalling pathway[125, 137, 142, 153]. To test the effect of plasminogen activation on p130Cas phosphorylation, we treated 293/uPAR cells seeded on VN or FN with Pli (Fig. 9). In line with the RTCA data, treatment with Pli resulted in a clear reduction of p130Cas phosphorylation when cells were seeded on VN while an up-regulation was observed for cells seeded on FN.

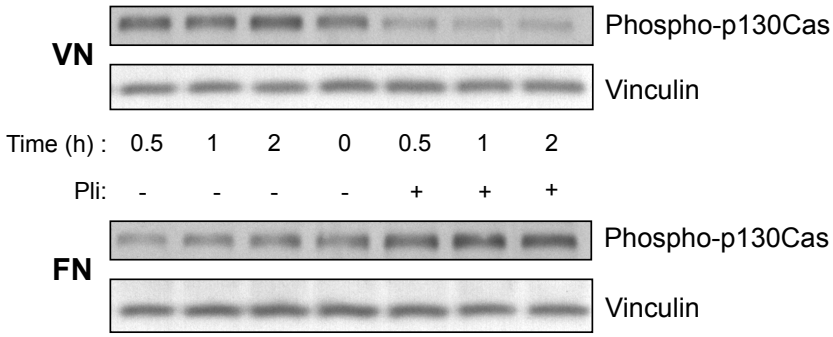

Figure 9: Plasminogen activation down-modulates uPAR-induced cell signalling on VN.

293/uPAR cells were seeded on VN- or FN-coated culture plates and allowed to adhere for about 1 hour before treatment with 30 nM Pli or vehicle. Cells were lysed at the indicated time points after treatment. Lysates were resolved by SDS-PAGE and p130Cas phosphorylation was assayed by immunoblotting. The blot is from a representative experiment.

These results document the existence of both positive and negative feedback loops between plasminogen activation and cell signalling and adhesion to VN and FN.

6.1.2 The catalytic activity of both uPA and Pli contributes to the negative feedback

The process of plasminogen activation is a reciprocal zymogen activation cascade in which the zymogen sc-uPA is converted into active tc-uPA and the zymogen Plg into active Pli, thus resulting in the concomitant generation of two distinct serine protease activities. To determine which of these activities is responsible for the negative feedback, we analyzed the cellular response to the isolated active proteases (Fig. 10). Both sc-uPA and active tc-uPA stimulated VN-adhesion to a similar extent and with similar kinetics, consistent with the fact that both contain the receptor binding GFD domain responsible for inducing uPAR-binding to VN[123, 126]. However, after the initial induction, the adhesion of tc-uPA treated cells started to decline as compared to cells treated with sc-uPA, demonstrating that the catalytic activity of uPA contributes directly to the feedback. The decline was not as steep as that observed with a combination of sc-uPA and Plg indicating that the catalytic

activity of uPA is involved but not sufficient to obtain the full magnitude of the feedback. Consistently, the addition of Plg to tc-uPA-treated cells further accelerated the feedback. To directly evaluate the contribution of Pli, we first treated cells with GFD to mimic the pro-adhesive effect of ligand-occupancy and then challenged the cells with Pli (Fig. 10). The treatment with Pli caused a rapid decrease in cell adhesion indicating that the proteolytic activity of Pli also contributes directly to the negative feedback.

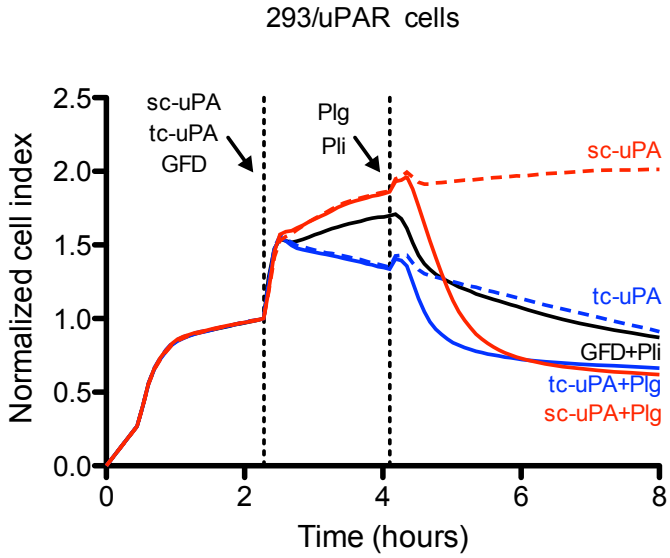

Figure 10: The catalytic activity of both uPA and Pli contributes to the negative feedback between plasminogen activation and cell adhesion.

RTCA experiments were conducted with 293/uPAR cells seeded in VN coated wells and treated as reported in the figure. A representative experiment is shown.

6.1.3 The negative feedback is partially caused by uPAR cleavage

It has been recognized for a long time that the linker region connecting D1 and D2D3 of uPAR is highly susceptible to proteolysis by various proteases including uPA and Pli[158, 159]. Since the binding site for VN in uPAR involves determinants in both D1 and D2D3[125, 126], cleavage of the linker region could possibly account for the negative feedback. To address this possibility, we generated HEK293 cells expressing a uPAR-variant where the reported uPA and Pli cleavage sites (^{83}R↓A and ^{89}R↓S)[159] have been disrupted by alanine

substitution of the arginine residues. The resulting receptor (uPAR$^{R83/89A}$) displayed largely intact VN binding that was stimulated by ligand-occupancy similarly to the wild-type receptor (Fig. 11). To gauge the role of uPAR cleavage, we therefore compared the effect of plasminogen activation on cell adhesion to VN mediated by uPAR^{WT} (Fig. 10) and uPAR$^{R83/89A}$ (Fig. 11). The onset of the negative feedback mediated by tc-uPA was markedly delayed indicating that uPAR-cleavage indeed contributes to the feedback. However, the mutational impairment of receptor cleavage did not fully phenocopy the effect of treatment with catalytically inactive sc-uPA. Furthermore, the treatment of 293/uPAR$^{R83/89A}$ cells with GFD followed by Pli resulted in a pronounced reduction in VN adhesion similar to that observed for 293/uPAR^{WT} cells (Fig. 10).

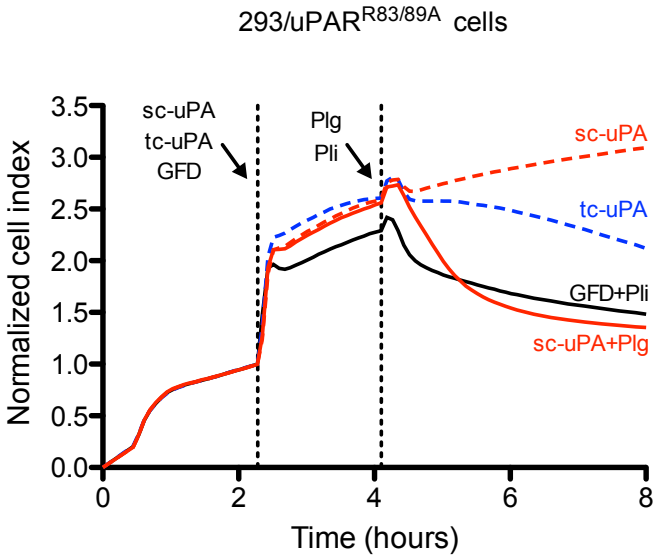

Figure 11: The cleavage of uPAR contributes partially to the negative feedback.

293/uPAR$^{R83/89A}$ cells were seeded on VN and treated as in Fig. 10. A representative experiment is shown.

Western blotting analysis confirmed that sc-uPA plus Plg, tc-uPA or Pli effectively cleave a significant fraction of uPAR^{WT}, but not uPAR$^{R83/89A}$ (Fig. 12).

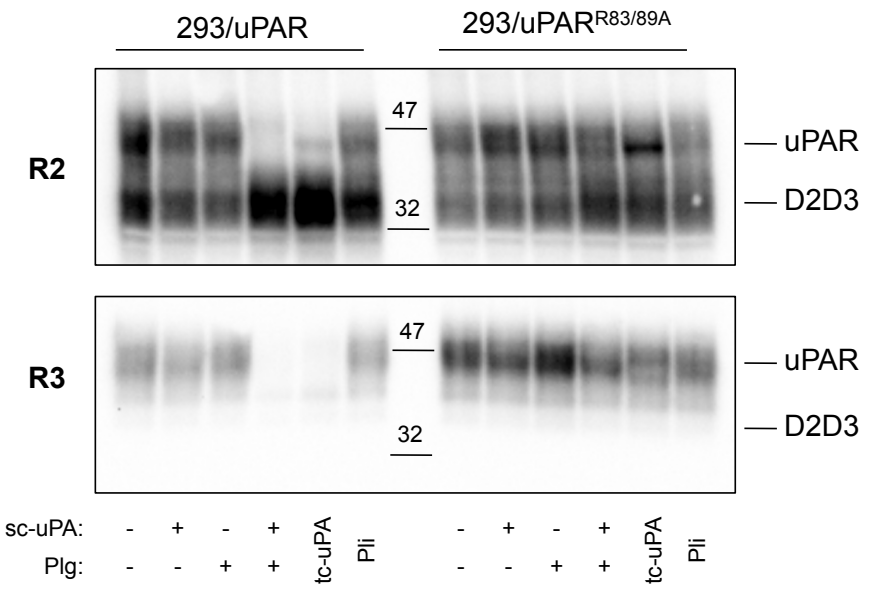

Figure 12: uPAR^{WT} but not uPAR$^{R83/89A}$ is cleaved by both uPA and Pli.

293/uPAR and 293/uPAR$^{R83/89A}$ cells were seeded on FN-coated culture plates and allowed to adhere for 1 h before treatment with the indicated reagents. After 1 h of treatment, cells were lysed, resolved by SDS-PAGE and analyzed by immunoblotting using monoclonal antibodies recognizing different epitopes in uPAR. R2 binds an epitope in D3 of uPAR and recognizes the full-length receptor (uPAR) as well as the cleaved form lacking D1 (D2D3). R3 binds an epitope in D1 and only recognizes full-length uPAR. The blot is from a representative experiment and the mobility of molecular weight standards is shown.

These data thus demonstrate that cleavage of uPAR by tc-uPA and Pli is only partially responsible for the negative feedback indicating that other functionally relevant uPA/Pli substrates are also involved in the process.

6.1.4 Pli cleaves the RGD-motif in VN

Pli has been shown to cleave VN at multiple locations *in vitro*[11, 177] and the treatment of VN-coated surfaces with Pli attenuates subsequent $\alpha_v\beta_5$-dependent adhesion of keratinocytes[178]. Consistent with these observations, we found that pre-treatment of VN coated surfaces with Pli, but not with tc-uPA, resulted in a dose-dependent reduction of cell adhesion (Fig. 13A). The inhibitory effect is not specific for uPAR-mediated cell

adhesion as the integrin-mediated adhesion of HeLa cells was also impaired (Fig. 13A). The inhibitory effect of Pli was however specific for VN as identical treatments of FN failed to modulate subsequent cell adhesion (Fig. 13B).

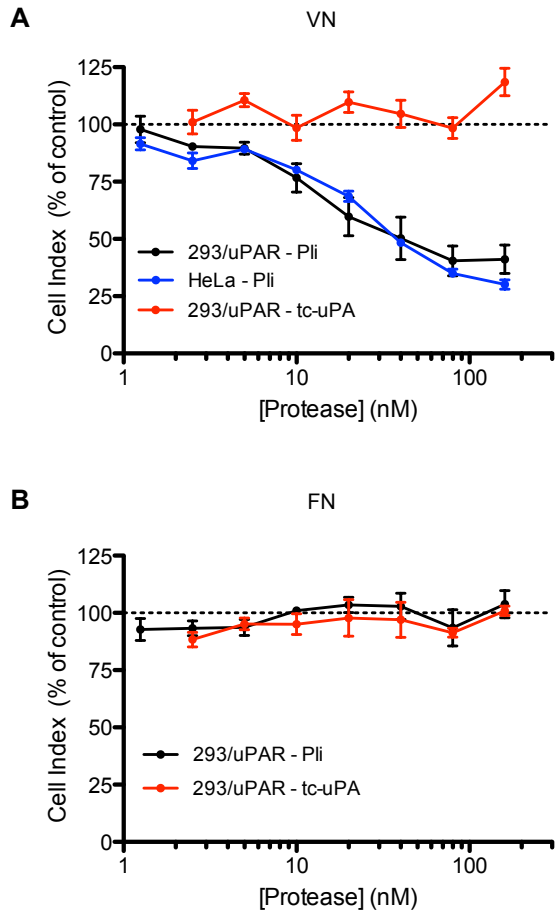

Figure 13: Pre-treatment of VN with Pli, but not uPA, inhibits subsequent cell adhesion mediated by uPAR and integrins. Wells coated with VN (A) or FN (B) were incubated with a dilution curve of Pli or tc-uPA for 1 h at 37˚C prior to cell seeding. After washing, 293/uPAR or HeLa cells were seeded and their adhesion was followed by RTCA. The cell indexes recorded 1 h after seeding are shown. Data are reported as percentage of the cell index measured in non-pre-treated wells and represent the mean ± standard error of the mean (SEM) of three independent experiments.

To investigate if the reported cleavage sites for Pli in VN were responsible for the negative feedback, we seeded 293/uPAR$^{R83/89A}$ cells on a recombinant form of VN (VN(1-64)-Fc) containing the N-terminal SMB domain responsible for uPAR binding and the flanking ^{45}RGD-motif interacting with integrin adhesion receptors, but none of the previously reported Pli cleavage sites located in the more C-terminal regions (^{88}K↓G, ^{348}K↓K and ^{361}R↓S[11, 177], see Fig. 14).

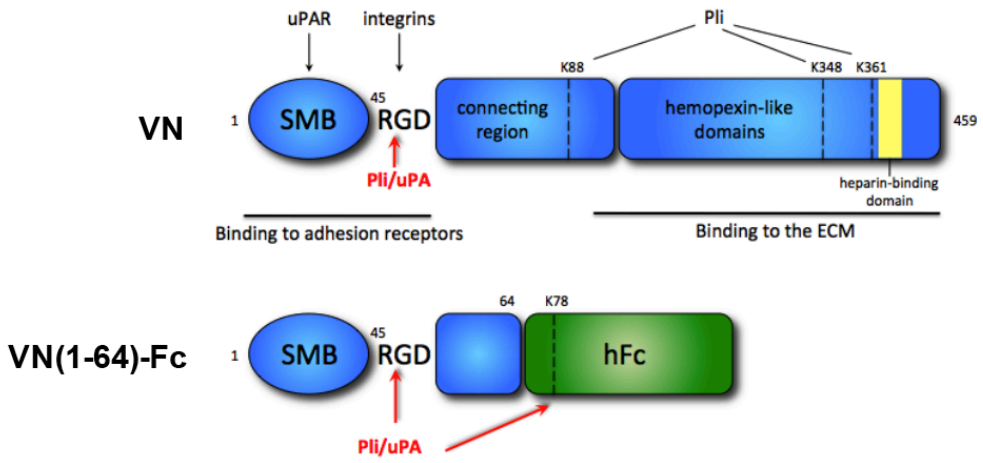

Figure 14: Cartoon illustrating the domain structure of human VN and the VN(1-64)-Fc chimera.

The N-terminal part of VN contains the SMB domain (residues 1-44) responsible for uPAR and PAI-1 binding as well as the flanking ^{45}RGD-motif responsible for integrin binding. The remaining C-terminal part contains hemopexin-like repeats intersected by a heparin binding site and it is responsible for binding to the ECM. The VN(1-64)-Fc chimera contains residues 1-64 of human VN fused to the Fc region of a human IgG heavy chain. The location of tc-uPA and Pli cleavage sites experimentally determined in this study are indicated in red while previously reported sites are reported in black.

Treatment of cells seeded on this substrate with tc-uPA, or sc-uPA plus Plg, still resulted in a robust negative feedback suggesting that the responsible cleavage site(s) are located within the N-terminal region of VN (Fig. 15).

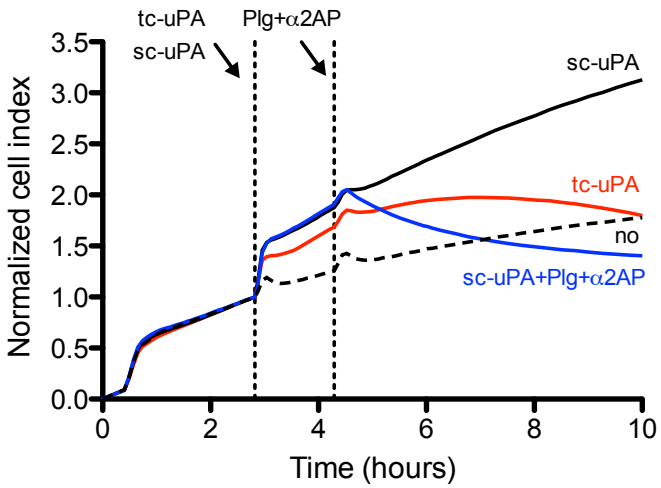

Figure 15: Cleavage site(s) responsible for the negative feedback are in the N-terminal region of VN.

RTCA experiment was performed on 293/uPAR$^{R83/89A}$ cells seeded on VN(1-64)-Fc and treated as reported. A representative experiment is shown.

Pli exhibits broad substrate specificity and cleaves peptide bonds after basic amino acid residues (lysine and arginine). To identify the Pli cleavage site(s) in the N-terminal part of VN, we individually mutated all basic residues present in this region into alanines, to abrogate proteolytic cleavage. VN variants so generated were used as coating substrate in RTCA experiments (Fig. 16 and 17). All mutants were comparably proficient in supporting uPAR-mediated 293/uPAR cells adhesion with the exception of the R8A mutant (Fig. 17). Notably, the R45A mutation was the only that abrogates both cell adhesion inhibition by Pli substrate pre-treatment (Fig. 16) and the negative feedback upon plasminogen activation (Fig. 17), indicating that cleavage at ^{45}R↓G in VN by Pli might be functionally responsible.

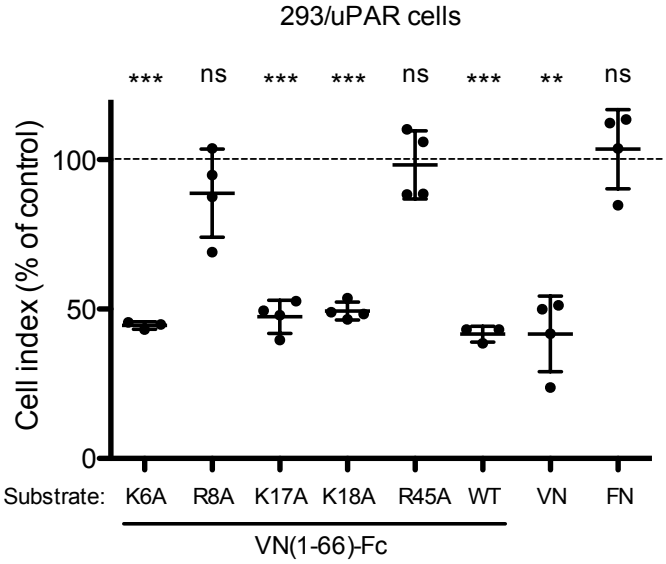

Figure 16: R45A mutation makes VN insensitive to Pli pre-treatment.

Wells were coated with VN, FN or VN(1-66)-Fc variants and incubated with 30 nM Pli or vehicle for 1 h at 37˚C prior to cell seeding. Subsequent 293/uPAR cells adhesion was followed by RTCA. The cell indexes recorded 1 h after seeding are shown as percentage of the cell index measured in non-pre-treated wells. Statistically significant difference between pre-treated and non-pre-treated wells was probed using Student's t-test (* = $p<0.05$, ** = $p<0.01$ and *** = $p<0.001$). Data are from a representative experiment, means ± standard deviation (SD) are shown.

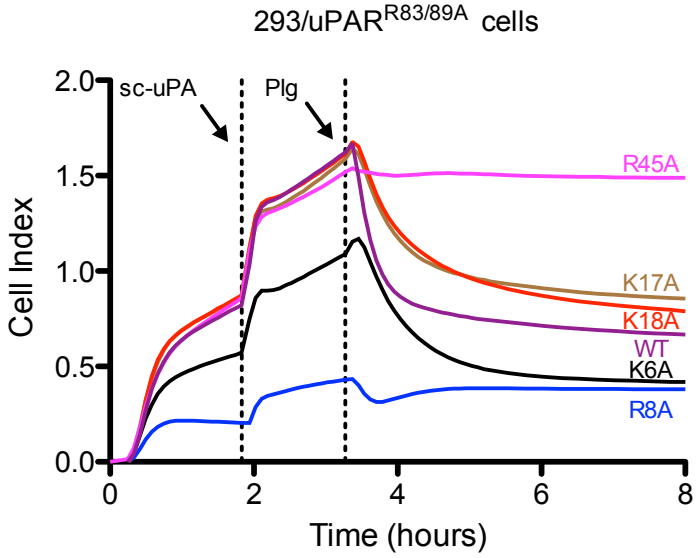

Figure 17: The R45A mutation in VN strongly impairs the negative feedback.

RTCA experiments were performed on 293/uPAR$^{R83/89A}$ cells seeded on VN(1-66)-Fc mutants and treated as reported. A representative experiment is shown.

To confirm this, we treated intact VN with Pli and analyzed the cleavage products by MALDI-TOF mass spectrometry (Fig. 18A). The molecular weight of the main peak observed in the resulting spectra closely matched that of an N-terminal VN-fragment (VN(1-45), theoretical average mass: 5159.71 Da) generated by ^{45}R↓GD cleavage. A peak with the same mass, but lower intensity, was also observed in spectra of non-treated VN (Fig. 18B), but not in spectra of Pli alone (Fig. 18C) suggesting that VN may be particularly prone to hydrolysis at this position and already partially cleaved. The same VN-fragment was also observed upon Pli-treatment of VN(1-64)-Fc (Fig. 18D), but not in a variant of this chimera (VN(1-64)^{R45A}-Fc) containing an alanine substitution of ^{45}R (Fig. 18E), conclusively identifying ^{45}R↓GD as a novel cleavage site for Pli in VN.

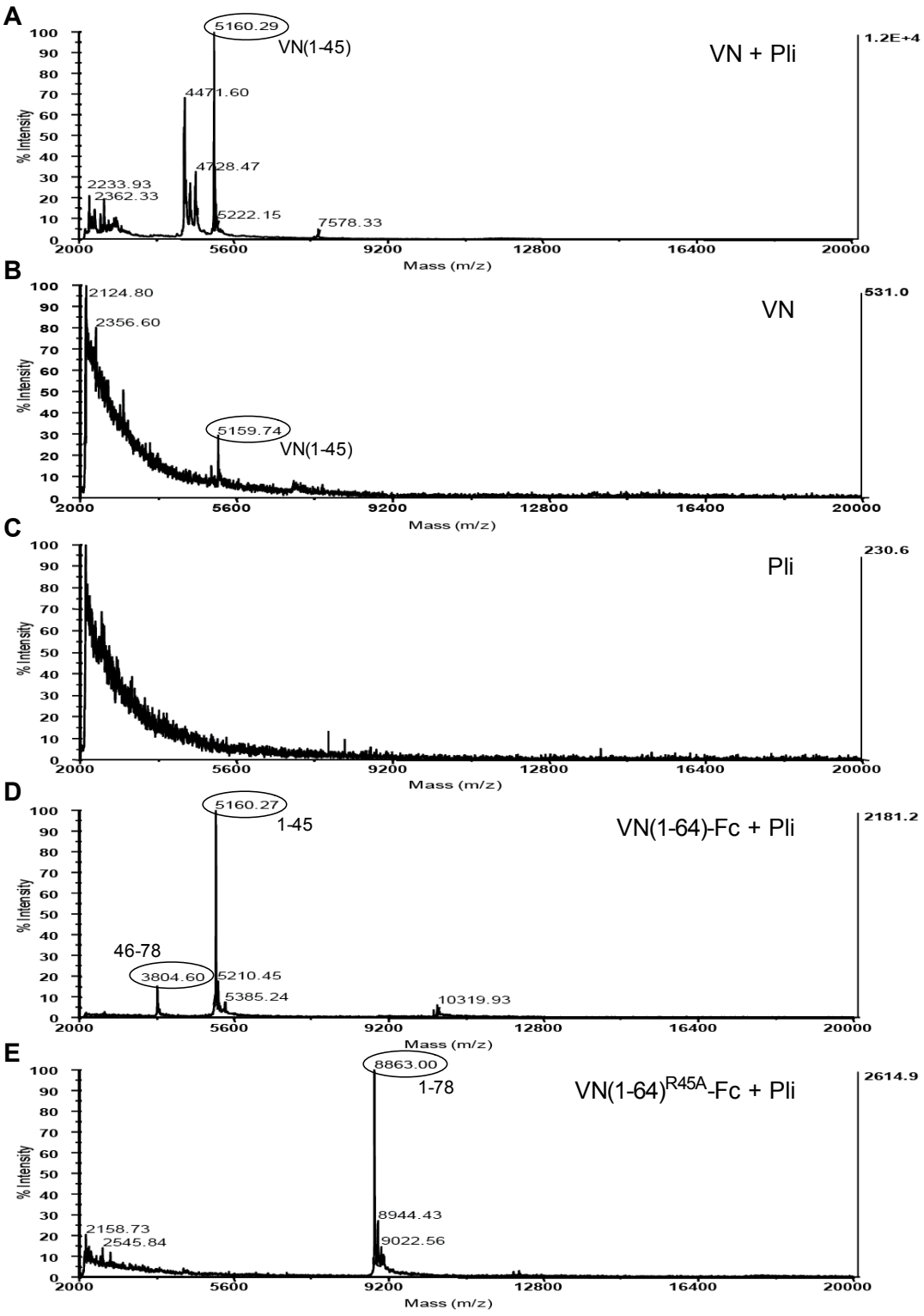

Figure 18: Pli cleaves VN in the RGD-motif after Arg45.

(A) Urea purified VN was incubated with Pli (substrate/enzyme ratio: 10:1 w/w) for 2 h at 37°C and the reactions were analyzed by MALDI-TOF mass spectrometry. A representative spectrum is shown. (B, C) Representative MALDI-TOF spectra of untreated VN (B) and Pli alone (C). (D, E) Representative MALDI-TOF spectra of VN(1-64)-Fc (D) and VN(1-64)^{R45A}-Fc (E) treated with Pli.

6.1.5 Cleavage of the RGD-motif in VN is responsible for the negative feedback between plasminogen activation and cell adhesion

To determine if the observed ^{45}R↓GD cleavage is functionally responsible for the feedback between plasminogen activation and cell adhesion to VN, we performed RTCA experiments using 293/uPAR$^{R83/89A}$ cells seeded on VN and different VN-variants where cleavage has been prevented by alanine substitution of ^{45}R in the RGD-motif (see cartoon in Fig. 14). Since the ^{45}R→A substitution, introduced to prevent cleavage, also results in impaired integrin-binding, we generated a second variant carrying the ^{46}G→A substitution that also abrogates integrin binding, but should have limited effect on cleavage. A representative experiment, illustrating the effect of the ^{45}R→A and ^{46}G→A substitutions on the proteolytic feedback, is shown in Fig. 19 and the quantified data from multiple experiments are presented in Fig. 20A and B.

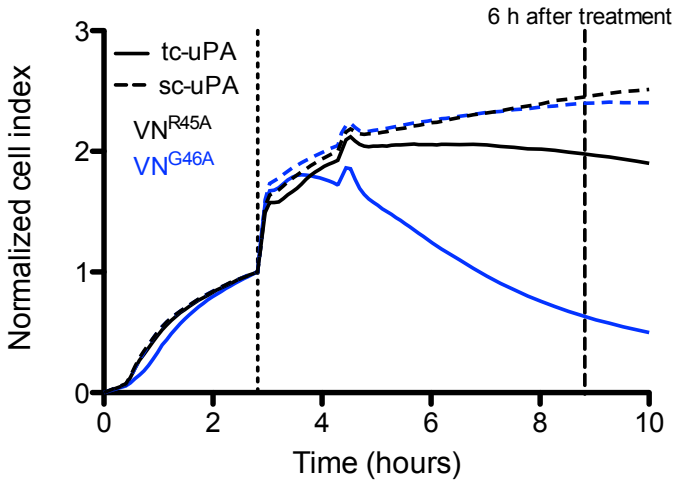

Figure 19: R45A mutation in VN strongly impairs tc-uPA mediated negative feedback.
293/uPAR$^{R83/89A}$ cells were seeded on VN^{R45A} or VN^{G46A} and treated with sc-uPA or tc-uPA at the indicated time-point (stippled vertical line). A representative RTCA experiment is shown. The time-point (6 h after treatment) at which the analysis shown in Fig. 20 was performed is depicted as vertical dashed line.

Introduction of the cleavage-blocking ^{45}R→A substitution in both intact VN and the shorter VN(1-64)-Fc chimera significantly and almost completely impaired the proteolytic feedback mediated by tc-uPA alone (Fig. 19 and Fig. 20A), demonstrating that the ^{45}R

cleavage site in the RGD-motif of VN is indeed functionally responsible for the bulk of the negative feedback mediated by active tc-uPA. The minor residual feedback observed on VN(1-64)-Fc was mediated by cleavage at a lysine residue (^{78}K) located in the Fc-part of the chimera. When cells were treated with a combination of sc-uPA, Plg and α2AP (Fig. 20B), the ^{45}R→A substitution had little effect on the proteolytic feedback on intact VN suggesting that other cleavage sites for Pli in VN are also important, or become important when the primary cleavage site has been inactivated. Nevertheless, the ^{45}R→A substitution did significantly impair the feedback on the shorter VN(1-64)-Fc chimera documenting that ^{45}R↓GD-cleavage may indeed contribute to the feedback. As observed for tc-uPA alone, the feedback was completely impaired by introduction of the ^{78}K substitution in the Fc-tag. Unexpectedly, the control mutation (^{46}G→A) significantly potentiated the negative feedback induced by tc-uPA. Although we have not investigated this point further, one explanation may be that the wild type ^{45}RGD-motif is partially protected from cleavage when bound by integrins. Therefore, the ^{46}G→A mutation may promote cleavage by preventing integrin binding.

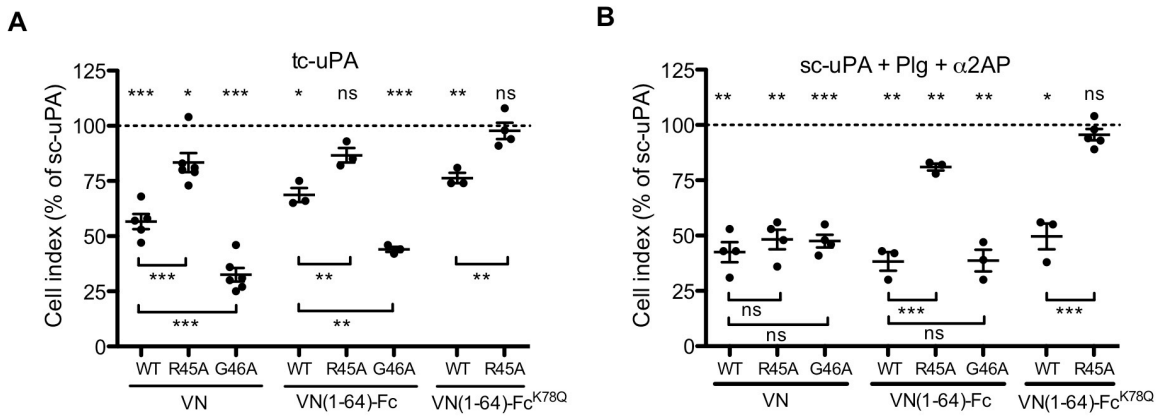

Figure 20: Cleavage of VN in the RGD-motif is responsible of the negative feedback.

RTCA analysis of 293/uPAR$^{R83/89A}$ cells seeded on different VN variants and treated with tc-uPA (A) or a combination of sc-uPA, Plg and α2AP (B). To merge independent experiments, the cell index measured after 6 h of treatment is shown as percentage of the one measured for cells seeded on the same substrate, but treated with sc-uPA, as depicted in Fig. 19. Dots are data from independent experiments and means ± SEM are shown. The significance levels were probed using Student's t-test.

Having identified a VN-variant largely refractory to the proteolytic feedback (VN(1-64)^{R45A}-Fc^{K78Q}, see Fig. 20A and B), we utilized this substrate to reinvestigate the contribution of uPAR-cleavage to the feedback. We generated 293 cells expressing uPAR-variants in which the two published cleavage sites are mutated individually or in combination (Fig. 21). This analysis revealed that cleavage both at ^{83}R↓ and ^{89}R↓ contribute to the negative feedback and that these sites are the only important ones as the alanine substitution of both completely abolished the feedback.

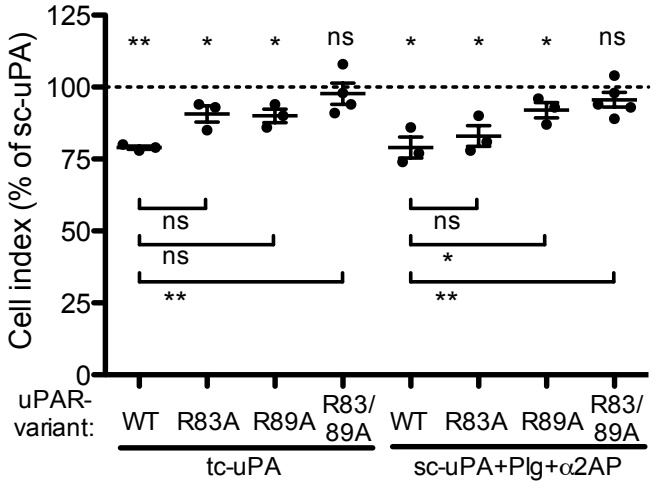

Figure 21: Cleavage of uPAR by uPA and Pli contributes to the negative feedback.

RTCA analysis of 293/uPAR^{WT} or mutant cells (as indicated) seeded on VN(1-64)^{R45A}-Fc^{K78Q} and treated with sc-uPA, tc-uPA or with a combination of sc-uPA, Plg and α2AP. Independent experiments were merged as described for Fig. 20.

These data thus demonstrate that the proteolytic feedback between plasminogen activation and cell adhesion to VN is functionally mediated by cleavage of both VN and uPAR and catalyzed by both tc-uPA and Pli. In the process, the cleavage of VN appears to be relatively more important than cleavage of uPAR. The main cleavage site in VN responsible for the negative feedback is ^{45}R↓ in the ^{45}RGD-motif even if other functionally relevant cleavage sites may exist.

6.1.6 Development of an immunoassay for the detection of N-terminal VN fragments

Proteolytic cleavage of matrix bound VN in the RGD-motif is expected to result in the release of an N-terminal VN-fragment (i.e. the SMB domain) from the connecting region and C-terminal hemopexin-like domains, which mediate the binding of VN to ECM components[87, 89]. To generate antibodies recognizing the N-terminal SMB domain of VN, we immunized $VN^{-/-}$ mice with a chimera protein containing the N-terminal region of human VN (residues 1-66) fused to the Fc region of a human IgG1 (VN(1-66)-Fc). We obtained three antibodies (namely HU3, HF6 and IO35) reactive with the antigen, but non-reactive with human IgG1 (data not shown). To map the binding epitopes, we used VN(1-66)-Fc variants containing selected amino acid substitutions (Fig. 22).

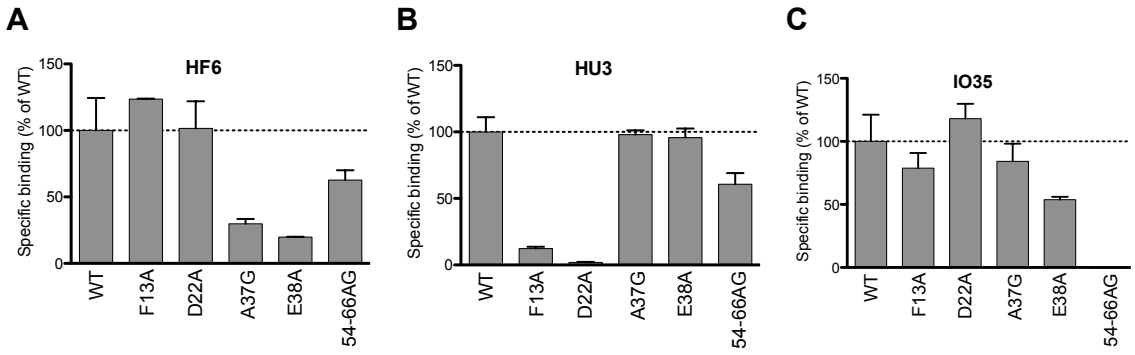

Figure 22: Mapping of the binding epitopes of HF6, HU3 and IO35.

96-well plates were coated with HF6 (A), HU3 (B) or IO35 (C), and incubated with VN(1-66)-Fc (100 ng/mL) carrying different amino acid substitutions as indicated. The 54-66AG is a substitution of the residues 54-66 with a stretch of alternating alanine and glycine residues. Bound VN(1-66)-Fc was detected using an Eu^{3+}-labeled secondary antibody directed against the human Fc moiety. Data are reported as percentage of the VN(1-66)-Fc WT, means ± SD of a representative experiment are shown.

This analysis showed that HU3 binds to an epitope (called Bin A) in VN comprising residues Phe13 and Asp22 as alanine substitution of any of these two residues strongly reduced binding. Residues Phe13 and Asp22 of VN are well-described to be involved in the binding of the natural VN-ligands uPAR and PAI-1[124, 179] as well as the previously

described antibody mAb153[180]. In contrast, HF6 binds to a second epitope (called Bin B) comprising residues Ala37 and Glu38. To our knowledge, antibodies against this epitope have not been described previously. Alanine substitution of Phe13 or Asp22 did not impair binding of HF6 and substitution of Ala37 (to glycine) or Glu38 did not impair binding of HU3 suggesting that the two epitopes are different and potentially non-overlapping. A third antibody, IO35, was found to bind downstream of the SMB-domain with a critical epitope (called Bin C) involving one or more residues in the VN(54-66) region, as the substitution of this region with a stretch of alternating Ala/Gly-residues prevents binding of the antibody. A cartoon of the binding epitopes is shown in Fig. 23.

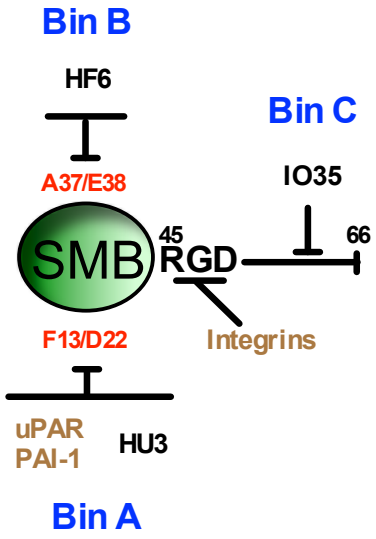

Figure 23: Cartoon illustrating the binding epitopes for HU3, HF6 and IO35 in VN.

HU3 and HF6 bind to two different epitopes within the SMB domain, critical residues for the binding are F13 and D22 for HU3 (Bin A) and A37 and E38 for HF6 (Bin B). uPAR and PAI-1 share the same binding site of HU3. IO35 binds downstream the SMB domain and the RGD motif with critical residues in the region 54-66 of VN (Bin C).

To test whether combinations of these antibodies could be used in a sandwich assay to measure SMB-containing VN fragments, we tested the ability of the different antibody pairs to contemporarily bind short un-tagged VN-fragments (Fig. 24). As predicted from the epitope mapping, pairs of antibodies belonging to different epitope bins were indeed able to detect short un-tagged VN-fragments demonstrating that the different epitope bins represent non-overlapping binding sites.

The combination of HU3 for coating and biotinylated HF6 for detection was chosen for further validation and optimization as this pair of antibodies yielded a high signal and

comparable detection of short and longer VN-fragments. The combination of HU3 as coating antibody and IO35 as detection antibody displayed a marked specificity towards longer fragments, consistent with the IO35 epitope being located in the region 54-66. It can therefore be used to discriminate between short N-terminal VN fragments (generated upon cleavage at ^{45}R↓GD) and longer fragments or the full length protein.

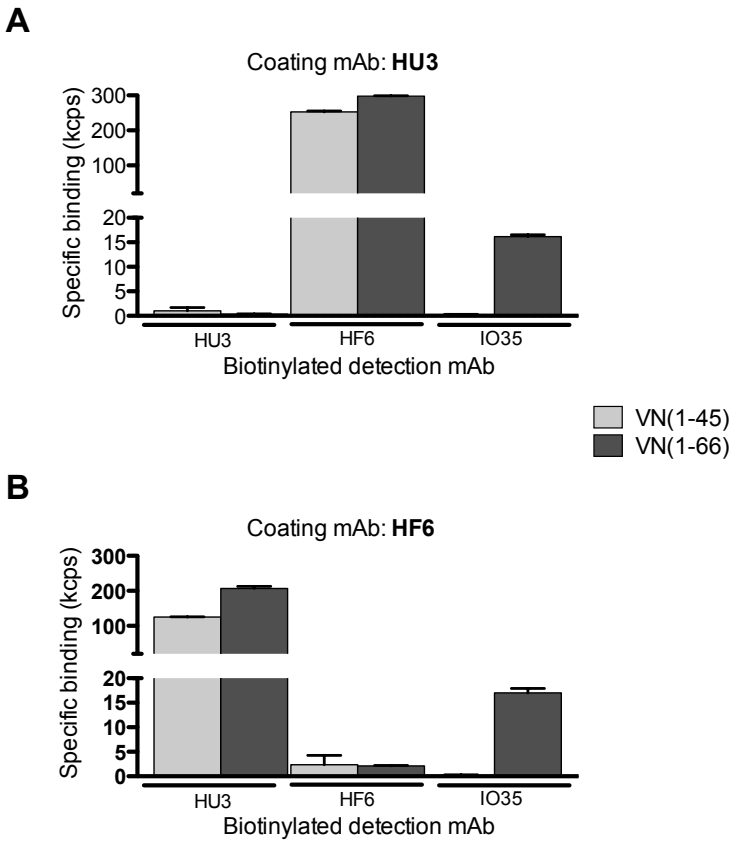

Figure 24: Recognition of short N-terminal VN fragments by HF6, HU3 and IO35.

Plates coated with HU3 (A) and HF6 (B) were incubated with conditioned medium of CHO cells expressing VN(1-45) (light grey columns) or VN(1-66) (dark grey columns) and the bound material was detected using biotinylated HF6, HU3 and IO35 as indicated. Means ± SD of a representative experiment are shown.

6.1.7 uPAR-expressing cells accelerate the cleavage of matrix VN by uPA and Pli

To investigate the occurrence of N-terminal VN fragments release, we treated VN immobilized on plastic with different forms of uPA and Plg in the absence or presence of 293/uPAR cells and quantified the levels of released SMB-containing VN-fragments (Fig.

25). In the absence of cells only the treatment with Pli was found to release VN-fragments, consistent with the pre-treatment experiments (Fig. 13) whereas the presence of 293/uPAR cells resulted in a highly significant release of VN-fragments also by tc-uPA and the combination of sc-uPA, Plg and α2AP.

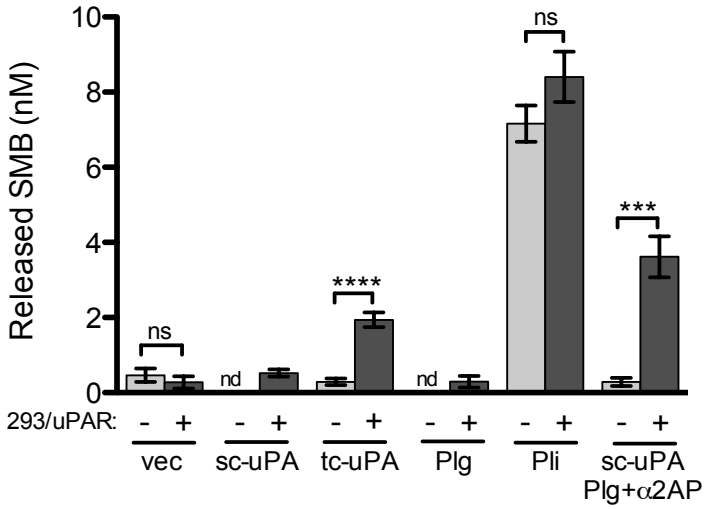

Figure 25: Plasminogen activation results in the release of N-terminal VN-fragments containing the SMB-domain.

293/uPAR cells were seeded on VN and treated as indicated for 2 h at 37˚C. The supernatants were harvested and the level of SMB-containing VN-fragments was measured by HU3/HF6 immunoassay (see material and methods). Values represent the mean ± SEM of at least 3 independent experiments. The statistical significance was probed using Student's t-test.

To exclude that tc-uPA mediated release could be due to trace amount of Pli, we used the Pli inhibitor aprotinin that does not have any activity towards uPA (Fig. 26). Indeed, aprotinin treatment did not have any effect on release by tc-uPA while was highly inhibitory for the treatment with sc-uPA, Plg and α2AP.

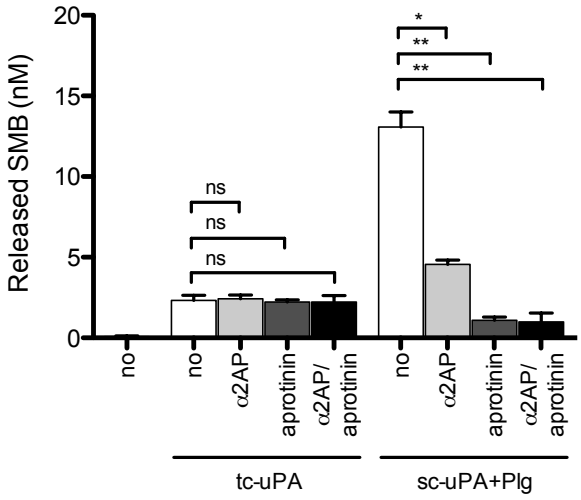

Figure 26: tc-uPA mediated release is not due to trace amount of Pli in the preparation.

293/uPAR cells were plated on VN and treated with tc-uPA or with a combination of sc-uPA and Plg in the presence or absence of Pli inhibitors (α2AP and aprotinin). Supernatants were analyzed as described in the legend to Fig. 25. Values represent the mean ± SEM of 3 independent experiments. The statistical significance was probed using Student's t-test.

Furthermore, tc-uPA mediated release requires: (i) uPAR expression, as mock transfected cells did not induce release (Fig. 27A); (ii) uPA binding to uPAR, as the release was impaired by the GFD domain of uPA; (iii) uPAR binding to VN, as cells expressing a VN-binding deficient uPAR mutant ($uPAR^{R91A}$) failed to promote the release and because an antibody blocking the interaction with VN (mAb 8B12, see material section) also prevented release (the mode of action of the different compounds/mutations utilized is depicted in Fig 28). Similar results were observed for the treatment with sc-uPA, Plg and α2AP (Fig. 27B), even if the inhibition by GFD and the impairment by the uPAR $^{91}R \rightarrow A$ substitution were incomplete and did not reach significance.

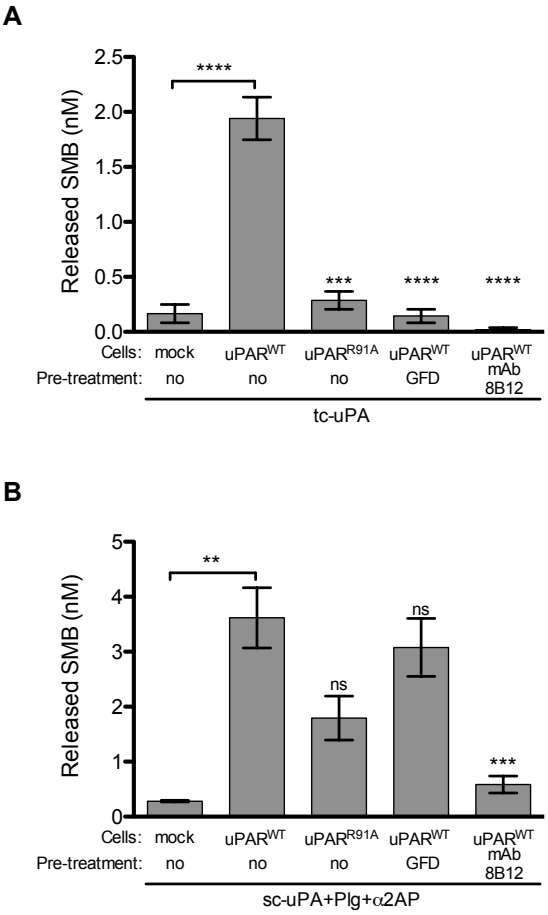

Figure 27: The generation of soluble VN-fragments containing the SMB-domain requires binding of both uPA and VN to uPAR.

Cells were plated on VN and treated with tc-uPA (A) or with a combination of sc-uPA, Plg and α2AP (B). Where indicated, 30 minutes pre-incubation with GFD or 8B12 was performed. Conditioned media were analyzed as described in Fig. 25. Values represent the mean ± SEM of 3 independent experiments. The statistical significance was probed using Student's t-test.

Figure 28: Cartoon illustrating the mechanism of action of the different compounds/mutations used in Fig. 27

The monoclonal antibody 8B12 is a competitive inhibitor of the interaction between uPAR and VN. The Arg91 residue in uPAR is part of the VN-binding epitope of the receptor. The GFD domain of uPA is a competitive antagonist of uPA-binding to uPAR.

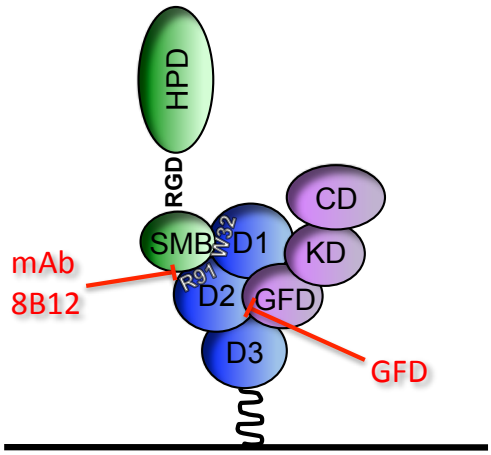

These data show that VN-fragments containing the SMB-domain are released from VN containing matrices upon plasminogen activation in a highly specific process that requires the binding of both uPA and VN to uPAR.

6.1.8 Binding of VN to uPAR accelerates cleavage by uPA

The above data suggest that uPAR directly "catalyzes" the cleavage of VN through a mechanism of substrate presentation in which the receptor coordinates the enzyme (uPA) and its substrate (VN) favouring the contact between the catalytic triad in uPA and the RGD-motif in VN. If true, this model predicts that uPAR catalyzes VN-cleavage even in the absence of cells. To test this hypothesis, we incubated VN-coated wells with a fixed concentration of uPA together with increasing concentrations of an Fc-tagged soluble uPAR and measured the concomitant release of VN-fragments (Fig. 29A). Consistent with the hypothesis, the addition of soluble uPAR indeed resulted in a dose dependent release of SMB-containing VN-fragments. The release requires catalytically active tc-uPA as no release was observed with sc-uPA and requires binding of uPAR to VN as no significant release was induced by a VN-binding deficient variant of uPAR ($uPAR^{W32/R91A}$-Fc).

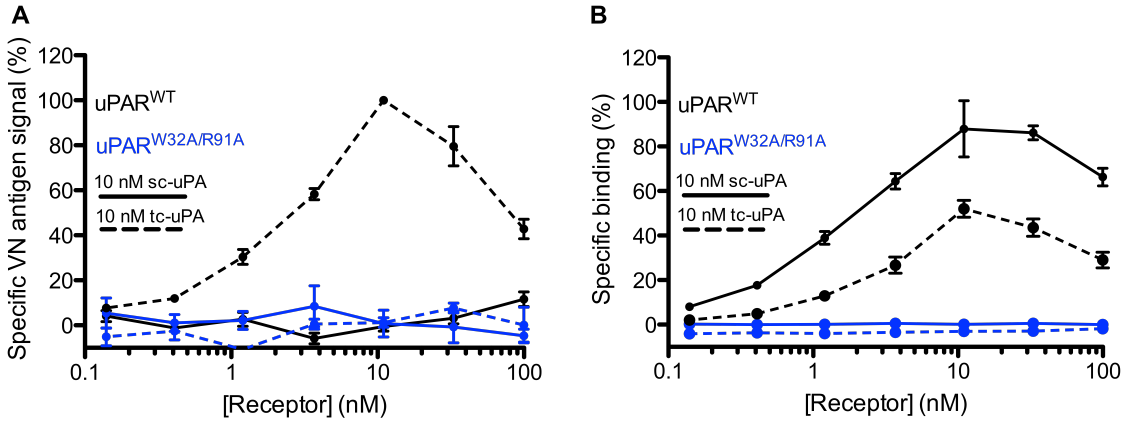

Figure 29: uPAR accelerate the generation of SMB-containing VN-fragments by uPA.

(A) Immobilized VN was incubated with 10 nM sc-uPA or tc-uPA together with a concentration curve of a soluble Fc-tagged uPAR ($uPAR^{WT}$) or a mutant form specifically deficient in VN-binding ($uPAR^{W32A/R91A}$). After 1 h of incubation, the supernatants were collected and analyzed for the presence of N-terminal VN-fragments by HU3/HF6 immunoassay. The release is reported as percentage of the maximal signal observed in the experiment (10 nM $uPAR^{WT}$ + tc-uPA). (B) After the recovery of supernatants for VN-fragment quantification, wells were washed and probed for bound uPAR-Fc using an Eu^{3+}-labeled anti-Fc antibody. The specific binding is reported as percentage of the maximal binding observed in the experiment (10 nM $uPAR^{WT}$ + sc-uPA). Data points represent the mean ± SEM of three independent experiments.

The levels of uPAR binding to VN (Fig. 29B) and the amounts of released SMB were directly proportional (Pearson r = 0.94, p < 0.0001, Fig. 30).

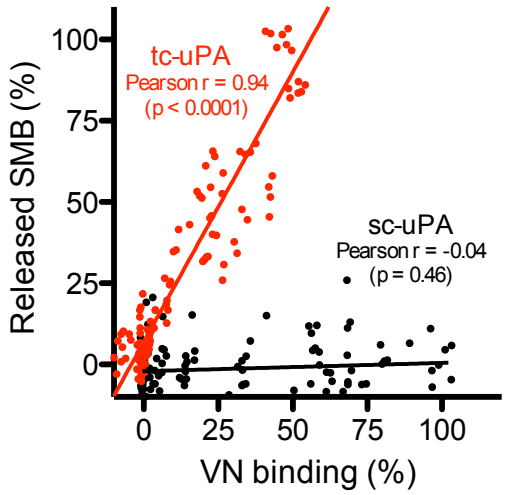

Figure 30: Levels of uPAR binding to VN and the release of VN fragments are strongly correlated.
All the individual data points recorded in three experiments shown in Fig. 29A and B were analyzed by plotting uPAR-binding to VN versus SMB release. Pearson correlations are shown.

To test whether these results could be an artefact of the forced uPAR dimerization caused by the presence of the Fc-tag, we repeated the same experiments comparing Fc-tagged soluble uPAR and un-tagged monomeric soluble uPAR (Fig. 31A and 31B). The presence of monomeric uPAR resulted in a dose dependent release of VN fragments but with lower efficiency compared to the Fc-tagged uPAR (Fig. 31A). This was paralleled by a less efficient VN binding of the monomeric uPAR compared to the Fc-tagged (Fig.31B). The correlation analysis between uPAR binding to VN and VN fragments release (Fig. 32) shows that comparable levels of binding to VN correspond to comparable release of VN fragments between monomeric and dimeric uPAR, further corroborating the concept that a key aspect for uPAR-mediated “catalysis” is its ability to bind VN. The release of VN fragments was not inhibited by an excess of aprotinin, thus excluding the presence of Pli contaminations in the different soluble uPAR preparations.

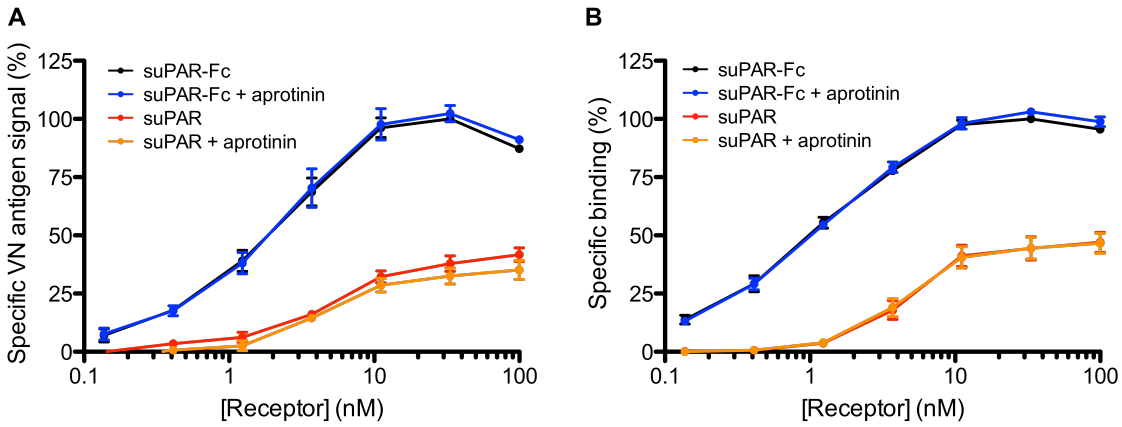

Figure 31: Monomeric soluble uPAR induces tc-uPA mediated cleavage of VN.

(A) Experiments were conducted as described for Fig. 29, using a fix concentration of tc-uPA (10 nM) and comparing soluble uPAR-Fc and soluble untagged uPAR, in the presence or absence of 300 nM aprotinin. (B) uPAR binding to VN was quantified by incubation with R2 antibody followed by incubation with Eu^{3+}-labeled anti-mouse Fc antibody. Data points represent the mean ± SEM of three independent experiments.

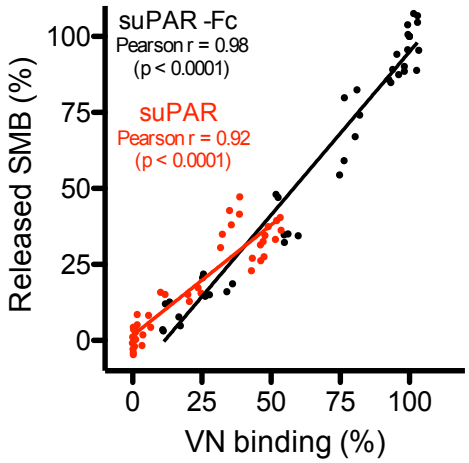

Figure 32: The VN-binding capability of uPAR determines the extent of cleavage acceleration.

All the individual data points recorded in three experiments shown in Fig. 31A and B were analyzed by plotting uPAR-binding to VN versus SMB release. Pearson correlations are shown.

To obtain a quantitative estimation of the extent of cleavage acceleration mediated by uPAR, we incubated VN-coated wells with tc-uPA in the presence of uPAR-Fc or with 100 times more tc-uPA in the absence of uPAR-Fc. Supernatants were collected at different time-points and analyzed for the presence of SMB-containing VN fragments (Fig. 33). The

release curves clearly show that the presence of uPAR results in higher cleavage acceleration compared to a 100-fold increase in the protease concentration. By linear regression of the initial part of the curves and slopes calculation, we estimated that the presence of uPAR results in a 300-fold increase in tc-uPA mediated cleavage of VN.

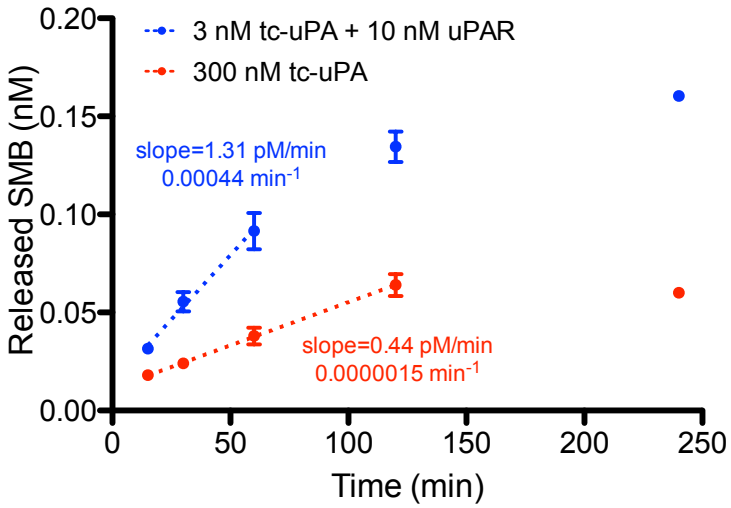

Figure 33: uPAR increases more than 100-fold the cleavage of VN mediated by tc-uPA.

VN immobilized in 96-well plates was incubated with 3 nM tc-uPA in the presence of 10 nM soluble Fc-tagged uPAR or with 300 nM tc-uPA alone. Supernatants were recovered at given time-points and analyzed for the presence of N-terminal VN-fragments by HU3/HF6 immunoassay. Dots represent the means ± SD of a representative experiment. Fitting of the initial part of the curves and slopes determination were done by linear regression using the GraphPad Prism (V6.0b) software. Estimation of the enzyme turnover rate was calculated dividing the slopes over the enzyme concentrations.

To confirm these data by an independent method and to conclusively identify the cleavage site(s) for uPA in VN, MALDI-TOF analysis was conducted on VN incubated with tc-uPA in the presence or absence of uPAR. Both in the absence (Fig. 34A) and in the presence of the receptor (Fig. 34B), a molecular species corresponding to VN(1-45) was observed, but the intensity of this peak was consistently and significantly higher in reactions containing also uPAR (Fig. 35).

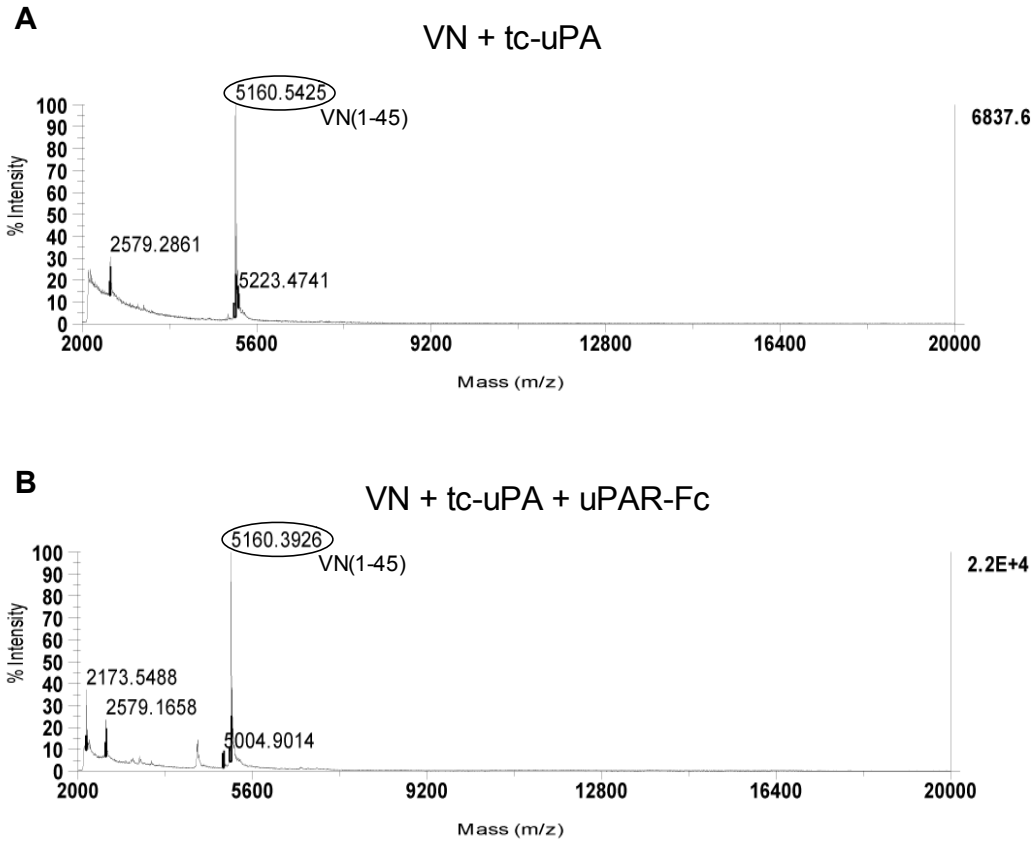

Figure 34: uPAR catalyzes uPA-mediated cleavage of the ^{45}RG peptide bond – MALDI spectra.

VN was subjected to tc-uPA digestion in the presence (B) or absence (A) of uPAR-Fc. Reactions were analyzed by MALDI-TOF mass spectrometry. Representative spectra are shown.

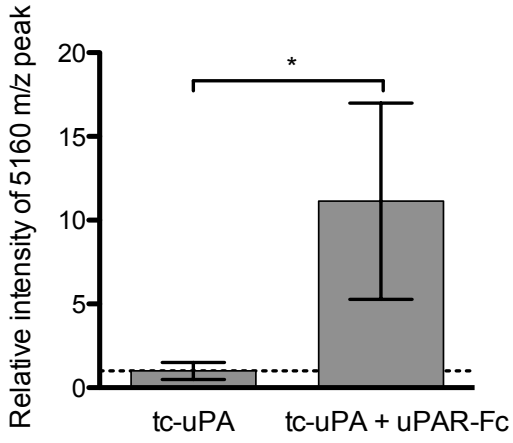

Figure 35: uPAR catalyzes uPA-mediated cleavage of ^{45}RG peptide bond in VN – peak intensity.

The experiment described in Fig. 34 was repeated 4 times and the intensity of 5160 Da peak was recorded. The graph shows the average relative intensity ± SEM of the 5160 Da peak from the 4 independent experiments, where the intensity of the 5160 Da peak of the tc-uPA alone condition of each experiment was set equal to 1. The statistical significance was probed using paired Student's t-test.

These data thus demonstrate that uPAR accelerates uPA-catalyzed VN-cleavage and that the predominant cleavage position is ^{45}R↓G consistently with the functional data.

6.1.9 SMB-containing VN fragments are released by cancer cell lines

We have shown that plasminogen activation results in the generation and release of N-terminal VN fragments. To test if it occurs also in non over-expressing conditions, we exploited the NCI-60 panel, which is a collection of 60 human cancer cell lines belonging to 9 different cancer types (breast, central nervous system CNS, renal, ovarian, prostate, colorectal, lung, melanoma and leukemia). All the cell lines were tested for the ability to generate VN fragments when seeded on immobilized VN in the presence or absence of exogenously added Plg and α2AP (Fig.36). In the absence of Plg, very low levels of SMB release were scored with the exception of a leukemic cell line (HL60) (Fig.36A). On the contrary, Plg addition resulted in a significant increase of fragments release in all tumour types, except for leukemia cell lines (Fig.36B). The data thus indicate that cell lines expressing patho-physiological levels of uPAR are indeed capable to release N-terminal VN fragments and that this capability is not restricted to few cancer types. Notably, the extent of VN fragments release displays a marked variability among the different cell lines even within the same cancer type, suggesting that it may be associated with peculiar tumour characteristics.

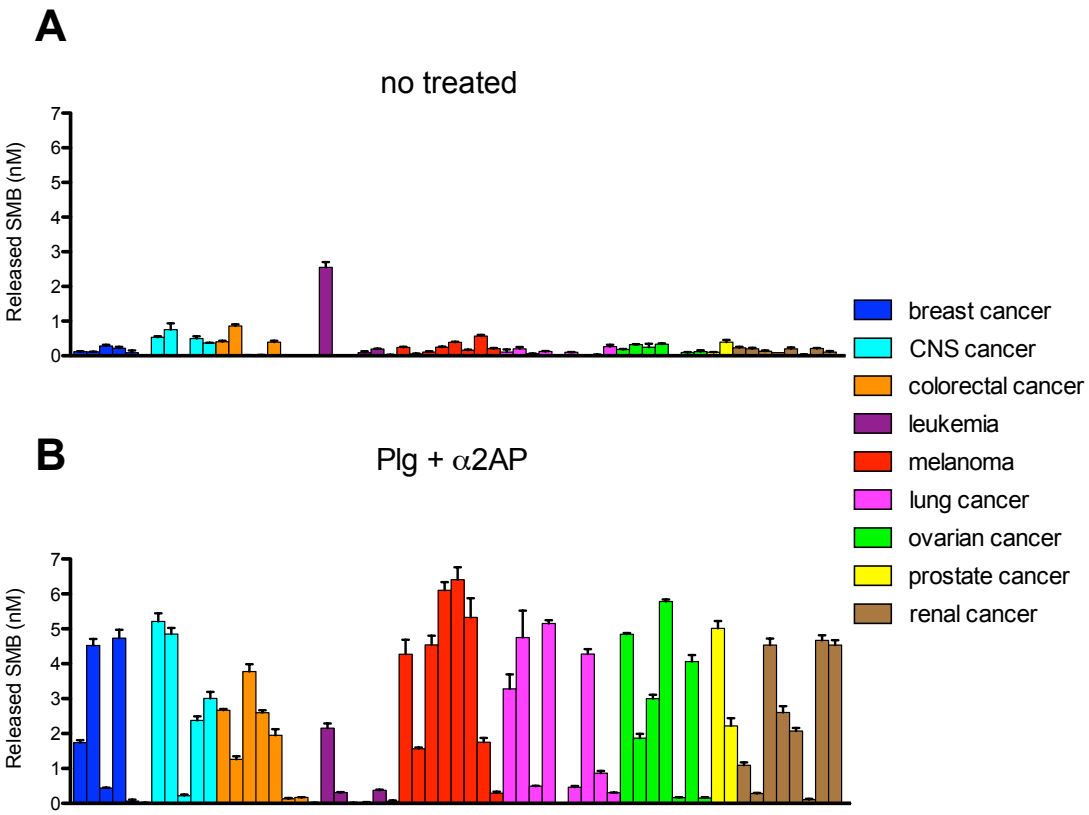

Figure 36: VN fragments are released by cancer cell lines.

All the NCI-60 cell-lines were seeded on VN and treated with Plg + α2AP (B) or vehicle (A). The supernatants were harvested after 16 h and the level of SMB-containing VN-fragments was measured by HU3/HF6 immunoassay. Values represent the mean ± SD.

To determine in an unbiased way what are the key cellular characteristics (i.e. genes) responsible for the release, we submitted the concentrations of VN fragments release in the absence or presence of Plg and α2AP as "patterns" to the CellMiner web tool[181]. This is an open-access bioinformatics tool that allows for pattern comparison between an input pattern of interest (i.e. VN fragments concentration) and gene expression across the NCI-60 panel. The outputs of the analysis are all the possible correlations between the input pattern and the expression levels of about 26.000 genes. When submitting the pattern coming from no-treated cells, 881 genes were found to positively correlate ($p<0.05$) and 387 to be negatively correlated with the levels of released VN fragments. The top one ($r = 0.844$) was the gene *ELANE* encoding for the serine protease neutrophils elastase. *PLG*

gene was also positively correlated (r = 0.32, rank = 440), indicating a possible direct involvement of the two endogenously expressed proteases in the cleavage of VN. The genes encoding for uPA (*PLAU*) and uPAR (*PLAUR*) were not found among the significant correlations. On the other hand, the analysis of the pattern of VN fragments release measured for Plg-treated cells resulted in the identification of 1033 positively and 1258 negatively correlated genes. A first preliminary data analysis did not reveal any obvious connection between the top 10 genes and the studied biological process. Importantly, however, *PLAU* was found to be positively correlated (r = 0.402, rank = 59). Of note, when restricting the analysis to the cancer cell lines of epithelial origin (n = 38), *PLAU* ranked number two with a strong and highly significant correlation (Fig. 37A), indicating, at least for epithelial cells, a strong connection between the expression of uPA and the ability of cancer cells to cleave VN. On the contrary, *PLAUR* still displayed no significant correlation (Fig. 37B).

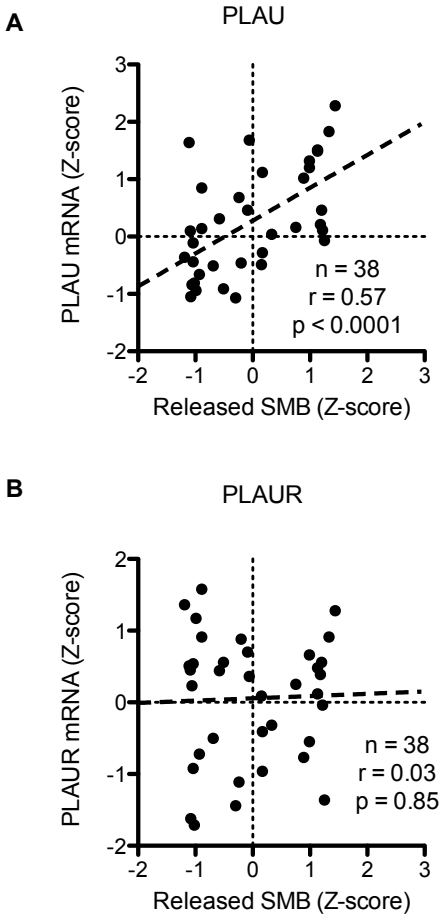

Figure 37: uPA expression but not uPAR correlates with the released SMB levels.

Correlation analysis between *PLAU* (A) and *PLAUR* (B) mRNA expression levels with released SMB levels (Fig. 36B). The analyzed variables are expressed as Z-score that is a mathematical transformation used by CellMiner to centre and normalize the data. Pearson correlations are shown.

6.1.10 N-terminal VN fragments are detectable in human urines

Because of the small size of the VN-fragments generated by proteolytic cleavage by uPA and Pli, it is reasonable to think that if these are generated *in vivo* they are most likely filtered rapidly to the urinary compartment where they should be detectable.

To test this hypothesis, we analyzed human urines samples from healthy volunteers with the HU3/HF6 immunoassay. All samples analyzed (n = 7) were positive for the presence of VN fragments (data not shown). However, a clear limitation of the assay is the lack of specificity as it can recognize SMB-containing VN fragments as well as the full-length protein. To discriminate between short and long VN fragments, we exploited the different specificity of the HU3/IO35 immunoassay, which does not detect short VN fragments generated upon cleavage at Arg45 (see Fig. 24). We calculated the ratio between the concentrations obtained with the two different assays (i.e. HU3/IO35 concentration divided by the HU3/HF6 concentration). When reported in percentage, a ratio of 100 means that the sample contains fragments that are longer than 1-66, on the contrary a ratio close to 0 indicates the presence of shorter fragments. Consistently, when conditioned medium of CHO cells expressing VN(1-45) was analyzed, it resulted in a ratio equal to 6.5%, while conditioned medium of CHO cells expressing VN(1-66) displayed a ratio of 92% (Fig. 38). The same analysis conducted on urine samples showed that they mainly contain short VN-fragments as evidenced by a ratio close to zero (average = 10.5%, Fig. 38). As control, we also analyzed a serum sample and we obtained a ratio of about 100, consistent with the high concentration of full length VN present in human blood.

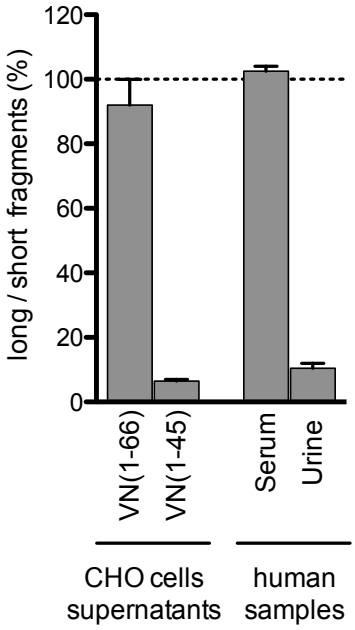

Figure 38: Human urines contain short N-terminal VN fragments.

Indicated samples were analyzed by HU3/IO35 and HU3/HF6 immunoassays. The HU3/IO35 extrapolated concentrations were divided over the concentrations calculated using HU3/HF6 measurements. Results are shown as percentage: a ratio of 100 (meaning equal recognition by the two assays) is indicative of samples containing long N-terminal VN fragments (≥1-66) while a ratio close to zero means that the sample contains shorter VN fragments.

To identify the molecular species present in human urines, urine samples from healthy volunteers were immunoprecipitated with the HF6 antibody and the adsorbed material analyzed by MALDI-TOF. A representative spectrum is shown in Fig. 39. Three molecular species could readily be assigned to N-terminal VN-fragments: VN(1-41) (theoretical m/z = 4676.11), VN(1-42) (theoretical m/z = 4804.24), VN(1-44) (theoretical m/z = 5004.48). The N-terminal VN-fragments observed in urine are presumably generated from longer precursor fragments (possibly VN(1-45)) by progressive removal of C-terminal residues by yet to be determined carboxypeptidases.

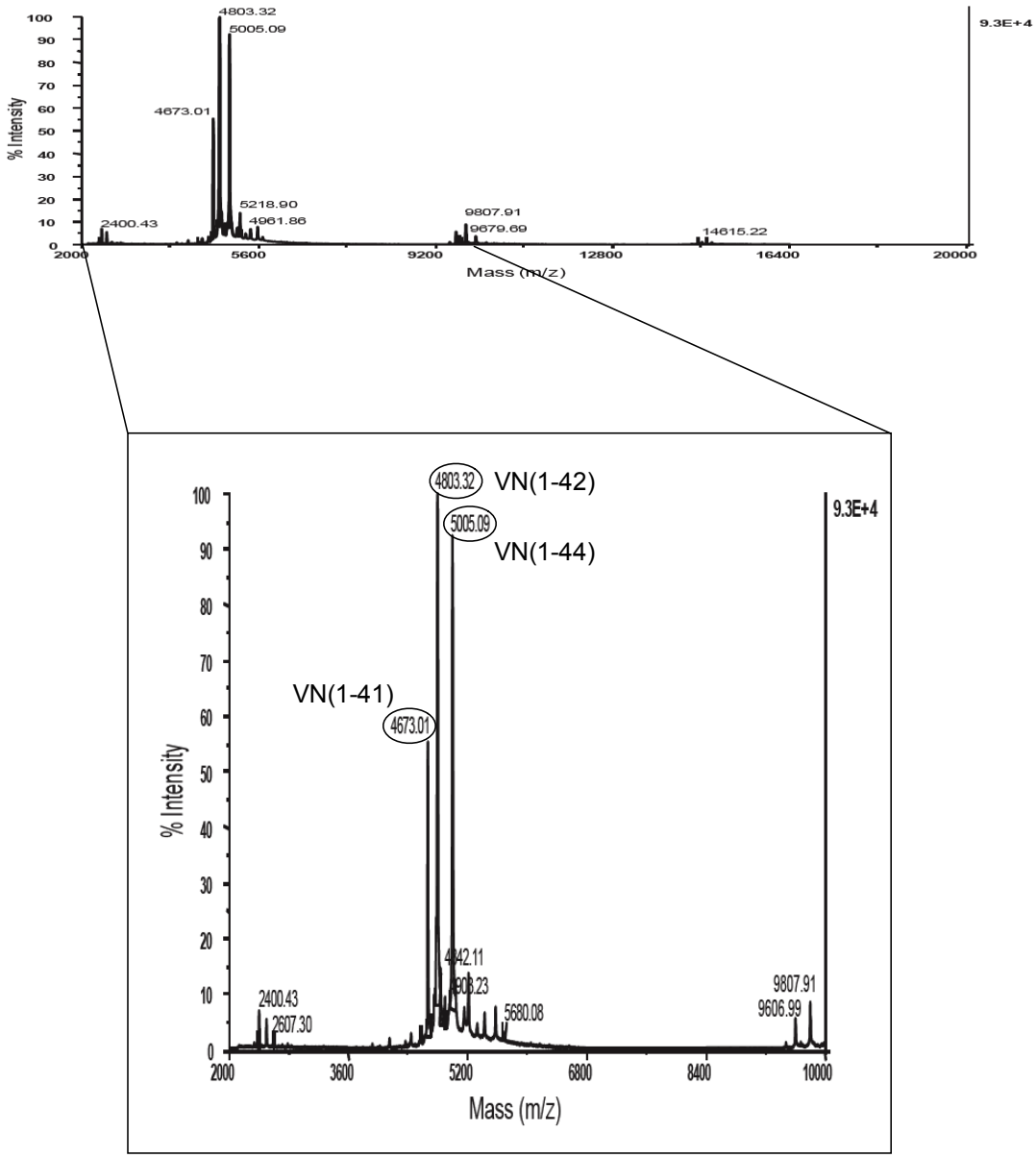

Figure 39: Three different molecular species of VN fragments are present in human urines.

Human urine samples were immunoprecipitated with HF6-conjugated beads and the eluted material was analyzed by MALDI-TOF mass spectrometry. A representative spectrum (MW range = 2-20 kDa) and a magnification (MW range = 2-10 kDa) are shown.

6.2 OPTIMIZATION AND VALIDATION OF THE HU3/HF6 IMMUNOASSAY FOR USE AS A CLINICAL GRADE ASSAY FOR THE DETECTION AND QUANTIFICATION OF URINARY N-TERMINAL VN-FRAGMENTS

We have recently shown that the interaction between uPAR and VN plays an important role in cancer progression[182]. Since the generation of VN-fragments *in vitro* requires this molecular interaction and VN fragments are indeed release by cancer cell lines *in vitro* and detectable in human urines, it is tempting to speculate that the levels of VN-fragments in urine might represent a novel biomarker in cancer patients, as a surrogate for the activity of the plasminogen activation system in tumour tissues.

To explore this possibility, we first needed to perform an exhaustive validation of the HU3/HF6 immunoassay to test its reliability and robustness.

6.2.1 Dynamic range and assay precision

To determine the dynamic range of the assay, a dilution curve of the reference protein (VN(1-61)) was prepared in assay buffer and the signal dose-response recorded (Fig. 40). The lower detection limit, defined as the concentration of VN(1-61) yielding a signal above background + 3 SD was found to be 3.3 fM. Similar, the upper detection limit defined by the concentration of VN(1-61) yielding a signal equal to saturation levels – 3 SD was found to be 33 pM. The assay thus has a dynamic range of approximately four orders of magnitude.

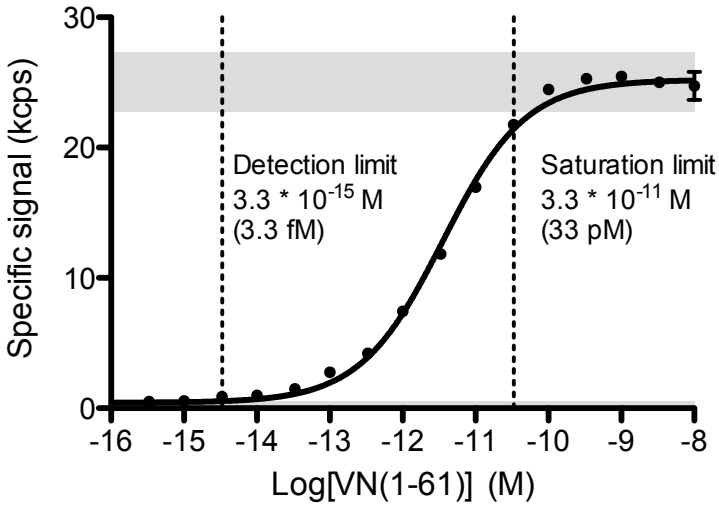

Figure 40: Dynamic range of the HU3/HF6 immunoassay.

Plates were coated with HU3 and incubated with a dilution curve of purified VN(1-61). Bound VN(1-61) was detected by subsequent incubations with biotin labeled HF6 and Eu^{3+}-conjugated streptavidin. The binding curve was fitted to the experimental data by non-linear regression fit as described in Material and methods. The dynamic range of the assay is given by the detection limit and the saturation limit and is indicated by stippled vertical lines. The lower detection limit was calculated as the concentration of VN(1-61) yielding a signal above background + 3 SD. The upper detection limit was calculated as the concentration of VN(1-61) yielding a signal equal to the saturation level – 3 SD. Grey zones indicate the average signal and noise +/- 3 times the SD recorded for the 16 negative and 16 positive control samples described in Fig. 41.

The quality of an assay depends on both the S/N ratio as well as the data variability and the latter may be quantified using the Z-factor[183]. To determine the Z-factor for the HU3/HF6 immunoassay, we measured the signal for 16 replicates of a negative control (assay buffer only) and 16 replicates of a positive control (10 nM VN(1-61) in assay buffer) and computed the Z-factor according to the formula: Z-factor = ((mean of positive controls – 3 x SD) – (mean of negative controls + 3 x SD))/(mean of positive controls – mean of negative controls). The resulting S/N-ratio was 59 and the Z-factor 0.9, representing an excellent assay (Fig. 41).

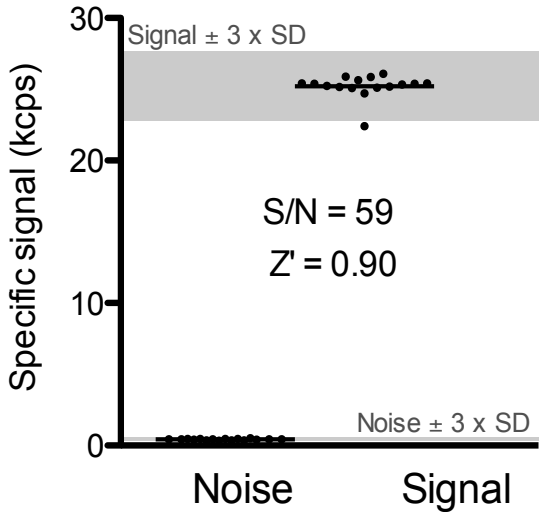

Figure 41: S/N ratio and Z-factor of the assay.

16 independent negative control samples (assay buffer alone, "Noise") and 16 independent positive control samples (sample buffer containing 10 nM VN(1-61), "Signal") were analyzed and the S/N-ratio and Z-factor calculated. The S/N-ratio was calculated as the mean signal of positive controls divided by the mean signal of the negative controls. The Z-factor was calculated as: ((mean positive controls – 3xSD) – (mean of negative controls + 3xSD)) divided by (mean positive controls – mean of negative controls). Grey zones indicate the average signal and noise +/- 3xSD recorded for the 16 negative and 16 positive control samples.

6.2.2 Linearity of the assay

To assess the optimal dilution of urine to use in the assay, a range of dilutions of the four different calibrator samples was made and assayed (Fig. 42). Compared to a reference dilution (1:1.600), the assay was found to be linear (+/- 20%) for sample dilutions in the range from 1:400 to 1:12.800 for all four calibrator samples. A urine sample dilution of 1:1.000 was chosen for subsequent measurements.

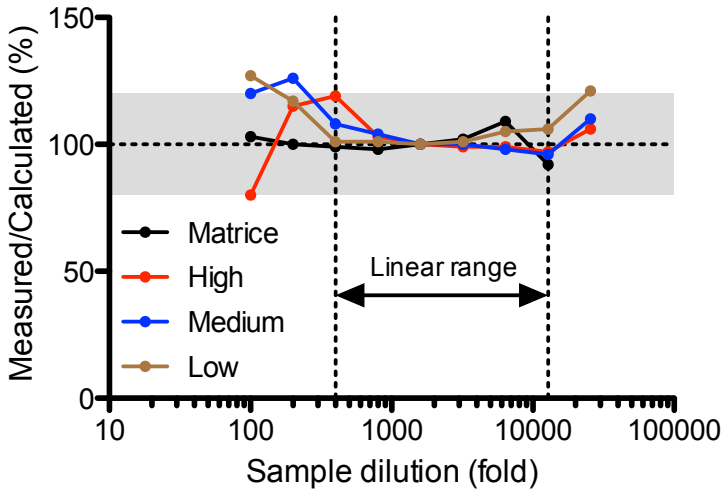

Figure 42: Assay linearity.

Dilution curves of four calibrator samples (high, medium, low and matrice) were prepared in assay buffer and the apparent ("Measured") concentration of VN-antigen quantified by extrapolation from a standard curve of VN(1-61). The actual ("Calculated") concentration of VN-antigen in the samples was obtained by first setting the measured concentration at 1:1.600-fold dilution to 100% and then deriving the concentration at other dilutions by numerical correction for the different dilutions. The grey zone indicates 100 +/- 20% linearity. The vertical stippled lines indicate the dilution range for which all four calibrators display a linear response +/- 20%.

6.2.3 Assay recovery

To determine the recovery of the assay, the four calibrator samples were spiked with a curve of VN(1-61) and the apparent analyte concentrations measured and compared to the same spike-in curve prepared in assay buffer (Fig. 43). The spike in with VN(1-61) resulted in linear response curves with similar slopes to the curve observed for the spike in curve prepared in assay buffer demonstrating a complete recovery of analyte. The data demonstrate that urine at the analyzed dilution does not contain components that interfere with the accurate detection and quantification of N-terminal VN-fragments.

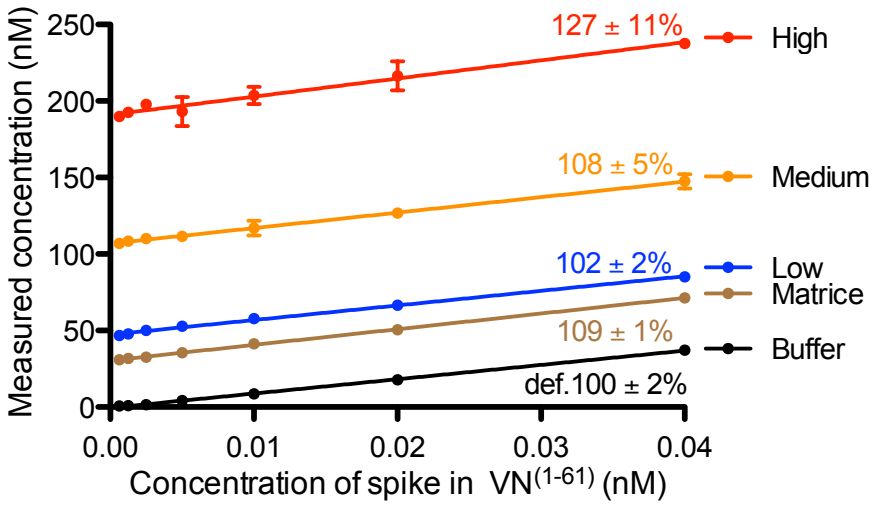

Figure 43: Assay recovery.

Assay buffer and the four calibrators (diluted 1:1.000) were spiked with a curve of VN(1-61) and the apparent concentration of VN-antigen measured. The slope of the curves is indicated in % of the slope calculated for VN(1-61) diluted in assay buffer.

6.2.4 Assay variability

To determine the assay variability within a single experiment (intra-assay variability) and between independent experiments (inter-assay variability) the four calibrators were measured 8 independent times in a single assay and in 9 independent assays (Fig. 44). The intra-assay variability (coefficient of variation) for the four calibrators was on average 3.5% (range: 2.9-4.3%) and the inter-assay variability 10% (range: 8.3-12%).

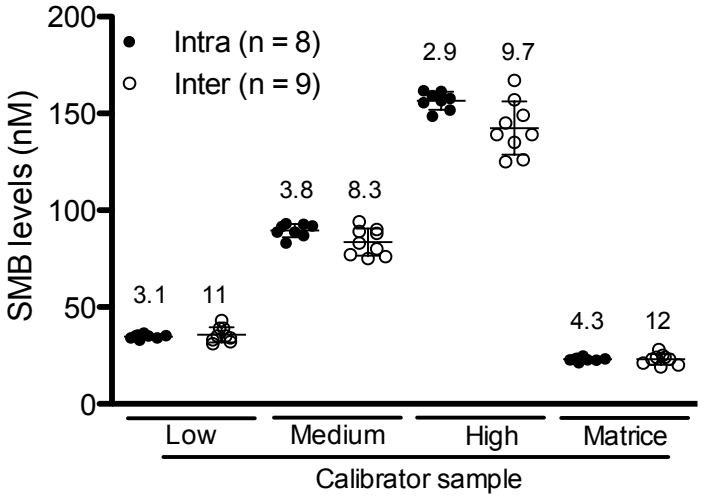

Figure 44: Intra- and inter-assay variability.

8 independent dilutions (1:1.000) of the four calibrators were measured in the same assay (same day, same plate) to determine the intra-assay variability, depicted with black dots. To measure the inter-assay variability, dilutions of the four calibrators were measured in 9 independent assays (different days), depicted with white dots. The calculated coefficients of variation (CV) are shown.

6.2.5 Assay robustness

To investigate the assay robustness in terms of sample storage temperature and freeze/thaw cycles, duplicate aliquots of the four calibrators were stored for three days at 4˚C, 25˚C and 37˚C or subjected to six complete freeze/thaw cycles on consecutive days. The different samples were then measured in a single assay and the recorded values compared to those obtained for the same samples stored at -80˚C until the assay (Fig. 45). The storage at different temperature or multiple freeze/thaw cycles did not result in any reduction of measured concentration demonstrating that the analyte is very stable. The different treatments did result in an increased variability (average 11%, range 9.5-12%) not explainable by ordinary intra-assay variability (3.5%, see Fig. 44) suggesting that a consistent sample handling is desirable.

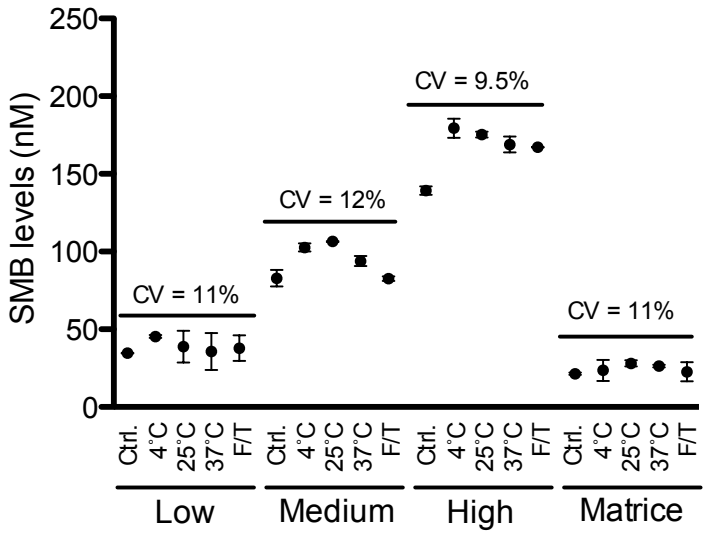

Figure 45: Assay robustness.

Aliquots (n = 2) of the four calibrators were measured after storage for 3 days at the indicated temperatures or after 6 complete freeze/thaw cycles. The CV for the different calibrators is shown.

6.2.6 Circadian variability

An important property of a good biomarker is that it should be relatively stable at base line so that altered levels may be correlated with pathological processes such as disease and possibly also treatment efficacy. To address the long term stability of urinary levels of VN-fragments, we measured the levels in consecutive early morning urine samples collected daily for a period of one month in one healthy male individual and one healthy female individual (Fig. 46A). The CV over one month for both individuals was 46%, however, after normalization for urinary creatinine levels (Fig. 46B) this variability was reduced 3-fold to approximately 15%.

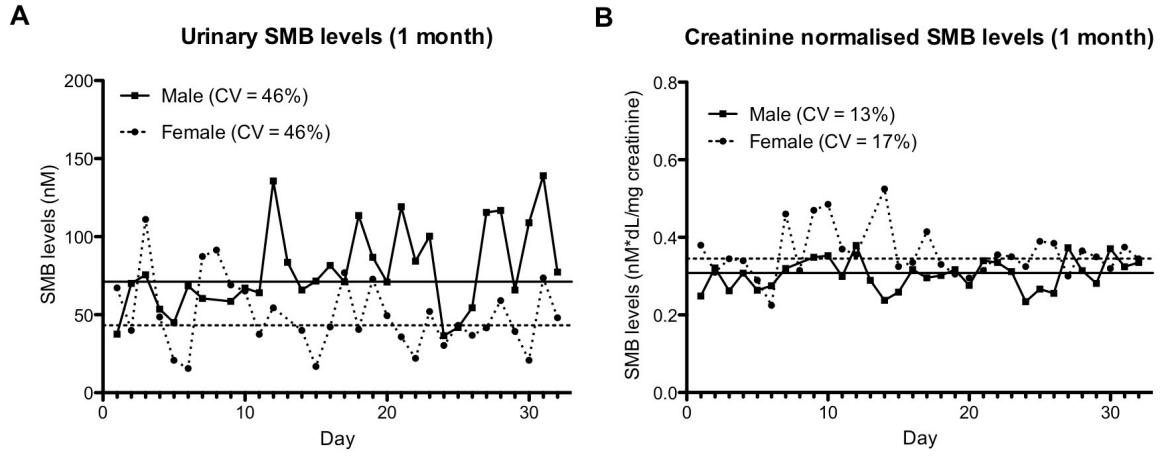

Figure 46: Long-term variations in urinary VN-antigen levels.

Early morning urine samples were collected every day for a month by two healthy volunteers (one male and one female) and the levels of VN-antigen measured. Graphs show measured VN fragments concentrations (A) and measured concentrations normalized on urinary creatinine levels (B) over time. Average levels are depicted by horizontal lines. The CVs are shown.

The variability within a single day was measured in 3 healthy males and 4 healthy females and was found to be 64% before normalization (Fig. 47A) and about 3-fold lower (20%) after creatinine normalization (Fig. 47B).

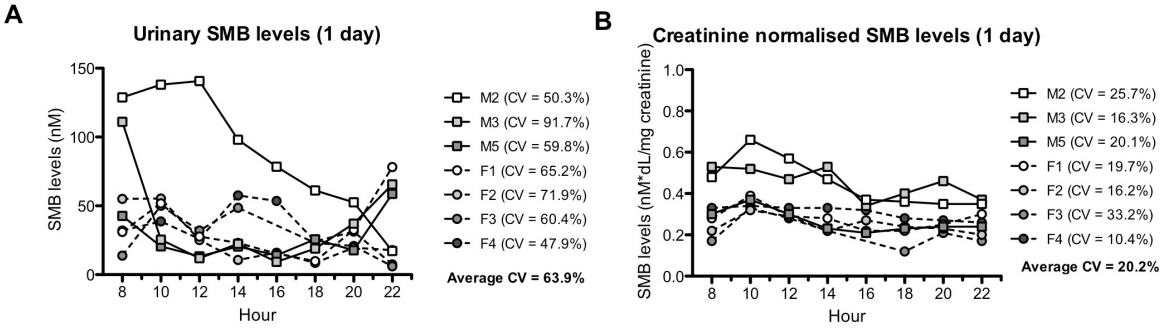

Figure 47: Short-term variations in urinary VN-antigen levels.

To determine the short-term variability in urinary SMB levels, three healthy male (M2, M3 and M5) and four healthy female (F1, F2, F3 and F4) volunteers collected urine samples every second hour from 8AM to 10PM. In panel A, the measured levels of VN-antigen are presented in function of the sampling hour. Creatinine normalized values are shown in panel B. The CVs are shown.

As the monthly variability is lower than the daily variability, these results show that the best accuracy is achieved by collecting the urine sample at the same time (i.e. early

morning urine) and normalizing for creatinine levels. The data furthermore confirm that urinary VN-fragments can be reliably measured and represent a stable biomarker.

6.3 uPA·PAI-1 IS A SUPER-AGONIST OF THE uPAR-VN INTERACTION

6.3.1 The uPA·PAI-1 complex is a super-agonist of the uPAR mediated cell adhesion to VN

We have shown that the plasminogen activation cascade exerts regulative feedback loops on uPAR mediated cell adhesion on VN. A prediction of these findings is that specific inhibitors of the proteolytic activity of uPA and Pli may functionally act to enhance and stabilize cell adhesion in conditions where the plasminogen activation system is active. In this context, PAI-1 has peculiar characteristics. Indeed, complex formation between uPA and PAI-1 results in the loss of two activities that normally suppress cell adhesion i.e. competitive binding of PAI-1 to VN and proteolytic degradation of uPAR and VN by uPA and Pli, while the pro-adhesive effect of uPA is maintained. Therefore, we reason that the uPA·PAI-1 complex, in contrast to its molecular precursors, will be a stable and irreversible agonist of uPAR-mediated cell adhesion to VN.

To address this hypothesis directly, we compared the individual and combined effect of uPA and PAI-1 on uPAR-mediated cell adhesion to VN (Fig. 48). As predicted from the competitive binding of uPAR and PAI-1 to the SMB of VN, the treatment with PAI-1 caused a marked reduction in cell adhesion to VN mediated by uPAR. Similarly, the treatment with tc-uPA resulted inhibitory following the initial increase in cell adhesion. In contrast to the individual treatments, the combined treatment with tc-uPA and PAI-1 had a strong and persistent pro-adhesive effect. This result is fully consistent with our hypothesis, but the magnitude of the agonistic effect was unexpected. In fact, the treatment with a combination of tc-uPA and PAI-1, or purified uPA·PAI-1 complex, was clearly more agonistic than treatment with sc-uPA that represents a strong prototypic agonist.

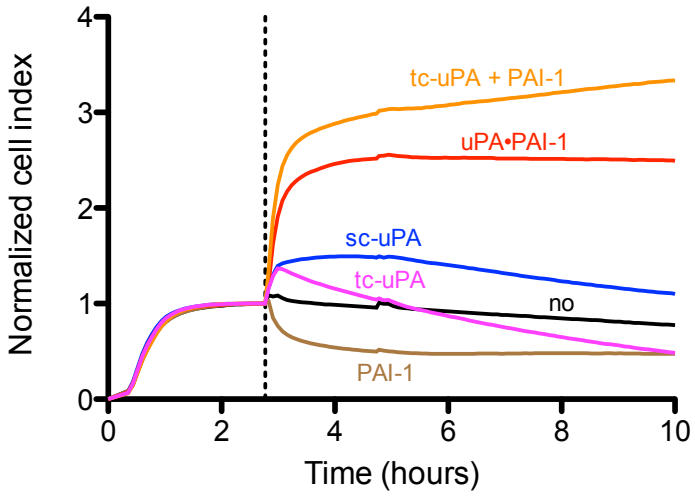

Figure 48: uPA·PAI-1 complex is a super-agonist of uPAR-mediated cell adhesion to VN.

RTCA analysis of 293/uPAR cells seeded on VN and treated at the indicated time-point. A representative experiment is shown.

The "super-agonistic" effect of the complex resulted in a spread cell morphology (Fig. 49) even if the cell-matrix contact area (Fig. 50) did not increase as compared to treatment with the canonical agonist sc-uPA. Treatment with PAI-1 had the opposite effects causing evident rounding up of the cells and a reduced cell matrix contact area.

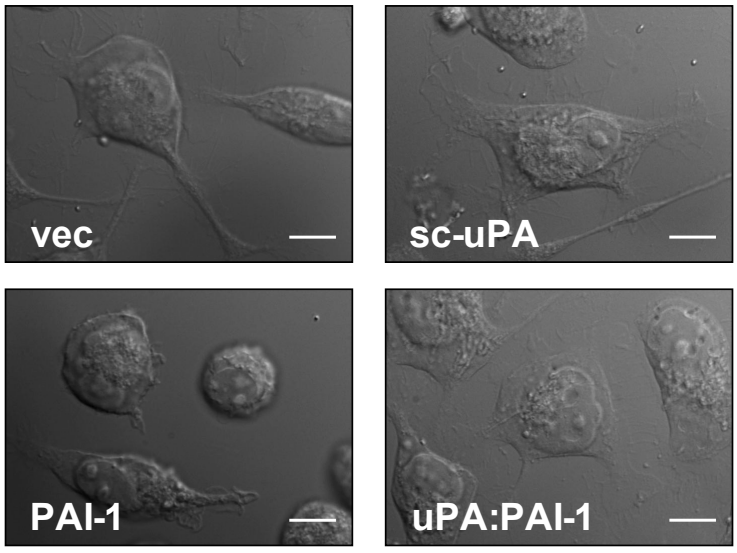

Figure 49: Morphology of 293/uPAR cells treated with different ligands.

293/uPAR cells were seeded on VN-coated cover-slips, allowed to adhere and treated with different ligands for 1 h. The cells were fixed and DIC images recorded. Representative DIC images are shown. Scale bar, 10 μM.

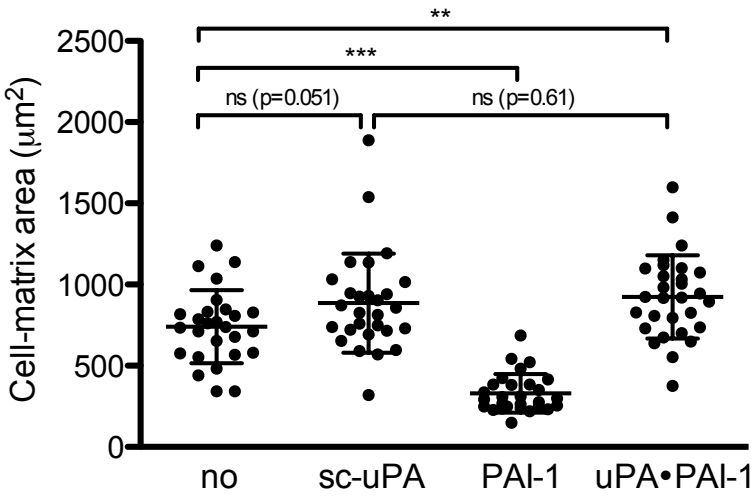

Figure 50: uPA·PAI-1 super-agonistic effect on uPAR-mediated adhesion to VN is not due to increased cell spreading.

Cell-matrix contact area was quantified in the DIC images, collected in the experiment described in the legend to Fig. 49, using ImageJ. Twenty-five cells were quantified for each condition. Means ± SD of a representative experiment are shown. Statistical significance was probed using Student's t-test.

Of note, treatment with both PAI-1 and the uPA·PAI-1 complex inhibited cell migration (Fig. 51 and Movies 2 and 3). The cause of inhibition of migration was however clearly the opposite in support of the paradigm that both too strong (i.e. uPA·PAI-1 treated cells) and too weak (i.e. PAI-1 treated cells) cell adhesion preclude efficient cell migration. The block of cell migration by PAI-1 is transient, possibly because of inactivation of its VN binding activity by latency conversion.

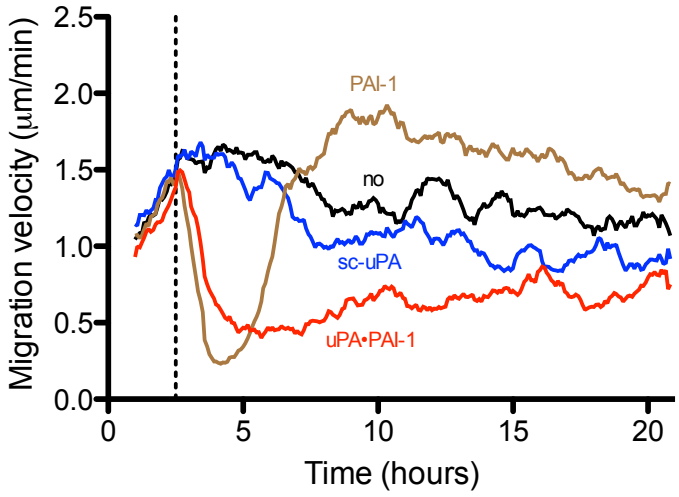

Figure 51: Effect of uPAR ligands on 2D cell migration on VN.

293/uPAR cells were seeded in VN-coated wells and treated as indicated. Cells were imaged by time-lapse microscopy. Cell migration was quantified by manual tracking using the ImageJ software suite and the "manual tracking" plugin. The migration speed at a given time point was calculated as the average cell migration speed over the 30 minutes preceding the time point. The curves represent the average migration speed of 50 or more individual cells for each condition. The time at which cells were treated is depicted with a vertical dashed line.

These data thus document that the uPA·PAI-1 complex is a stable agonist of the uPAR-mediated cell adhesion to VN. Moreover, we here show for the first time that the complex is endowed with super-agonistic properties.

6.3.2 PAI-1 counteracts the negative feedback and behaves as a proteolysis-dependent agonist of the uPAR-mediated cell adhesion on VN

To investigate if the super-agonistic activity of the uPA·PAI-1 complex manifests itself in conditions where plasminogen activation is triggered, we conducted RTCA experiments with sequential additions of the proteases in their native zymogen forms as well as their inhibitors (Fig. 52). 293/uPAR cells were seeded on VN, allowed to adhere, and then treated with sc-uPA, PAI-1 or a mixture of the two. As predicted, the treatment with PAI-1

markedly reduced adhesion while sc-uPA was stimulatory. The cumulative effect of the pro-adhesive activity of sc-uPA and the anti-adhesive activity PAI-1 was a reduction in cell adhesion as compared to sham treated cells. To activate cell surface associated plasminogen activation, Plg and α2AP were added in a second step. Addition of Plg+α2AP to sc-uPA treated cells resulted in a steady decline in cell adhesion. In strong contrast the addition of Plg+α2AP to cells pre-treated with both sc-uPA and PAI-1 resulted in a sharp wave of cell adhesion. Addition of Plg+α2AP to sham or PAI-1 pre-treated cells had no effect (data not shown).

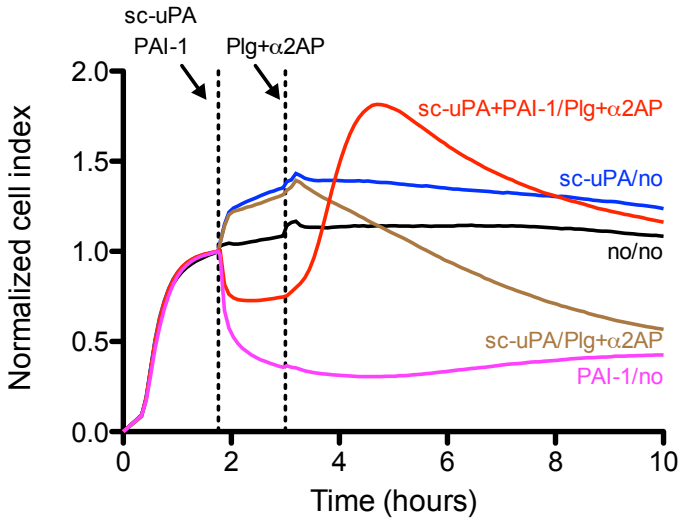

Figure 52: uPA generated during plasminogen activation stimulates cell adhesion to VN-coated matrices in the presence of PAI-1.

RTCA analysis of 293/uPAR cells seeded on VN and treated as indicated. A representative experiment is shown.

The data show that PAI-1 simultaneously blocks the negative feedback and enhances uPAR-VN interaction, thus behaving as a proteolysis-dependent stimulator of cell adhesion to VN.

6.3.3 uPA·PAI-1 complex directly enhances uPAR-VN interaction

It has been shown that the GFD domain of uPA is required and sufficient to induce the conformational change in uPAR that increases the receptor affinity for VN[126]. sc-uPA, tc-uPA and the uPA·PAI-1 complex all contain this domain and display very similar binding affinity towards uPAR[117]. To understand if the super-agonistic activity of the uPA·PAI-1 complex is mediated by an increase in the binding reaction between uPAR and VN or if other cellular processes are also involved, we compared the agonistic activity of sc-uPA, tc-uPA and uPA·PAI-1 in inducing uPAR-binding to immobilized VN using purified components (Fig. 53). Both sc-uPA and tc-uPA induced uPAR-binding to VN with similar EC_{50}, but the B_{max} was higher for sc-uPA presumably because of the uPAR and/or VN cleavage occurring during the binding reaction. Notably, the uPA·PAI-1 complex was clearly a stronger agonist displaying about three-fold lower EC_{50} and twice the B_{max} as compared to sc-uPA.

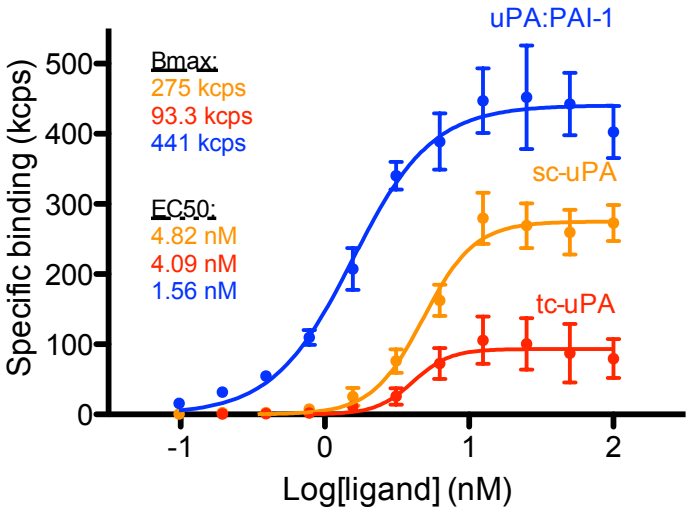

Figure 53: The uPA·PAI-1 complex is a super-agonist of the interaction between uPAR and VN.

96-well immunoplates were coated with VN and incubated with a fixed concentration of Fc-tagged uPAR (10 nM) in the presence of a dilution curve of sc-uPA, tc-uPA and uPA·PAI-1 complex as indicated. After 2 h of binding, plates were washed and probed for bound uPAR-Fc using an Eu^{3+}-labeled anti-Fc antibody. Dots represent the means ± SD of a representative experiment. Curves fitting and determination of EC_{50} and B_{max} were done by non-linear regression using the log[agonist] vs. response – variable slope (four parameter) algorithm and the GraphPad Prism (V6.0b) software.

The strong agonistic activity of the uPA·PAI-1 complex is unlikely to be caused by increased uPAR-binding as it is, if anything, a weaker antagonist of the uPA/uPAR-interaction (Fig. 54). It thus appears plausible that the strong pro-adhesive activity of the uPA·PAI-1 complex is caused by an increased stability of the PAI-1·uPA·uPAR·VN complex as compared to the sc-uPA·uPAR·VN complex.

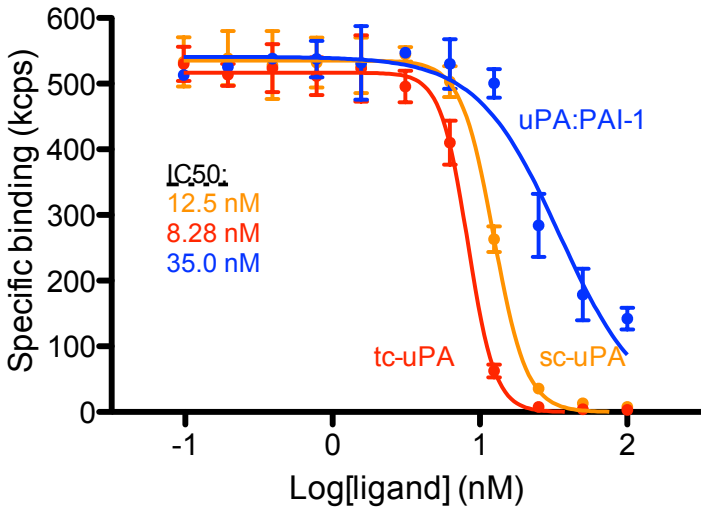

Figure 54: uPA·PAI-1 super-agonistic activity is not due to higher affinity of the uPA·PAI-1 complex for uPAR.

The same reaction mixtures used in Fig. 53 were also tested for uPAR-binding activity towards immobilized sc-uPA. This assay was conducted exactly as described for Fig. 53 with the only exception that plates had been coated with sc-uPA. Dots represent the means ± SD of a representative experiment. Curves fitting and determination of IC_{50} values were performed by non linear regression using the log[inhibitor] vs. response – Variable slope (four parameters) algorithm and the GraphPad Prism (V6.0b) software.

6.3.4 Mechanism of the PAI-1·uPA·uPAR·VN complex formation

As the interaction with VN stabilizes PAI-1 in an active conformation[52], it is likely that the physiologically relevant inactivation of uPA by PAI-1 occurring in tissues may predominantly happen between uPAR-bound uPA and VN-bound PAI-1. To investigate if these conditions can be reconstituted using purified components, we analyzed the binding

of sc-uPA/tc-uPA-bound uPAR to immobilized VN saturated with PAI-1 (Fig. 55). Saturation of VN with PAI-1 completely blocked the subsequent binding of the sc-uPA·uPAR-complex consistent with the fact that the binding of PAI-1 and uPAR to VN are mutually exclusive and that the affinity of PAI-1 for VN is higher that the affinity of uPAR for VN[131]. In contrast, uPAR in the presence of tc-uPA bound very efficiently to VN surfaces pre-saturated with PAI-1, consistent with the agonistic effect of the uPA·PAI-1 complex.

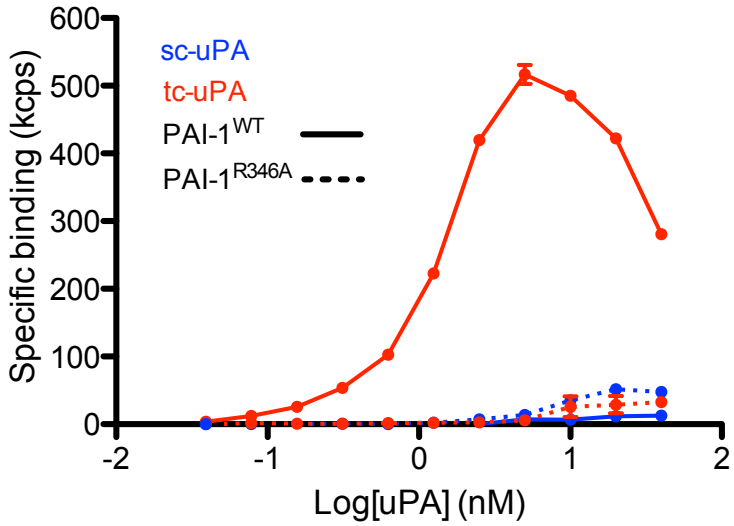

Figure 55: Complex formation between uPA and PAI-1 is required to promote uPAR binding to VN. 96-well immunoplates were coated with VN and saturated with PAI-1 or PAI-1^{R346A} mutant and washed extensively. Wells were added a fixed concentration of uPAR-Fc mixed with a dilution curved of sc-uPA or tc-uPA as indicated. Bound uPAR-Fc was detected as described in the legend to Figure 53. Dots represent means ± SD of a representative experiment.

The inactivation of uPA by PAI-1 involves major conformational changes in the inhibitor that results in a complete loss of binding activity towards VN[184]. The inhibition hereby causes the dissociation of PAI-1 from VN, liberating the SMB-domain and possibly allowing for the binding of uPAR. As only catalytically active tc-uPA reacts with PAI-1[185], the difference in binding of uPAR to PAI-1 saturated VN induced by sc-uPA and tc-uPA may thus be accounted for PAI-1 dissociation induced only by tc-uPA. To address this hypothesis directly, we repeated the binding experiment using a PAI-1 variant carrying a

RCL mutation (PAI-1^{R346A}) that prevents its interaction with tc-uPA[48], but maintain normal binding to VN[132]. Consistent with the hypothesis, the pre-incubation of VN with PAI-1^{R346A} prevented the subsequent binding of uPAR loaded not only with sc-uPA, but also with tc-uPA (Fig. 55).

Dissociation of PAI-1 from VN is required to liberate the binding site for uPAR. To test this in our *in vitro* setting, we repeated the experiments using an active site mutant uPA (tc-uPA^{S356A}) that binds PAI-1, but fails to hydrolyze the RCL of PAI-1. As RCL cleavage is the event that triggers the conformational change in PAI-1, this mutant should therefore not dissociate PAI-1 from VN and consequently not liberate the binding site for uPAR. Nevertheless, the tc-uPA^{S356A} mutant was a potent inducer of uPAR binding to VN coated surfaces incubated with PAI-1 (Fig. 56). This could be due to the existence of a quaternary complex intermediate, uPAR·uPA·PAI-1·VN, that transiently connects uPAR to VN even if the two molecules do not touch each other. The half-life of this quaternary complex is expected to be short, as the reaction of uPA with PAI-1 rapidly leads to the disassociation of the latter from VN. As tc-uPA^{S356A} binds to PAI-1, but fails to induce its dissociation from VN, the linear quaternary complex (uPAR·uPA^{S356A}·PAI-1·VN) may be stable and provide the link between uPAR and VN (see cartoon Fig. 60).

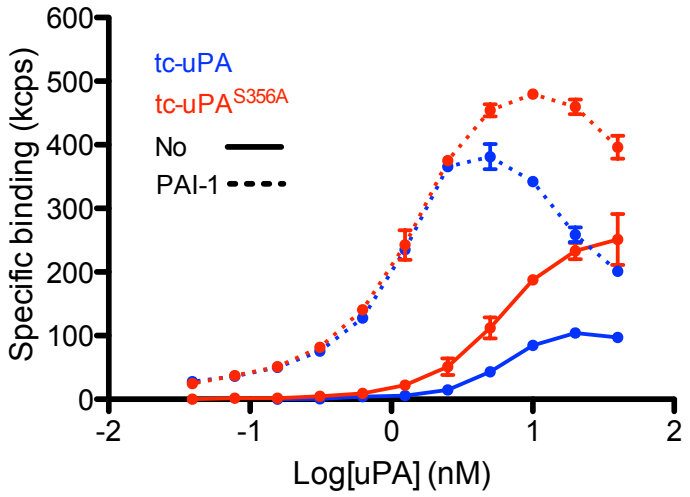

Figure 56: Pre-incubation of VN with PAI-1 increases subsequent uPAR binding induced by uPA and the catalytic activity of uPA is dispensable.

VN-coated wells were saturated with PAI-1 or left untreated (no) and incubated with a fixed concentration of uPAR-Fc (10 nM) mixed with a dilution curve of tc-uPA or an uPA variant (tc-uPA^{S356A}) which does bind PAI-1, but lacks catalytic activity. Binding of uPAR to VN was quantified as for Fig. 53. Dots represent means ± SD of a representative experiment.

A hallmark difference between the linear (uPAR·uPA·PAI-1·VN) and the branched (VN·uPAR·uPA·PAI-1) quaternary complexes is the requirement for direct uPAR binding to VN. In fact only for the branched complex, this interaction should be important. To test this prediction, we conducted binding assays using a receptor mutant (uPAR$^{W32A/R91A}$) that displays a complete and specific deficiency in VN binding[186]. Consistent with the model, this mutant readily supported tc-uPA^{S356A} induced uPAR binding to PAI-1 treated VN coated surfaces, but not VN binding induced by tc-uPA^{WT} (Fig. 57).

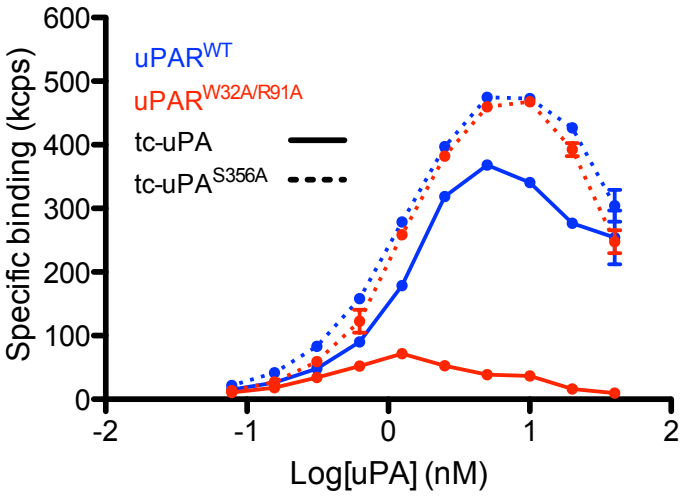

Figure 57: The VN binding site is required for tc-uPA mediated uPAR binding and dispensable for tc-uPA^{S356A} induced binding.

VN-coated wells were saturated with PAI-1 and incubated with a fixed concentration of uPAR-Fc or uPAR$^{W32A/R91A}$-Fc mixed with a dilution curve of tc-uPA or tc-uPA^{S356A} as indicated. Binding of uPAR-Fc variants to VN was measured as for Fig. 53. Dots represent means ± SD of a representative experiment.

Control experiments confirmed that the uPAR$^{W32A/R91A}$ variant is indeed VN-binding deficient as no or little binding to VN was observed with this receptor variant (Fig. 58). As shown above, the VN-binding of uPAR^{WT} observed in the presence of the uPA·PAI-1 complex the is superior to the binding observed in the presence of sc-uPA confirming the super-agonistic activity of the uPA·PAI-1 complex also in this assay.

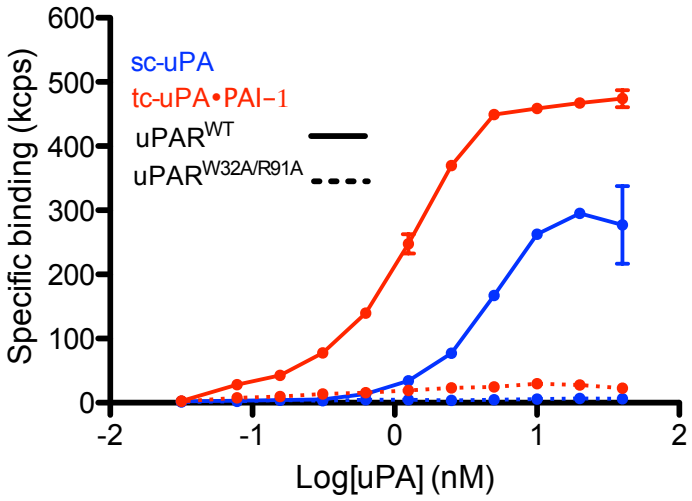

Figure 58: The VN binding site in uPAR is required for both sc-uPA and uPA·PAI-1 induced VN binding.

Constant concentrations of uPAR-Fc and uPAR$^{W32A/R91A}$-Fc were mixed with dilution curves of sc-uPA and uPA·PAI-1 complex and added to VN coated wells. uPAR binding to VN was measured as described for Fig. 53. Dots represent means ± SD of a representative experiment.

As we found that receptor binding to VN in the presence of uPA·PAI-1 is mediated almost exclusively by the VN binding site in uPAR, the model also predicts that the VN-binding site in PAI-1 should be dispensable. To verify this, we measured the binding of uPAR to VN in the presence of tc-uPA and a PAI-1 mutant (PAI-1$^{R103A/M112A/Q125A}$) that displays normal reactivity with uPA, but completely fails to bind VN[187]. In these experiments (Fig. 59), we found that PAI-1 and PAI-1$^{R103A/M112A/Q125A}$ are equally efficient in inducing uPAR binding to VN demonstrating that the main VN binding site in PAI-1, involving residues Arg103, Met112 and Gln125, does not contribute to the VN binding activity of the uPAR·uPA·PAI-1 complex.

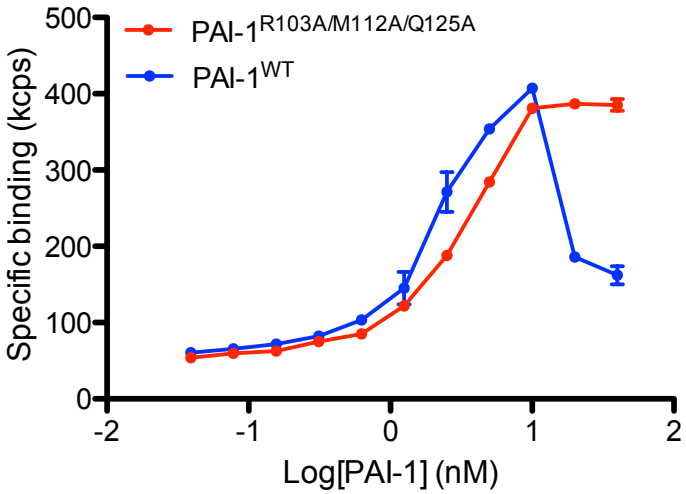

Figure 59: The VN binding site in PAI-1 is dispensable for the super-agonistic activity of the uPA·PAI-1 complex in inducing uPAR binding to VN.

Constant concentrations of uPAR-Fc (10 nM) was mixed with a constant concentration of tc-uPA (5 nM) and a dilution curve of PAI-1 WT or mutant. The mixtures were added to VN coated wells and uPAR binding measured as described for Fig. 53. Dots represent means ± SD of a representative experiment.

Taken together these data unequivocally demonstrate the mechanism outlined in Fig. 60, in which the complex formation by uPA and PAI-1 promotes uPAR binding to VN, through a series of discrete binding and dissociation reactions.

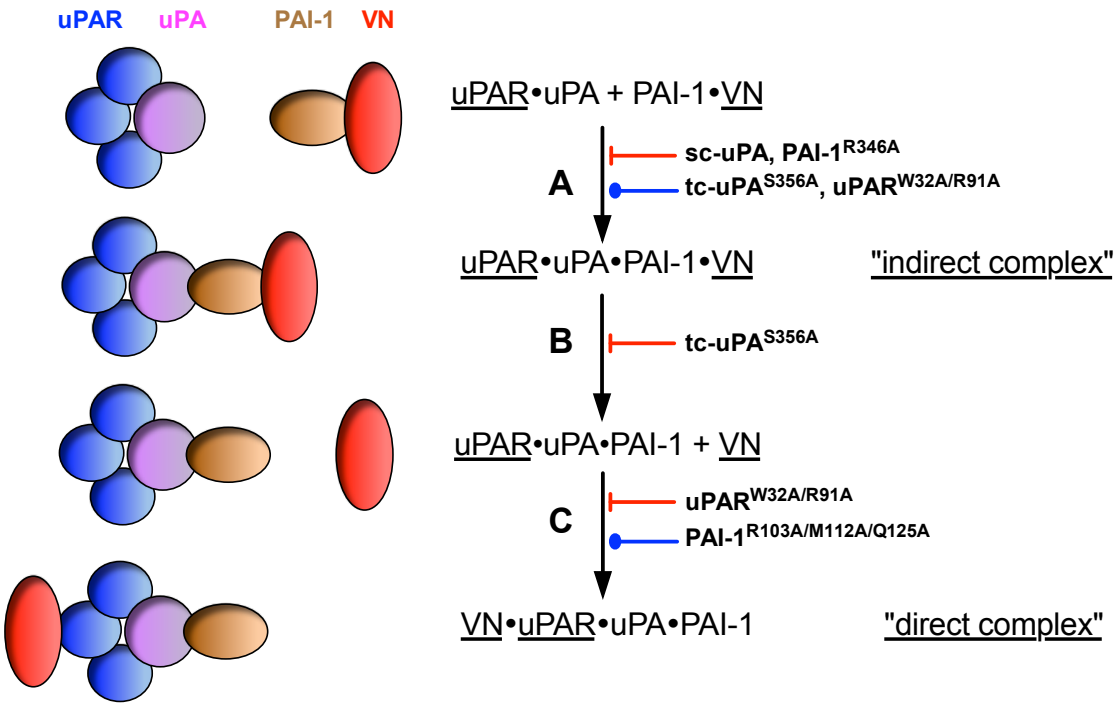

Figure 60: Cartoon depicting the mechanism responsible for uPAR binding to VN mediated by complex formation between uPA and PAI-1.

Active uPA (i.e. tc-uPA) bound to uPAR reacts with VN-bound PAI-1 to generate a linear quaternary complex ("indirect complex"). This complex formation (reaction A) requires interactions between uPA and PAI-1 as both sc-uPA and PAI^{R346A} mutant fail to support binding (Fig. 55). The formation of this complex does not involve the catalytic activity of uPA (Fig. 56) or the VN binding site in uPAR (Fig. 57). As PAI-1 is released from VN when it reacts with uPA the linear quaternary is instable (reaction B), however, the dissociation is blocked by catalytically inactive uPA (tc-uPA^{S356A}) (Fig. 57). Dissociation of the uPAR·uPA·PAI-1 from VN liberates the uPAR binding site in VN and is therefore followed by the generation of branched "direct complex" mediated by a direct interaction between uPAR and VN (Fig. 58). The VN binding site in PAI-1 is not involved for the generation of this complex (Fig. 59).

Our data document the mechanism by which complex formation between uPA and PAI-1 promotes uPAR binding to VN, however, they do not explain why the apparent affinity and capacity of uPAR binding to VN is higher when in complex with uPA·PAI-1 as compared to uPA. It is reasonable to assume that yet-to-be-described protein-protein interactions present in the quaternary VN·uPAR·uPA·PAI-1 complex, but absent in the VN·uPAR·uPA complex, are responsible for the increased binding. However, to our best

knowledge there are no well-documented interactions described in the literature and a systematic experimental approach will therefore be required to determine the structural basis for the increased stability.

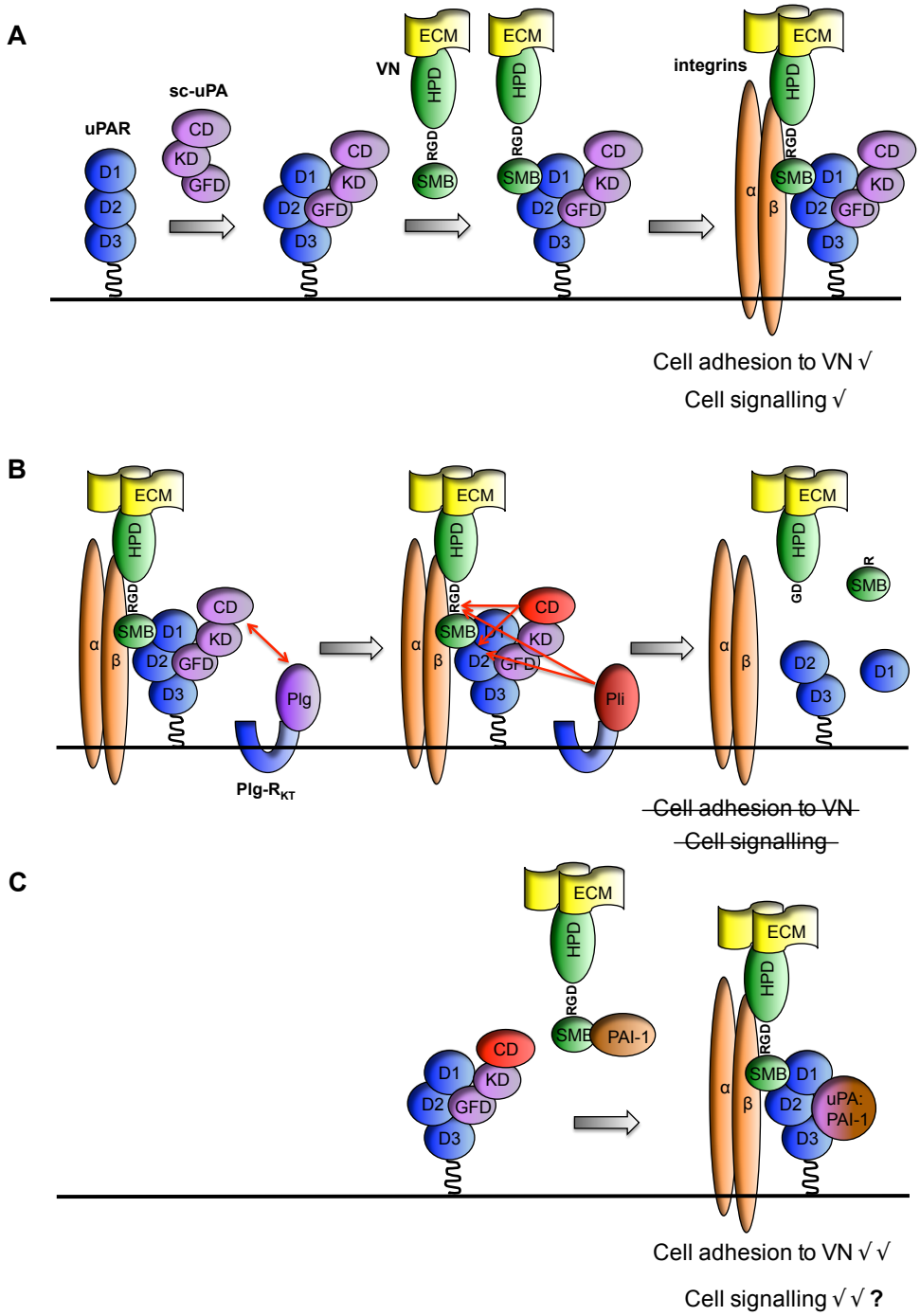

Figure 61: Cartoon illustrating the molecular mechanism of the cross-talk between plasminogen activation and cell adhesion to VN.

(A) Binding of sc-uPA to uPAR alters the conformation of the receptor increasing its affinity for VN. Binding of uPAR to VN in the ECM promotes cell adhesion and the contact between integrin receptors and the RGD-motif of VN. (B) uPAR-bound sc-uPA is prone to activation by other membrane associated serine proteases including Pli and once it becomes activated it will revert cell adhesion by proteolytic inactivation of the RGD-motif in VN as well as by cleavage of uPAR. (C) PAI-1 counteracts the negative feedback and behaves as a uPA-dependent super-agonist of the uPAR-VN interaction.

7. DISCUSSION

7.1 NEGATIVE FEEDBACK BETWEEN uPAR INDUCED EXTRACELLULAR PROTEOLYSIS AND CELL ADHESION TO VN

We here report that the proteolytic activities of uPA and Pli exert a major negative feedback on integrin- and uPAR-mediated cell adhesion on VN. We show that uPA and Pli inactivate the adhesive activities of VN predominantly through cleavage of the ^{45}R↓G peptide bond in the N-terminal region of the molecule. Proteolysis at this position directly inactivates the ^{45}RGD-motif responsible for integrin binding and results in the separation of the uPAR and PAI-1 binding determinants, located in the N-terminal SMB domain, from the connecting region and hemopexin-like repeats responsible for the tethering of VN to the ECM (Fig. 61B).

7.1.1 uPAR cleavage

As previously hypothesized[158], the proteolytic feedback is partially mediated by uPA/Pli catalyzed proteolytic inactivation of uPAR, but this mechanism appears to be quantitatively less important than the direct cleavage of VN. The fact that the cleavage of the anchoring receptor (i.e. uPAR) responsible for the high adhesion of 293/uPAR cells to VN is of little importance is somehow unexpected. A possible explanation has been given by a recent study in which it has been shown, using surface plasmon resonance, that the complex between the D1 of uPAR and sc-uPA displays a high affinity binding to immobilized D2D3[188]. As a consequence, the cleavage of uPAR in the D1-D2 linker region may not result in a fast dissociation of D1, leaving a VN-binding competent receptor on the cell surface.

7.1.2 VN cleavage

Pli has been previously shown to cleave VN at multiple locations in the central and C-terminal regions of the protein[11, 177] and cleavage in or close to the RGD-motif has been reported for other enzymes. The serine protease granzyme B, released by cytotoxic T-cells, has been shown to cleave VN immediately downstream of the RGD-motif (^{45}RGD↓V)[189] and the cancer-related serine protease tissue kallikrein 14 has been shown to cleave within the RGD-motif (^{45}R↓GDV)[190] at the same location reported for uPA and Pli here. In addition, it has also been reported that members of the MMPs family cleave VN in more C-terminal regions[191, 192].

Treatment of VN with Pli has been shown to prevent subsequent $\alpha_v\beta_5$-mediated adhesion of the keratinocyte cell line HaCaT[178], however if VN was actually cleaved, and where, was not addressed in the study. uPAR-dependent cell surface plasminogen activation has also been shown to cause the retraction of cultured human umbilical vein endothelial cell monolayers[175], but whether this effect was mediated by cleavage of VN was not addressed. The evidence presented here clearly provides an appealing mechanism by which these observations may be explained at the molecular level.

7.1.3 uPAR "catalyzes" the cleavage of VN mediated by uPA

In contrast to Pli, uPA is endowed with very narrow substrate specificity. Only two substrates (i.e. Plg and uPAR) have been carefully characterized and, in addition, PAI-1 may be considered as a peculiar uPA substrate. We here identify VN as a novel and the first described uPAR-dependent substrate for uPA. Indeed, the cleavage of VN by uPA is dependent upon uPAR both *in vitro*, using purified proteins, as well as in cell culture suggesting that uPAR catalyzes the cleavage reaction by a mechanism of substrate presentation in which the receptor coordinates the protease (uPA) and the substrate (VN) in

a ternary complex in which the hydrolysis reaction is greatly favoured. We have estimated that the presence of uPAR accelerates the cleavage of VN mediated by uPA more than 300 times. However, the use of immobilized VN as substrate does not allow us to calculate kinetics parameters such as K_m, V_{max} and K_{cat}. To this end, a fluorophore/quencher approach may be employed, by preparation of short labelled recombinant VN variant (e.g. VN(1-61)).

7.1.4 Cancer cells lines release SMB-containing fragments in vitro

Using the NCI-60 panel of cancer cell lines, we have shown that VN fragments are released also by cells expressing patho-physiological uPAR levels.

In the absence of exogenous Plg, only the human promyelocytic leukemic HL60 cells were capable of efficiently release N-terminal VN fragments. Remarkably, this cell line is the one in the panel that expresses the highest levels of neutrophil elastase and Plg, indicating a possible role of these proteases in the cleavage of VN. In contrast to Pli, no cleavage sites are known for neutrophil elastase in VN. However, it has been reported that neutrophil elastase can increase fibrinolysis through cleavage and inactivation of PAI-1[193] as well as through the conversion of Glu-Plg to the more susceptible form Lys-Plg[194].

In the presence of Plg, the release of VN fragments is significantly increased in several cancer cell lines belonging to all the cancer types present in the panel, with the exception of leukemic cell lines. Remarkably, the levels of fragment release in the cancer cell lines with epithelial origin is highly correlated with *PLAU* expression levels, clearly identifying a strong connection between uPA expression and the ability of cells to cleave VN. Since uPA levels are a well-known marker of poor prognosis, this finding corroborates the idea that N-terminal VN fragments may have similar prognostic value, at least for epithelial cancers.

Despite the highly significant correlation between uPA expression levels and the extent of VN fragments release in epithelial cancer cell lines (rank = 2, r = 0.57, p < 0.0001, Fig. 37A), the expression of uPAR gene is not significantly correlated with VN fragments release (r = 0.03, p = 0.85, Fig. 37B). This finding is clearly not in accordance neither with our experiments performed with uPAR-overexpressing cells and with purified proteins *in vitro* nor with fact that uPAR should be a central regulator of cell surface plasminogen activation. We currently have no explanation for this finding. One possibility is that uPA cell surface receptors different from uPAR are relatively more important. Another possible explanation is that the long Plg incubation performed in the experiments (16 h) has allowed free uPA to activate cell surface Plg, despite the low catalytic efficiency of uPA when present in solution-phase[109].

7.1.5 Implications and future perspectives

It is widely believed that the function of uPAR in extracellular proteolysis is to accelerate plasminogen activation and to localize the activated proteases on the cell surface. The data presented here show that matrix VN is a substrate for these membrane-associated proteolytic enzymes. While Pli is crucial for fibrin surveillance *in vivo*[113], the only process that has been well-documented to require the binding of uPA to uPAR *in vivo* is the suppression of inflammation secondary to fibrin deposition[115]. We propose that while Pli is responsible for the resolution of fibrin deposits in the provisional matrix subsequent to tissue injury, the primary function of uPAR/uPA may be to bind and promote the focused resolution also of the VN component present in these lesions.

Experiments with cells expressing physiological levels of uPAR will give us more hints to hypothesize about the possible functional relevance of VN cleavage. On the one hand, we are currently exploiting the NCI-60 panel to perform a correlative analysis as already done for the SMB release. On the other hand, migration, chemotaxis and invasion experiments

using cancer cell lines, leukocytes or fibroblasts may also give important indications. However, the localization of the uPA and Pli cleavage site in VN represents a major issue to perform such structure-function experiments. Indeed, it is currently not possible to block the cleavage of VN (i.e. using the ^{45}R→A mutation in VN) without also blocking integrin binding. As integrins are predominantly responsible for cell adhesion to VN, virtually all the cell lines will adhere poorly to VN variants carrying mutations in the RGD motif. The use of mixed coating (e.g. VN plus FN or collagen embedded with the different VN variants) may represent a possible solution to this problem and also provide a more physiological matrix compared to the single purified components.

Finally, future studies with knock-in animals may shed light on the *in vivo* relevance of the VN cleavage. VN$^{-/-}$ mice are viable and fertile with no major phenotypes[195], therefore the introduction of single amino acid substitution in the VN gene is not expected to result in severe phenotypes. However, VN$^{-/-}$ mice display detectable phenotypes when challenged with external insults. Indeed, the mice display impaired leukocytes recruitment at site of inflammation and ischemia[196] and a slight delay in skin wounds closure[197]. Comparing knock-in animals, bearing the ^{45}R→A and the ^{46}G→A substitution or the intact RGD, may reveal a role of the cleavage of VN in these processes. We have recently shown that VN and specifically the uPAR-VN interaction plays an important role in tumour growth *in vivo*[182]; similar experiments with the VN mutants knock-in animals may contribute to further characterize the role of VN, and VN cleavage, in tumour progression and dissemination.

7.3 SMB-CONTAINING FRAGMENTS ARE PRESENT *IN VIVO*

We here show that SMB-containing N-terminal VN fragments are present in human urines. Three different species, corresponding to VN(1-41), VN(1-42) and VN(1-44) are readily detected and present at variable relative concentrations in all urine samples analyzed so far

(Fig. 39 and data not shown). Preliminary data on urines of cancer patients show no qualitative difference in the fragment pattern of cancer patients compared to healthy volunteers.

These fragments may derive from longer precursors, such as VN(1-45), further trimmed by carboxypeptidases present in the blood circulation as well as in urines. In particular, a specific subgroup of carboxypeptidases, called carboxypeptidases B (basic), is composed of proteases that specifically cleave C-terminal basic residues (i.e. Lys and Arg). They could account for the absence of the VN(1-45) fragment, whose terminal Arg residue might be readily removed by such enzymes. The thrombin-activatable fibrinolytic inhibitor (TAFI) may represent an interesting candidate. Indeed, TAFI is a metallocarboxypeptidase that removes C-terminal basic residues. It is present in the blood stream and activated by thrombin in the coagulation cascade as well as by Pli in the fibrinolytic process[198].

The smallest fragment detected is VN(1-41). Remarkably, the residue 41 of VN is a Pro. Among the 21 amino acids, Pro is the only secondary amine and its peculiar structure makes peptide bonds with Pro as P1' residue resistant to proteolysis. Specific prolyl carboxypeptidases remove C-terminal residues adjacent to a Pro, but they do not remove Pro residues. This may explain why we do not observe shorter fragments in urine samples.

Similar N-terminal VN fragments have previously been described. Indeed, the SMB domain was discovered in the 1970's as a circulating peptide in human plasma[199, 200]. The presence of additional N-terminal VN fragments in hemofiltrates of patients with end stage renal disease has also been reported[201]. In addition to VN(1-44), other three molecular species, i.e. VN(1-48), VN(1-49) and VN(1-50), have been described. We do not observe such fragments in our samples, even if their molecular weight (less than 5.7 kDa) would allow their filtration in the urinary compartment. This may suggest that the accumulation of those fragments in the circulation is peculiar of patients with kidney disease and therefore not present in the blood of healthy individuals or cancer patients. Alternatively, these fragments, even if present in the blood stream, may be further digested in the urines

and therefore not detected in our MALDI spectra. Moreover, the absence of VN(1-41) and VN(1-42) fragments in the hemofiltrates[201] may indicate that the removal of Gln42, Val43 and Thr44 is specifically catalyzed by urinary carboxypeptidases.

The presence of SMB-containing peptides in human urines has also been previously documented[202]. SMB immunoreactivity was observed in the urines of 8 adult healthy individuals. Notably, the 85.9% of the SMB present in urines is found in a "free" form, whereas the SMB present in the plasma of the same subjects is described as almost completely (more than 95%) "bound to serum proteins". We know now that the SMB is the N-terminal domain of VN but, when this study was performed, VN had not been characterized yet. These findings are therefore consistent with our data (Fig. 38), which show that about the 90% of the SMB-containing antigen present in urine samples represents short N-terminal VN fragments, while in blood samples virtually 100% of the signal is given by longer fragments, presumably the full length VN.

7.4 THE USE OF N-TERMINAL VN FRAGMENTS AS CANCER BIOMARKER

High levels of uPAR and/or uPA/PAI-1 have been shown to have a strong prognostic value in several carcinomas, including breast, lung, colon and gastric cancers. In particular, uPA and PAI-1 levels in breast tumour tissues are, together with *ERBB2*-status, the only novel breast cancer biomarkers to be fully supported by the highest level of evidence (LOE-1) of clinical utility[203, 204]. Indeed, it has been shown that node negative breast cancer patients can be stratified using uPA/PAI-1 levels in tumour extracts: low levels indentify a low risk group having a very good prognosis, whereas patients with high levels of uPA/PAI-1 display higher relapse risk and derive significant benefit from an adjuvant chemotherapy regimen. The use of uPA and PAI-1 has been included in the 2007 update of the American Society of Clinical Oncology recommendations for clinical decision-making in node-negative breast cancer patients. Nevertheless, the use of these biomarkers is not

widespread mainly for the logistic limitation of requiring fresh-frozen specimens, which may be not available in all hospitals.

We here propose the use of urinary N-terminal VN fragments as a novel cancer biomarker. The idea stems from previous work done in the lab in which we have shown that the interaction between uPAR and VN plays a pivotal role in tumour growth *in vivo*[182]. Since efficient VN cleavage requires this interaction, our hypothesis is that the levels of VN fragments in urine samples may represent a novel biomarker in cancer patients, as a surrogate for the activity of the plasminogen activation system in the tumour tissue. Potential uses may be prognosis (i.e. high levels of urinary VN fragments might correlate with a poor prognosis) and patient stratification. At present, despite all the evidences linking the uPA-system with cancer, no targeted therapy against components of the uPA-system is available for cancer patients. uPAR inhibitors and specifically inhibitors of the uPAR-VN interaction have been developed in our lab and are currently undergoing extensive pre-clinical studies. In view of an anti-uPAR therapy, our immunoassay may represent a suitable tool for patient stratification, to select patients more likely to respond, as well as for non-invasive monitoring of the response to therapy.

The nature of the specimen required (i.e. early morning urine) clearly facilitates the use of this biomarker compared to uPA/PAI-1. However, it also implies some limitations, for instance it can not be used for patients with kidney disease who suffer from proteinuria, as high levels of full length VN are likely to be present in the urines of such patients. Similarly, follow-up measurements of urinary VN fragments will not be possible in patients subjected to therapy associated with nephrotoxicity side-effects (e.g. some chemotherapeutics). In addition, enzymes such granzyme B[189] and tissue kallikrein 14[190] have been reported to cleave VN *in vitro* close or within the RGD motif of the protein, thus potentially generating VN fragments similar to those generated by uPA and Pli. These fragments would be detected by our immunoassay and might therefore represent a signal not related to the uPA-system activity in the tumour tissue. Possibly, some of these issues

may be overcome by developing an immunoassay specific for the VN(1-44) fragments, which therefore would allow the analysis of blood samples.

A small exploratory study on breast cancer patients' urine samples is already planned. We will analyze urine samples of newly diagnosed primary breast cancer patients, with the objective of evaluating the basic parameters of urinary VN fragments. Correlation analyses between VN fragments urinary levels and standard clinical-pathological parameters (e.g. age, tumour size, number of lymph nodes involved and hormone receptor and *ERBB2* status) will be performed to evaluate the feasibility of larger future studies.

7.5 VALIDATION OF THE HU3/HF6 IMMUNOASSAY

Our immunoassay for the detection of SMB-containing VN fragments is based on a sandwich-type TR-FIA. Two monoclonal antibodies, with non-overlapping epitopes within the SMB domain of VN, are used for the capturing (HU3) and the detection (HF6) of the antigen. This design is clearly not specific for VN fragments and therefore prevents us from measuring such fragments in serum or plasma samples that are rich in VN. Hence, we focused on urine samples where the SMB antigen signal is mainly given by short N-terminal fragments (shorter that 1-65, Fig. 38).

A robust validation of the assay is a key aspect for a biomarker success. To this end, we have assessed a number of assay parameters to optimize the assay and evaluate its overall quality (Fig. 40-45). The assay exhibits a large dynamic range and linearity range and high sensitivity (detection limit in the femtomolar range). The precision (in term of CV) in repeated analyses of calibrator samples is expected to vary less than 25-30% in ELISA-based measurements of macromolecules[205]. The variability, both intra- and inter-day, was found to be less than 5% and 15% respectively, thus indicating that our immunoassay is indeed highly reproducible and precise. Since an analyte-free matrix is non available (i.e. SMB depleted human urines), the standard curve is prepared in dilution buffer (i.e. PBS +

0.1% Tween). To specifically test whether the difference between the diluent and the sample matrix may affect the assay results, we performed spike-in experiments and found that the analyte recovery is virtually 100% in all four calibrators samples. Finally, we assessed the stability to storage and freezing/thawing cycles of the VN fragments in urine samples. Results show a high stability with little variability associated with the different storage conditions. Taken together, these data clearly indicate that the HU3/HF6 immunoassay has very good performance characteristics and can be employed to reliably measure N-terminal VN fragments in human urine samples. Depletion and mass spectrometry experiments are still missing to complete the validation process.

A key characteristic of a biomarker is the constancy under normal physiological conditions. Urinary levels of the VN fragments showed little fluctuations when normalized on the creatinine concentration, particularly when analyzing early morning urine samples. However, the analysis of healthy volunteers samples also showed quite high basal levels (around 50 nM) compared for instance with suPAR levels in urines, which are in the picomolar range[206]. As a consequence, detecting eventual increases due to pathological conditions might be problematic.

7.6 THE uPA·PAI-1 COMPLEX IS A SUPER-AGONIST OF THE uPAR/VN INTERACTION

We here report that PAI-1 counteracts the negative feedback mediated by uPA and Pli and behaves as a proteolysis-dependent super-agonist of the uPAR-VN interaction (Fig. 61C). Indeed, PAI-1, in the absence of active uPA, inhibits uPAR-mediated cell adhesion by competing for the binding to the SMB domain of VN. On the other hand, we have shown that the complex formation between tc-uPA and PAI-1 results in a potent agonistic effect on the uPAR-VN interaction and cell adhesion to VN, which is stronger than the effect mediated by sc-uPA. Using purified components *in vitro*, we have shown that this strong

induction does not involve proteins other than uPA, uPAR, PAI-1 and VN. We have characterized the mechanism of the uPA·PAI-1 complex formation and shown the existence of a quaternary intermediate uPAR·uPA·PAI-1·VN. However, at the moment, we do not know the structural basis of the increased affinity of uPAR for VN induced by the uPA·PAI-1 complex. Indeed, the uPA·PAI-1 complex induces uPAR binding to VN with a much lower EC_{50} compared to sc-uPA. Unexpectedly, the complex also displays a double B_{max} compared to sc-uPA. The B_{max} is a measure of the number of binding sites present in the well and therefore should be identical as the VN coating was not changed between the two conditions. This suggests that the difference between the two ligands may be due to an increased stability of the PAI-1·uPA·uPAR·VN complex compared to the sc-uPA·uPAR·VN complex. The VN-binding epitope in uPAR seems to be the same in the presence of the different ligands, as mutation of the Trp32 and Arg91 is sufficient to abrogate both sc-uPA and complex induced binding to VN. However, further experiments are needed to clarify this issue.

7.6.1 Future investigations

Our data are preliminary and many aspects still need to be addressed. Some are briefly described below.

PAI-1 has three potential N-glycosylation sites, with only two that are actually utilized (N209 and N265)[207]. The basic serpin inhibitory mechanism is not different between glycosylated and non-glycosylated PAI-1 (for instance, they display virtually identical second rate constant for the reaction with uPA). However, the presence of glycosylations has been shown to affect latency transition rate and binding to different monoclonal antibodies[207]. It has been suggested that glycans, at both positions, may establish several hydrogen bonds and hydrophobic interactions with the surrounding amino acids, thus changing the conformation of those regions of the protein. Since in our experiments, we

have employed recombinant PAI-1 expressed in *E. coli* and therefore lacking glycosylations, it will be important to confirm the super-agonist behaviour of the uPA·PAI-1 complex using PAI-1 expressed in eukaryotic cells such as HEK293 cells.

It is well-known that uPAR-bound uPA·PAI-1 complex is endocytosed by several members of the LDLR family, including LRP-1A, LRP-1B and VLDLR (reviewed in [49]). In the HEK293 Flp-In cells, these proteins are not or poorly expressed, as determined by microarray analysis performed in our lab. One important point will be to assess whether these endocytic receptors are still capable to internalize the PAI-1·uPA·uPAR complex, when it is engaged with VN. On the other hand, it will be important to test the effect of uPA·PAI-1 treatment on cells with endogenous uPAR and LDLR.

Other serpins have been shown to inhibit uPA *in vitro*. Testing the ability of such complexes (e.g. uPA·PAI-2 and uPA·PN-1) to induce uPAR binding to VN in binding experiments may clarify whether the super-agonist properties are peculiar of the uPA·PAI-1 complex or a more general characteristic of the uPA·serpin complexes. This could also help in understanding the structural basis of such high affinity.

7.6.2 Implications

Historically, the uPA-system has been firstly linked with the promotion of pericellular proteolysis. The detection of uPA and uPAR at the invasive front of tumours[74, 75] has further substantiated the notion that uPA is involved in cancer cell migration and dissemination. The specific uPA inhibitor, PAI-1, was therefore expected to be a marker of favourable outcome for cancer patients. On the contrary, PAI-1 clearly emerged as a potent prognostic marker of poor clinical outcome. Moreover, the combined assessment of uPA and PAI-1 was found to provide even superior prognostic information than either molecule alone[208]. This represents the so-called “uPA/PAI-1 paradox”.

A partial answer to this paradox has been given by the finding that the uPA-system exerts biological functions that are independent of the catalytic activity of uPA and mediated through the interaction with proteins in the pericellular space, such as VN, and the initiation of intracellular signalling. In this context, uPA and PAI-1 may have different and non-opposing functions.

The finding that the uPA·PAI-1 complex is a super-agonist of the uPAR/VN interaction provides a possible mechanistic explanation to the paradox. uPA and PAI-1 have opposite effects on uPAR-mediated adhesion to VN, when considered individually. The former is a well-established inducer of the uPAR/VN interaction[122, 126], whereas the latter competitively inhibits the binding of uPAR to the SMB domain of VN[102]. In sharp contrast, the formation of the covalent complex between uPA and PAI-1 blocks these opposing effects and empowers the two molecules with potent agonistic properties.

Since the uPAR/VN interaction has been shown to be necessary and sufficient to activate p130Cas and ERK pathways[125, 137], the formation of the uPA·PAI-1 complex and the subsequent induction of the uPAR-binding to VN may be responsible for the triggering of migratory and mitogenic signals involved in tumour progression.

Remarkably, the levels of the uPA·PAI-1 complex in tumour extracts have been shown to have independent prognostic as well as predictive values in breast cancer patients. Specifically, high levels of the complex correlate with poor prognosis in lymph node negative breast carcinomas[209] and predict response to adjuvant systemic therapy in primary breast cancers[210] as well as to endocrine therapy in advanced breast cancers[211]. Since, the formation of the complex requires active uPA and PAI-1, the authors suggest that the assessment of the complex levels may be a functional measurement of the active uPA and PAI-1 present in the tumour tissue and therefore provides more meaningful information compared to total PAI-1/uPA. We propose that the complex between uPA and PAI-1 is not only a measure of a past activity but is importantly endowed with peculiar characteristics

(i.e. super-agonist activity on the uPAR-mediated adhesion to VN) that directly contribute to the malignant phenotype.

8. REFERENCES

1. Puente, X.S., Sanchez, L.M., Overall, C.M. & Lopez-Otin, C. Human and mouse proteases: a comparative genomic approach. *Nat Rev Genet* 4, 544-558 (2003).

2. Raum, D. *et al.* Synthesis of human plasminogen by the liver. *Science* 208, 1036-1037 (1980).

3. Zhang, L. *et al.* Plasminogen has a broad extrahepatic distribution. *Thromb Haemost* 87, 493-501 (2002).

4. Robbins, K.C., Summaria, L., Hsieh, B. & Shah, R.J. The peptide chains of human plasmin. Mechanism of activation of human plasminogen to plasmin. *J Biol Chem* 242, 2333-2342 (1967).

5. Lyons, R.M., Gentry, L.E., Purchio, A.F. & Moses, H.L. Mechanism of activation of latent recombinant transforming growth factor beta 1 by plasmin. *J Cell Biol* 110, 1361-1367 (1990).

6. Taipale, J., Koli, K. & Keski-Oja, J. Release of transforming growth factor-beta 1 from the pericellular matrix of cultured fibroblasts and fibrosarcoma cells by plasmin and thrombin. *J Biol Chem* 267, 25378-25384 (1992).

7. Saksela, O. & Rifkin, D.B. Release of basic fibroblast growth factor-heparan sulfate complexes from endothelial cells by plasminogen activator-mediated proteolytic activity. *J Cell Biol* 110, 767-775 (1990).

8. Whitelock, J.M., Murdoch, A.D., Iozzo, R.V. & Underwood, P.A. The degradation of human endothelial cell-derived perlecan and release of bound basic fibroblast growth factor by stromelysin, collagenase, plasmin, and heparanases. *J Biol Chem* 271, 10079-10086 (1996).

9. Matsuoka, H., Sisson, T.H., Nishiuma, T. & Simon, R.H. Plasminogen-mediated activation and release of hepatocyte growth factor from extracellular matrix. *Am J Respir Cell Mol Biol* 35, 705-713 (2006).

10. Liotta, L.A. *et al.* Effect of plasminogen activator (urokinase), plasmin, and thrombin on glycoprotein and collagenous components of basement membrane. *Cancer Res* 41, 4629-4636 (1981).

11. Chain, D., Kreizman, T., Shapira, H. & Shaltiel, S. Plasmin cleavage of vitronectin. Identification of the site and consequent attenuation in binding plasminogen activator inhibitor-1. *FEBS Lett* 285, 251-256 (1991).

12. Deryugina, E.I. & Quigley, J.P. Cell surface remodeling by plasmin: a new function for an old enzyme. *J Biomed Biotechnol* 2012, 564259.

13. He, C.S. *et al.* Tissue cooperation in a proteolytic cascade activating human interstitial collagenase. *Proc Natl Acad Sci U S A* 86, 2632-2636 (1989).

14. Mazzieri, R. *et al.* Control of type IV collagenase activity by components of the urokinase-plasmin system: a regulatory mechanism with cell-bound reactants. *EMBO J* 16, 2319-2332 (1997).

15. Romer, J. *et al.* Impaired wound healing in mice with a disrupted plasminogen gene. *Nat Med* 2, 287-292 (1996).

16. Ploplis, V.A., French, E.L., Carmeliet, P., Collen, D. & Plow, E.F. Plasminogen deficiency differentially affects recruitment of inflammatory cell populations in mice. *Blood* 91, 2005-2009 (1998).

17. Wiman, B. & Collen, D. Purification and characterization of human antiplasmin, the fast-acting plasmin inhibitor in plasma. *Eur J Biochem* 78, 19-26 (1977).

18. Hall, S.W., Humphries, J.E. & Gonias, S.L. Inhibition of cell surface receptor-bound plasmin by alpha 2-antiplasmin and alpha 2-macroglobulin. *J Biol Chem* 266, 12329-12336 (1991).

19. Law, R.H. *et al.* The X-ray crystal structure of full-length human plasminogen. *Cell Rep* 1, 185-190.

20. Han, J. *et al.* Monoclonal antibodies detect receptor-induced binding sites in Glu-plasminogen. *Blood* 118, 1653-1662.

21. Miles, L.A., Dahlberg, C.M. & Plow, E.F. The cell-binding domains of plasminogen and their function in plasma. *J Biol Chem* 263, 11928-11934 (1988).

22. Felez, J. *et al.* Characterization of cellular binding sites and interactive regions within reactants required for enhancement of plasminogen activation by tPA on the surface of leukocytic cells. *Thromb Haemost* 76, 577-584 (1996).

23. Swaisgood, C.M., Schmitt, D., Eaton, D. & Plow, E.F. In vivo regulation of plasminogen function by plasma carboxypeptidase B. *J Clin Invest* 110, 1275-1282 (2002).

24. Miles, L.A. *et al.* Role of cell-surface lysines in plasminogen binding to cells: identification of alpha-enolase as a candidate plasminogen receptor. *Biochemistry* 30, 1682-1691 (1991).

25. Andronicos, N.M. *et al.* Proteomics-based discovery of a novel, structurally unique, and developmentally regulated plasminogen receptor, Plg-RKT, a major regulator of cell surface plasminogen activation. *Blood* 115, 1319-1330.

26. Lighvani, S. *et al.* Regulation of macrophage migration by a novel plasminogen receptor Plg-R KT. *Blood* 118, 5622-5630.

27. Cesarman-Maus, G. & Hajjar, K.A. Molecular mechanisms of fibrinolysis. *Br J Haematol* 129, 307-321 (2005).

28. Carmeliet, P. *et al.* Physiological consequences of loss of plasminogen activator gene function in mice. *Nature* 368, 419-424 (1994).

29. Kobayashi, H. *et al.* Cathepsin B efficiently activates the soluble and the tumor cell receptor-bound form of the proenzyme urokinase-type plasminogen activator (Pro-uPA). *J Biol Chem* 266, 5147-5152 (1991).

30. Lee, S.L., Dickson, R.B. & Lin, C.Y. Activation of hepatocyte growth factor and urokinase/plasminogen activator by matriptase, an epithelial membrane serine protease. *J Biol Chem* 275, 36720-36725 (2000).

31. Kilpatrick, L.M. *et al.* Initiation of plasminogen activation on the surface of monocytes expressing the type II transmembrane serine protease matriptase. *Blood* 108, 2616-2623 (2006).

32. Moran, P. *et al.* Pro-urokinase-type plasminogen activator is a substrate for hepsin. *J Biol Chem* 281, 30439-30446 (2006).

33. List, K. *et al.* Plasminogen-independent initiation of the pro-urokinase activation cascade in vivo. Activation of pro-urokinase by glandular kallikrein (mGK-6) in plasminogen-deficient mice. *Biochemistry* 39, 508-515 (2000).

34. Nagamine, Y., Medcalf, R.L. & Munoz-Canoves, P. Transcriptional and posttranscriptional regulation of the plasminogen activator system. *Thromb Haemost* 93, 661-675 (2005).

35. Kawano, T., Morimoto, K. & Uemura, Y. Partial purification and properties of urokinase inhibitor from human placenta. *J Biochem* 67, 333-342 (1970).

36. Astedt, B., Lecander, I., Brodin, T., Lundblad, A. & Low, K. Purification of a specific placental plasminogen activator inhibitor by monoclonal antibody and its complex formation with plasminogen activator. *Thromb Haemost* 53, 122-125 (1985).

37. Scott, R.W. *et al.* Protease nexin. Properties and a modified purification procedure. *J Biol Chem* 260, 7029-7034 (1985).

38. Thorsen, S., Philips, M., Selmer, J., Lecander, I. & Astedt, B. Kinetics of inhibition of tissue-type and urokinase-type plasminogen activator by plasminogen-activator inhibitor type 1 and type 2. *Eur J Biochem* 175, 33-39 (1988).

39. Simpson, A.J., Booth, N.A., Moore, N.R. & Bennett, B. Distribution of plasminogen activator inhibitor (PAI-1) in tissues. *J Clin Pathol* 44, 139-143 (1991).

40. Hakkert, B.C., Rentenaar, J.M. & van Mourik, J.A. Monocytes enhance the bidirectional release of type I plasminogen activator inhibitor by endothelial cells. *Blood* 76, 2272-2278 (1990).

41. Samad, F., Yamamoto, K. & Loskutoff, D.J. Distribution and regulation of plasminogen activator inhibitor-1 in murine adipose tissue in vivo. Induction by tumor necrosis factor-alpha and lipopolysaccharide. *J Clin Invest* 97, 37-46 (1996).

42. Brogren, H. *et al.* Platelets synthesize large amounts of active plasminogen activator inhibitor 1. *Blood* 104, 3943-3948 (2004).

43. Brogren, H., Wallmark, K., Deinum, J., Karlsson, L. & Jern, S. Platelets retain high levels of active plasminogen activator inhibitor 1. *PLoS One* 6, e26762.

44. Andreasen, P.A. *et al.* Plasminogen activator inhibitor type-1: reactive center and amino-terminal heterogeneity determined by protein and cDNA sequencing. *FEBS Lett* 209, 213-218 (1986).

45. Ny, T., Sawdey, M., Lawrence, D., Millan, J.L. & Loskutoff, D.J. Cloning and sequence of a cDNA coding for the human beta-migrating endothelial-cell-type plasminogen activator inhibitor. *Proc Natl Acad Sci U S A* 83, 6776-6780 (1986).

46. Pannekoek, H. *et al.* Endothelial plasminogen activator inhibitor (PAI): a new member of the Serpin gene family. *EMBO J* 5, 2539-2544 (1986).

47. Ginsburg, D. *et al.* cDNA cloning of human plasminogen activator-inhibitor from endothelial cells. *J Clin Invest* 78, 1673-1680 (1986).

48. Sherman, P.M. *et al.* Saturation mutagenesis of the plasminogen activator inhibitor-1 reactive center. *J Biol Chem* 267, 7588-7595 (1992).

49. Dupont, D.M. *et al.* Biochemical properties of plasminogen activator inhibitor-1. *Front Biosci (Landmark Ed)* 14, 1337-1361 (2009).

50. Declerck, P.J., De Mol, M., Vaughan, D.E. & Collen, D. Identification of a conformationally distinct form of plasminogen activator inhibitor-1, acting as a noninhibitory substrate for tissue-type plasminogen activator. *J Biol Chem* 267, 11693-11696 (1992).

51. Hekman, C.M. & Loskutoff, D.J. Endothelial cells produce a latent inhibitor of plasminogen activators that can be activated by denaturants. *J Biol Chem* 260, 11581-11587 (1985).

52. Lindahl, T.L., Sigurdardottir, O. & Wiman, B. Stability of plasminogen activator inhibitor 1 (PAI-1). *Thromb Haemost* 62, 748-751 (1989).

53. Seiffert, D. & Loskutoff, D.J. Evidence that type 1 plasminogen activator inhibitor binds to the somatomedin B domain of vitronectin. *J Biol Chem* 266, 2824-2830 (1991).

54. Lawrence, D.A. *et al.* Characterization of the binding of different conformational forms of plasminogen activator inhibitor-1 to vitronectin. Implications for the regulation of pericellular proteolysis. *J Biol Chem* 272, 7676-7680 (1997).

55. Schar, C.R. *et al.* Characterization of a site on PAI-1 that binds to vitronectin outside of the somatomedin B domain. *J Biol Chem* 283, 28487-28496 (2008).

56. Schar, C.R., Blouse, G.E., Minor, K.H. & Peterson, C.B. A deletion mutant of vitronectin lacking the somatomedin B domain exhibits residual plasminogen activator inhibitor-1-binding activity. *J Biol Chem* 283, 10297-10309 (2008).

57. Wiman, B., Almquist, A., Sigurdardottir, O. & Lindahl, T. Plasminogen activator inhibitor 1 (PAI) is bound to vitronectin in plasma. *FEBS Lett* 242, 125-128 (1988).

58. Declerck, P.J. *et al.* Purification and characterization of a plasminogen activator inhibitor 1 binding protein from human plasma. Identification as a multimeric form of S protein (vitronectin). *J Biol Chem* 263, 15454-15461 (1988).

59. Stoop, A.A., Lupu, F. & Pannekoek, H. Colocalization of thrombin, PAI-1, and vitronectin in the atherosclerotic vessel wall: A potential regulatory mechanism of thrombin activity by PAI-1/vitronectin complexes. *Arterioscler Thromb Vasc Biol* 20, 1143-1149 (2000).

60. Roldan, A.L. *et al.* Cloning and expression of the receptor for human urokinase plasminogen activator, a central molecule in cell surface, plasmin dependent proteolysis. *EMBO J* 9, 467-474 (1990).

61. Ploug, M. *et al.* Cellular receptor for urokinase plasminogen activator. Carboxyl-terminal processing and membrane anchoring by glycosyl-phosphatidylinositol. *J Biol Chem* 266, 1926-1933 (1991).

62. Llinas, P. *et al.* Crystal structure of the human urokinase plasminogen activator receptor bound to an antagonist peptide. *EMBO J* 24, 1655-1663 (2005).

63. Krishnamachary, B. *et al.* Regulation of colon carcinoma cell invasion by hypoxia-inducible factor 1. *Cancer Res* 63, 1138-1143 (2003).

64. Sun, L. *et al.* MicroRNA-10b induces glioma cell invasion by modulating MMP-14 and uPAR expression via HOXD10. *Brain Res* 1389, 9-18.

65. Solberg, H., Ploug, M., Hoyer-Hansen, G., Nielsen, B.S. & Lund, L.R. The murine receptor for urokinase-type plasminogen activator is primarily expressed in tissues actively undergoing remodeling. *J Histochem Cytochem* 49, 237-246 (2001).

66. Romer, J. *et al.* The receptor for urokinase-type plasminogen activator is expressed by keratinocytes at the leading edge during re-epithelialization of mouse skin wounds. *J Invest Dermatol* 102, 519-522 (1994).

67. Uszynski, M., Perlik, M., Uszynski, W. & Zekanowska, E. Urokinase plasminogen activator (uPA) and its receptor (uPAR) in gestational tissues; Measurements and clinical implications. *Eur J Obstet Gynecol Reprod Biol* 114, 54-58 (2004).

68. Beschorner, R. *et al.* Lesion-associated accumulation of uPAR/CD87- expressing infiltrating granulocytes, activated microglial cells/macrophages and upregulation by endothelial cells following TBI and FCI in humans. *Neuropathol Appl Neurobiol* 26, 522-527 (2000).

69. Plesner, T. *et al.* The receptor for urokinase-type plasminogen activator and urokinase is translocated from two distinct intracellular compartments to the plasma membrane on stimulation of human neutrophils. *Blood* 83, 808-815 (1994).

70. Min, H.Y. *et al.* cDNA for Mo3, a monocyte activation antigen, encodes the human receptor for urokinase plasminogen activator. *J Immunol* 148, 3636-3642 (1992).

71. Nykjaer, A., Petersen, C.M., Moller, B., Andreasen, P.A. & Gliemann, J. Identification and characterization of urokinase receptors in natural killer cells and T-cell-derived lymphokine activated killer cells. *FEBS Lett* 300, 13-17 (1992).

72. Tjwa, M. *et al.* Membrane-anchored uPAR regulates the proliferation, marrow pool size, engraftment, and mobilization of mouse hematopoietic stem/progenitor cells. *J Clin Invest* 119, 1008-1018 (2009).

73. Allgayer, H. Translational research on u-PAR. *Eur J Cancer* 46, 1241-1251.

74. Pyke, C. *et al.* Urokinase-type plasminogen activator is expressed in stromal cells and its receptor in cancer cells at invasive foci in human colon adenocarcinomas. *Am J Pathol* 138, 1059-1067 (1991).

75. Pyke, C. *et al.* Immunohistochemical detection of the receptor for urokinase plasminogen activator in human colon cancer. *Histopathology* 24, 131-138 (1994).

76. Grondahl-Hansen, J. *et al.* Localization of urokinase-type plasminogen activator in stromal cells in adenocarcinomas of the colon in humans. *Am J Pathol* 138, 111-117 (1991).

77. Pyke, C. *et al.* Receptor for urokinase is present in tumor-associated macrophages in ductal breast carcinoma. *Cancer Res* 53, 1911-1915 (1993).

78. Nielsen, B.S., Sehested, M., Timshel, S., Pyke, C. & Dano, K. Messenger RNA for urokinase plasminogen activator is expressed in myofibroblasts adjacent to cancer cells in human breast cancer. *Lab Invest* 74, 168-177 (1996).

79. Nielsen, B.S. *et al.* Urokinase plasminogen activator is localized in stromal cells in ductal breast cancer. *Lab Invest* 81, 1485-1501 (2001).

80. Offersen, B.V. *et al.* The myofibroblast is the predominant plasminogen activator inhibitor-1-expressing cell type in human breast carcinomas. *Am J Pathol* 163, 1887-1899 (2003).

81. Duffy, M.J. The urokinase plasminogen activator system: role in malignancy. *Curr Pharm Des* 10, 39-49 (2004).

82. Holmes, R. Preparation from human serum of an alpha-one protein which induces the immediate growth of unadapted cells in vitro. *J Cell Biol* 32, 297-308 (1967).

83. Grinnell, F., Hays, D.G. & Minter, D. Cell adhesion and spreading factor. Partial purification and properties. *Exp Cell Res* 110, 175-190 (1977).

84. Hayman, E.G., Pierschbacher, M.D., Ohgren, Y. & Ruoslahti, E. Serum spreading factor (vitronectin) is present at the cell surface and in tissues. *Proc Natl Acad Sci U S A* 80, 4003-4007 (1983).

85. Seiffert, D., Keeton, M., Eguchi, Y., Sawdey, M. & Loskutoff, D.J. Detection of vitronectin mRNA in tissues and cells of the mouse. *Proc Natl Acad Sci U S A* 88, 9402-9406 (1991).

86. Seiffert, D., Crain, K., Wagner, N.V. & Loskutoff, D.J. Vitronectin gene expression in vivo. Evidence for extrahepatic synthesis and acute phase regulation. *J Biol Chem* 269, 19836-19842 (1994).

87. Izumi, M., Shimo-Oka, T., Morishita, N., Ii, I. & Hayashi, M. Identification of the collagen-binding domain of vitronectin using monoclonal antibodies. *Cell Struct Funct* 13, 217-225 (1988).

88. Skorstengaard, K., Halkier, T., Hojrup, P. & Mosher, D. Sequence location of a putative transglutaminase cross-linking site in human vitronectin. *FEBS Lett* 262, 269-274 (1990).

89. Ishikawa-Sakurai, M. & Hayashi, M. Two collagen-binding domains of vitronectin. *Cell Struct Funct* 18, 253-259 (1993).

90. Preissner, K.T., Holzhuter, S., Justus, C. & Muller-Berghaus, G. Identification of and partial characterization of platelet vitronectin: evidence for complex formation with platelet-derived plasminogen activator inhibitor-1. *Blood* 74, 1989-1996 (1989).

91. Izumi, M., Yamada, K.M. & Hayashi, M. Vitronectin exists in two structurally and functionally distinct forms in human plasma. *Biochim Biophys Acta* 990, 101-108 (1989).

92. Stockmann, A., Hess, S., Declerck, P., Timpl, R. & Preissner, K.T. Multimeric vitronectin. Identification and characterization of conformation-dependent self-association of the adhesive protein. *J Biol Chem* 268, 22874-22882 (1993).

93. Seiffert, D. & Schleef, R.R. Two functionally distinct pools of vitronectin (Vn) in the blood circulation: identification of a heparin-binding competent population of Vn within platelet alpha-granules. *Blood* 88, 552-560 (1996).

94. van Aken, B.E., Seiffert, D., Thinnes, T. & Loskutoff, D.J. Localization of vitronectin in the normal and atherosclerotic human vessel wall. *Histochem Cell Biol* 107, 313-320 (1997).

95. Koukoulis, G.K., Shen, J., Virtanen, I. & Gould, V.E. Vitronectin in the cirrhotic liver: an immunomarker of mature fibrosis. *Hum Pathol* 32, 1356-1362 (2001).

96. Gladson, C.L. & Cheresh, D.A. Glioblastoma expression of vitronectin and the alpha v beta 3 integrin. Adhesion mechanism for transformed glial cells. *J Clin Invest* 88, 1924-1932 (1991).

97. Tomasini-Johansson, B.R., Sundberg, C., Lindmark, G., Gailit, J.O. & Rubin, K. Vitronectin in colorectal adenocarcinoma--synthesis by stromal cells in culture. *Exp Cell Res* 214, 303-312 (1994).

98. Aaboe, M., Offersen, B.V., Christensen, A. & Andreasen, P.A. Vitronectin in human breast carcinomas. *Biochim Biophys Acta* 1638, 72-82 (2003).

99. Seiffert, D. & Loskutoff, D.J. Type 1 plasminogen activator inhibitor induces multimerization of plasma vitronectin. A suggested mechanism for the generation of the tissue form of vitronectin in vivo. *J Biol Chem* 271, 29644-29651 (1996).

100. Minor, K.H. & Peterson, C.B. Plasminogen activator inhibitor type 1 promotes the self-association of vitronectin into complexes exhibiting altered incorporation into the extracellular matrix. *J Biol Chem* 277, 10337-10345 (2002).

101. Leavesley, D.I. *et al.* Vitronectin--master controller or micromanager? *IUBMB Life* 65, 807-818.

102. Deng, G., Curriden, S.A., Wang, S., Rosenberg, S. & Loskutoff, D.J. Is plasminogen activator inhibitor-1 the molecular switch that governs urokinase receptor-mediated cell adhesion and release? *J Cell Biol* 134, 1563-1571 (1996).

103. Preissner, K.T. Specific binding of plasminogen to vitronectin. Evidence for a modulatory role of vitronectin on fibrin(ogen)-induced plasmin formation by tissue plasminogen activator. *Biochem Biophys Res Commun* 168, 966-971 (1990).

104. Moser, T.L., Enghild, J.J., Pizzo, S.V. & Stack, M.S. Specific binding of urinary-type plasminogen activator (u-PA) to vitronectin and its role in mediating u-PA-dependent adhesion of U937 cells. *Biochem J* 307 (Pt 3), 867-873 (1995).

105. Vassalli, J.D., Baccino, D. & Belin, D. A cellular binding site for the Mr 55,000 form of the human plasminogen activator, urokinase. *J Cell Biol* 100, 86-92 (1985).

106. Appella, E. *et al.* The receptor-binding sequence of urokinase. A biological function for the growth-factor module of proteases. *J Biol Chem* 262, 4437-4440 (1987).

107. Barinka, C. *et al.* Structural basis of interaction between urokinase-type plasminogen activator and its receptor. *J Mol Biol* 363, 482-495 (2006).

108. Gardsvoll, H. *et al.* Characterization of the functional epitope on the urokinase receptor. Complete alanine scanning mutagenesis supplemented by chemical cross-linking. *J Biol Chem* 281, 19260-19272 (2006).

109. Ellis, V., Behrendt, N. & Dano, K. Plasminogen activation by receptor-bound urokinase. A kinetic study with both cell-associated and isolated receptor. *J Biol Chem* 266, 12752-12758 (1991).

110. Estreicher, A., Muhlhauser, J., Carpentier, J.L., Orci, L. & Vassalli, J.D. The receptor for urokinase type plasminogen activator polarizes expression of the protease to the leading edge of migrating monocytes and promotes degradation of enzyme inhibitor complexes. *J Cell Biol* 111, 783-792 (1990).

111. Zhou, H.M., Nichols, A., Meda, P. & Vassalli, J.D. Urokinase-type plasminogen activator and its receptor synergize to promote pathogenic proteolysis. *EMBO J* 19, 4817-4826 (2000).

112. Bolon, I., Zhou, H.M., Charron, Y., Wohlwend, A. & Vassalli, J.D. Plasminogen mediates the pathological effects of urokinase-type plasminogen activator overexpression. *Am J Pathol* 164, 2299-2304 (2004).

113. Bugge, T.H. *et al.* Urokinase-type plasminogen activator is effective in fibrin clearance in the absence of its receptor or tissue-type plasminogen activator. *Proc Natl Acad Sci U S A* 93, 5899-5904 (1996).

114. Gyetko, M.R. *et al.* Urokinase receptor-deficient mice have impaired neutrophil recruitment in response to pulmonary Pseudomonas aeruginosa infection. *J Immunol* 165, 1513-1519 (2000).

115. Connolly, B.M. *et al.* Selective abrogation of the uPA-uPAR interaction in vivo reveals a novel role in suppression of fibrin-associated inflammation. *Blood* 116, 1593-1603.

116. Cubellis, M.V., Wun, T.C. & Blasi, F. Receptor-mediated internalization and degradation of urokinase is caused by its specific inhibitor PAI-1. *EMBO J* 9, 1079-1085 (1990).

117. Jensen, P.H., Christensen, E.I., Ebbesen, P., Gliemann, J. & Andreasen, P.A. Lysosomal degradation of receptor-bound urokinase-type plasminogen activator is enhanced by its inhibitors in human trophoblastic choriocarcinoma cells. *Cell Regul* 1, 1043-1056 (1990).

118. Conese, M., Olson, D. & Blasi, F. Protease nexin-1-urokinase complexes are internalized and degraded through a mechanism that requires both urokinase receptor and alpha 2-macroglobulin receptor. *J Biol Chem* 269, 17886-17892 (1994).

119. Nykjaer, A. *et al.* Purified alpha 2-macroglobulin receptor/LDL receptor-related protein binds urokinase.plasminogen activator inhibitor type-1 complex. Evidence that the alpha 2-macroglobulin receptor mediates cellular degradation of urokinase receptor-bound complexes. *J Biol Chem* 267, 14543-14546 (1992).

120. Nykjaer, A. *et al.* Recycling of the urokinase receptor upon internalization of the uPA:serpin complexes. *EMBO J* 16, 2610-2620 (1997).

121. Waltz, D.A. & Chapman, H.A. Reversible cellular adhesion to vitronectin linked to urokinase receptor occupancy. *J Biol Chem* 269, 14746-14750 (1994).

122. Wei, Y. *et al.* Identification of the urokinase receptor as an adhesion receptor for vitronectin. *J Biol Chem* 269, 32380-32388 (1994).

123. Kanse, S.M., Kost, C., Wilhelm, O.G., Andreasen, P.A. & Preissner, K.T. The urokinase receptor is a major vitronectin-binding protein on endothelial cells. *Exp Cell Res* 224, 344-353 (1996).

124. Huai, Q. *et al.* Crystal structures of two human vitronectin, urokinase and urokinase receptor complexes. *Nat Struct Mol Biol* 15, 422-423 (2008).

125. Madsen, C.D., Ferraris, G.M., Andolfo, A., Cunningham, O. & Sidenius, N. uPAR-induced cell adhesion and migration: vitronectin provides the key. *J Cell Biol* 177, 927-939 (2007).

126. Gardsvoll, H. & Ploug, M. Mapping of the vitronectin-binding site on the urokinase receptor: involvement of a coherent receptor interface consisting of residues from both domain I and the flanking interdomain linker region. *J Biol Chem* 282, 13561-13572 (2007).

127. Xu, X. *et al.* Crystal structure of the urokinase receptor in a ligand-free form. *J Mol Biol* 416, 629-641.

128. Sidenius, N., Andolfo, A., Fesce, R. & Blasi, F. Urokinase regulates vitronectin binding by controlling urokinase receptor oligomerization. *J Biol Chem* 277, 27982-27990 (2002).

129. Cunningham, O. *et al.* Dimerization controls the lipid raft partitioning of uPAR/CD87 and regulates its biological functions. *EMBO J* 22, 5994-6003 (2003).

130. Caiolfa, V.R. *et al.* Monomer dimer dynamics and distribution of GPI-anchored uPAR are determined by cell surface protein assemblies. *J Cell Biol* 179, 1067-1082 (2007).

131. Okumura, Y. *et al.* Kinetic analysis of the interaction between vitronectin and the urokinase receptor. *J Biol Chem* 277, 9395-9404 (2002).

132. Stefansson, S. & Lawrence, D.A. The serpin PAI-1 inhibits cell migration by blocking integrin alpha V beta 3 binding to vitronectin. *Nature* 383, 441-443 (1996).

133. Ferraris, G.M. & Sidenius, N. Urokinase plasminogen activator receptor: a functional integrator of extracellular proteolysis, cell adhesion, and signal transduction. *Semin Thromb Hemost* 39, 347-355.

134. Smith, H.W. & Marshall, C.J. Regulation of cell signalling by uPAR. *Nat Rev Mol Cell Biol* 11, 23-36.

135. Wei, Y. *et al.* Regulation of alpha5beta1 integrin conformation and function by urokinase receptor binding. *J Cell Biol* 168, 501-511 (2005).

136. Bass, R. & Ellis, V. Regulation of urokinase receptor function and pericellular proteolysis by the integrin alpha(5)beta(1). *Thromb Haemost* 101, 954-962 (2009).

137. Ferraris, G.M. *et al.* The interaction between uPAR and vitronectin triggers ligand-independent adhesion signalling by integrins. *EMBO J*.

138. Xue, W., Kindzelskii, A.L., Todd, R.F., 3rd & Petty, H.R. Physical association of complement receptor type 3 and urokinase-type plasminogen activator receptor in neutrophil membranes. *J Immunol* 152, 4630-4640 (1994).

139. Sitrin, R.G., Todd, R.F., 3rd, Albrecht, E. & Gyetko, M.R. The urokinase receptor (CD87) facilitates CD11b/CD18-mediated adhesion of human monocytes. *J Clin Invest* 97, 1942-1951 (1996).

140. Gyetko, M.R. *et al.* Function of the urokinase receptor (CD87) in neutrophil chemotaxis. *J Leukoc Biol* 58, 533-538 (1995).

141. Wei, C. *et al.* Modification of kidney barrier function by the urokinase receptor. *Nat Med* 14, 55-63 (2008).

142. Smith, H.W., Marra, P. & Marshall, C.J. uPAR promotes formation of the p130Cas-Crk complex to activate Rac through DOCK180. *J Cell Biol* 182, 777-790 (2008).

143. Zhang, F. *et al.* Distinct ligand binding sites in integrin alpha3beta1 regulate matrix adhesion and cell-cell contact. *J Cell Biol* 163, 177-188 (2003).

144. Wei, Y. *et al.* Urokinase receptors are required for alpha 5 beta 1 integrin-mediated signaling in tumor cells. *J Biol Chem* 282, 3929-3939 (2007).

145. Liu, D., Aguirre Ghiso, J., Estrada, Y. & Ossowski, L. EGFR is a transducer of the urokinase receptor initiated signal that is required for in vivo growth of a human carcinoma. *Cancer Cell* 1, 445-457 (2002).

146. Eastman, B.M., Jo, M., Webb, D.L., Takimoto, S. & Gonias, S.L. A transformation in the mechanism by which the urokinase receptor signals provides a selection advantage for estrogen receptor-expressing breast cancer cells in the absence of estrogen. *Cell Signal* 24, 1847-1855.

147. Kiyan, J., Kiyan, R., Haller, H. & Dumler, I. Urokinase-induced signaling in human vascular smooth muscle cells is mediated by PDGFR-beta. *EMBO J* 24, 1787-1797 (2005).

148. Resnati, M. *et al.* Proteolytic cleavage of the urokinase receptor substitutes for the agonist-induced chemotactic effect. *EMBO J* 15, 1572-1582 (1996).

149. Fazioli, F. *et al.* A urokinase-sensitive region of the human urokinase receptor is responsible for its chemotactic activity. *EMBO J* 16, 7279-7286 (1997).

150. Resnati, M. *et al.* The fibrinolytic receptor for urokinase activates the G protein-coupled chemotactic receptor FPRL1/LXA4R. *Proc Natl Acad Sci U S A* 99, 1359-1364 (2002).

151. de Paulis, A. *et al.* Urokinase induces basophil chemotaxis through a urokinase receptor epitope that is an endogenous ligand for formyl peptide receptor-like 1 and -like 2. *J Immunol* 173, 5739-5748 (2004).

152. Montuori, N., Carriero, M.V., Salzano, S., Rossi, G. & Ragno, P. The cleavage of the urokinase receptor regulates its multiple functions. *J Biol Chem* 277, 46932-46939 (2002).

153. Kjoller, L. & Hall, A. Rac mediates cytoskeletal rearrangements and increased cell motility induced by urokinase-type plasminogen activator receptor binding to vitronectin. *J Cell Biol* 152, 1145-1157 (2001).

154. Behrendt, N. *et al.* The ligand-binding domain of the cell surface receptor for urokinase-type plasminogen activator. *J Biol Chem* 266, 7842-7847 (1991).

155. Beaufort, N. *et al.* Proteolytic regulation of the urokinase receptor/CD87 on monocytic cells by neutrophil elastase and cathepsin G. *J Immunol* 172, 540-549 (2004).

156. Andolfo, A. *et al.* Metalloproteases cleave the urokinase-type plasminogen activator receptor in the D1-D2 linker region and expose epitopes not present in the intact soluble receptor. *Thromb Haemost* 88, 298-306 (2002).

157. Beaufort, N. *et al.* Interplay of human tissue kallikrein 4 (hK4) with the plasminogen activation system: hK4 regulates the structure and functions of the urokinase-type plasminogen activator receptor (uPAR). *Biol Chem* 387, 217-222 (2006).

158. Hoyer-Hansen, G. *et al.* Urokinase plasminogen activator cleaves its cell surface receptor releasing the ligand-binding domain. *J Biol Chem* 267, 18224-18229 (1992).

159. Hoyer-Hansen, G., Ploug, M., Behrendt, N., Ronne, E. & Dano, K. Cell-surface acceleration of urokinase-catalyzed receptor cleavage. *Eur J Biochem* 243, 21-26 (1997).

160. Hoyer-Hansen, G. *et al.* Urokinase-catalysed cleavage of the urokinase receptor requires an intact glycolipid anchor. *Biochem J* 358, 673-679 (2001).

161. Wilhelm, O.G. *et al.* Cellular glycosylphosphatidylinositol-specific phospholipase D regulates urokinase receptor shedding and cell surface expression. *J Cell Physiol* 180, 225-235 (1999).

162. Beaufort, N. *et al.* Plasmin cleaves the juxtamembrane domain and releases truncated species of the urokinase receptor (CD87) from human bronchial epithelial cells. *FEBS Lett* 574, 89-94 (2004).

163. Sidenius, N., Sier, C.F. & Blasi, F. Shedding and cleavage of the urokinase receptor (uPAR): identification and characterisation of uPAR fragments in vitro and in vivo. *FEBS Lett* 475, 52-56 (2000).

164. Selleri, C. *et al.* Involvement of the urokinase-type plasminogen activator receptor in hematopoietic stem cell mobilization. *Blood* 105, 2198-2205 (2005).

165. Selleri, C. *et al.* In vivo activity of the cleaved form of soluble urokinase receptor: a new hematopoietic stem/progenitor cell mobilizer. *Cancer Res* 66, 10885-10890 (2006).

166. Montuori, N. & Ragno, P. Multiple activities of a multifaceted receptor: roles of cleaved and soluble uPAR. *Front Biosci (Landmark Ed)* 14, 2494-2503 (2009).

167. Jo, M., Thomas, K.S., Wu, L. & Gonias, S.L. Soluble urokinase-type plasminogen activator receptor inhibits cancer cell growth and invasion by direct urokinase-independent effects on cell signaling. *J Biol Chem* 278, 46692-46698 (2003).

168. Hoyer-Hansen, G., Behrendt, N., Ploug, M., Dano, K. & Preissner, K.T. The intact urokinase receptor is required for efficient vitronectin binding: receptor cleavage prevents ligand interaction. *FEBS Lett* 420, 79-85 (1997).

169. Sidenius, N. & Blasi, F. Domain 1 of the urokinase receptor (uPAR) is required for uPAR-mediated cell binding to vitronectin. *FEBS Lett* 470, 40-46 (2000).

170. Montuori, N., Rossi, G. & Ragno, P. Cleavage of urokinase receptor regulates its interaction with integrins in thyroid cells. *FEBS Lett* 460, 32-36 (1999).

171. Bernstein, A.M., Twining, S.S., Warejcka, D.J., Tall, E. & Masur, S.K. Urokinase receptor cleavage: a crucial step in fibroblast-to-myofibroblast differentiation. *Mol Biol Cell* 18, 2716-2727 (2007).

172. Mazzieri, R., D'Alessio, S., Kenmoe, R.K., Ossowski, L. & Blasi, F. An uncleavable uPAR mutant allows dissection of signaling pathways in uPA-dependent cell migration. *Mol Biol Cell* 17, 367-378 (2006).

173. Madsen, C.D., Ferraris, G.M., Andolfo, A., Cunningham, O. & Sidenius, N. uPAR-induced cell adhesion and migration: vitronectin provides the key. *The Journal of cell biology* 177, 927-939 (2007).

174. Galfre, G., Howe, S.C., Milstein, C., Butcher, G.W. & Howard, J.C. Antibodies to major histocompatibility antigens produced by hybrid cell lines. *Nature* 266, 550-552 (1977).

175. Conforti, G., Dominguez-Jimenez, C., Ronne, E., Hoyer-Hansen, G. & Dejana, E. Cell-surface plasminogen activation causes a retraction of in vitro cultured human umbilical vein endothelial cell monolayer. *Blood* 83, 994-1005 (1994).

176. Atienza, J.M., Zhu, J., Wang, X., Xu, X. & Abassi, Y. Dynamic monitoring of cell adhesion and spreading on microelectronic sensor arrays. *J Biomol Screen* 10, 795-805 (2005).

177. Kost, C., Benner, K., Stockmann, A., Linder, D. & Preissner, K.T. Limited plasmin proteolysis of vitronectin. Characterization of the adhesion protein as morpho-regulatory and angiostatin-binding factor. *Eur J Biochem* 236, 682-688 (1996).

178. Reinartz, J., Schafer, B., Batrla, R., Klein, C.E. & Kramer, M.D. Plasmin abrogates alpha v beta 5-mediated adhesion of a human keratinocyte cell line (HaCaT) to vitronectin. *Exp Cell Res* 220, 274-282 (1995).

179. Zhou, A., Huntington, J.A., Pannu, N.S., Carrell, R.W. & Read, R.J. How vitronectin binds PAI-1 to modulate fibrinolysis and cell migration. *Nat Struct Biol* 10, 541-544 (2003).

180. Royle, G., Deng, G., Seiffert, D. & Loskutoff, D.J. A method for defining binding sites involved in protein-protein interactions: analysis of the binding of plasminogen activator inhibitor 1 to the somatomedin domain of vitronectin. *Anal Biochem* 296, 245-253 (2001).

181. Reinhold, W.C. *et al.* CellMiner: a web-based suite of genomic and pharmacologic tools to explore transcript and drug patterns in the NCI-60 cell line set. *Cancer Res* 72, 3499-3511.

182. Pirazzoli, V., Ferraris, G.M. & Sidenius, N. Direct evidence of the importance of vitronectin and its interaction with the urokinase receptor in tumor growth. *Blood* 121, 2316-2323.

183. Zhang, J.H., Chung, T.D. & Oldenburg, K.R. A Simple Statistical Parameter for Use in Evaluation and Validation of High Throughput Screening Assays. *J Biomol Screen* 4, 67-73 (1999).

184. Salonen, E.M. *et al.* Interaction of plasminogen activator inhibitor (PAI-1) with vitronectin. *J Biol Chem* 264, 6339-6343 (1989).

185. Andreasen, P.A. *et al.* Plasminogen activator inhibitor from human fibrosarcoma cells binds urokinase-type plasminogen activator, but not its proenzyme. *J Biol Chem* 261, 7644-7651 (1986).

186. Gardsvoll, H. *et al.* Mimicry of the regulatory role of urokinase in lamellipodia formation by introduction of a non-native interdomain disulfide bond in its receptor. *J Biol Chem* 286, 43515-43526.

187. Jensen, J.K. *et al.* Construction of a plasminogen activator inhibitor-1 variant without measurable affinity to vitronectin but otherwise normal. *FEBS Lett* 556, 175-179 (2004).

188. Mertens, H.D. *et al.* A flexible multidomain structure drives the function of the urokinase-type plasminogen activator receptor (uPAR). *J Biol Chem* 287, 34304-34315.

189. Buzza, M.S. *et al.* Extracellular matrix remodeling by human granzyme B via cleavage of vitronectin, fibronectin, and laminin. *J Biol Chem* 280, 23549-23558 (2005).

190. Borgono, C.A. *et al.* Expression and functional characterization of the cancer-related serine protease, human tissue kallikrein 14. *J Biol Chem* 282, 2405-2422 (2007).

191. Marchenko, G.N. *et al.* Characterization of matrix metalloproteinase-26, a novel metalloproteinase widely expressed in cancer cells of epithelial origin. *Biochem J* 356, 705-718 (2001).

192. Kenny, H.A., Kaur, S., Coussens, L.M. & Lengyel, E. The initial steps of ovarian cancer cell metastasis are mediated by MMP-2 cleavage of vitronectin and fibronectin. *J Clin Invest* 118, 1367-1379 (2008).

193. Wu, K. *et al.* The cleavage and inactivation of plasminogen activator inhibitor type 1 by neutrophil elastase: the evaluation of its physiologic relevance in fibrinolysis. *Blood* 86, 1056-1061 (1995).

194. Machovich, R. & Owen, W.G. An elastase-dependent pathway of plasminogen activation. *Biochemistry* 28, 4517-4522 (1989).

195. Zheng, X., Saunders, T.L., Camper, S.A., Samuelson, L.C. & Ginsburg, D. Vitronectin is not essential for normal mammalian development and fertility. *Proc Natl Acad Sci U S A* 92, 12426-12430 (1995).

196. Li, R. *et al.* Vitronectin increases vascular permeability by promoting VE-cadherin internalization at cell junctions. *PLoS One* 7, e37195.

197. Jang, Y.C., Tsou, R., Gibran, N.S. & Isik, F.F. Vitronectin deficiency is associated with increased wound fibrinolysis and decreased microvascular angiogenesis in mice. *Surgery* 127, 696-704 (2000).

198. Wyseure, T. & Declerck, P.J. Novel or expanding current targets in fibrinolysis. *Drug Discov Today* 19, 1476-1482.

199. Fryklund, L., Uthne, K. & Sievertsson, H. Isolation and characterization of polypeptides from human plasma enhancing the growth of human normal cells in culture. *Biochem Biophys Res Commun* 61, 950-956 (1974).

200. Fryklund, L. & Sievertsson, H. Primary structure of somatomedin B: a growth hormone-dependent serum factor with protease inhibiting activity. *FEBS Lett* 87, 55-60 (1978).

201. Standker, L. *et al.* Structural and functional characterization of vitronectin-derived RGD-containing peptides from human hemofiltrate. *Eur J Biochem* 241, 557-563 (1996).

202. Yalow, R.S., Hall, K. & Luft, R. Immunoreactive somatomedin B in urine. *J Clin Endocrinol Metab* 41, 638-639 (1975).

203. Hayes, D.F. *et al.* Tumor marker utility grading system: a framework to evaluate clinical utility of tumor markers. *J Natl Cancer Inst* 88, 1456-1466 (1996).

204. Harbeck, N. *et al.* Ten-year analysis of the prospective multicentre Chemo-N0 trial validates American Society of Clinical Oncology (ASCO)-recommended biomarkers uPA and PAI-1 for therapy decision making in node-negative breast cancer patients. *Eur J Cancer* 49, 1825-1835.

205. Cummings, J., Ward, T.H., Greystoke, A., Ranson, M. & Dive, C. Biomarker method validation in anticancer drug development. *Br J Pharmacol* 153, 646-656 (2008).

206. Sier, C.F. *et al.* Presence of urokinase-type plasminogen activator receptor in urine of cancer patients and its possible clinical relevance. *Lab Invest* 79, 717-722 (1999).

207. Gils, A. *et al.* Biochemical importance of glycosylation of plasminogen activator inhibitor-1. *Thromb Haemost* 90, 206-217 (2003).

208. Harbeck, N., Kates, R.E. & Schmitt, M. Clinical relevance of invasion factors urokinase-type plasminogen activator and plasminogen activator inhibitor type 1 for individualized therapy decisions in primary breast cancer is greatest when used in combination. *J Clin Oncol* 20, 1000-1007 (2002).

209. Manders, P. *et al.* Complex of urokinase-type plasminogen activator with its type 1 inhibitor predicts poor outcome in 576 patients with lymph node-negative breast carcinoma. *Cancer* 101, 486-494 (2004).

210. Manders, P. *et al.* Predictive impact of urokinase-type plasminogen activator: plasminogen activator inhibitor type-1 complex on the efficacy of adjuvant systemic therapy in primary breast cancer. *Cancer Res* 64, 659-664 (2004).

211. Manders, P. *et al.* The complex between urokinase-type plasminogen activator (uPA) and its type-1 inhibitor (PAI-I) independently predicts response to first-line endocrine therapy in advanced breast cancer. *Thromb Haemost* 91, 514-521 (2004).